STUDIES OF THE OFF-RESONANT NONLINEAR OPTICAL PROPERTIES OF AN ORGANIC MOLECULAR CRYSTAL AND SPECIFIC NONCONJUGATED CONDUCTIVE POLYMERS

Except where reference is made to the work of others, the work described in this dissertation is my own or was done in collaboration with my advisory committee. This dissertation does not include proprietary or classified information.

_____

Jitto Titus

Certificate of Approval:

_____	_____
Lloyd S. Riggs Professor Electrical and Computer Engineering	Mrinal Thakur, Chair Professor Mechanical Engineering
_____	_____
Dan Marghitu Professor Mechanical Engineering	Joe F. Pittman Interim Dean Graduate School

STUDIES OF THE OFF-RESONANT NONLINEAR OPTICAL PROPERTIES OF AN ORGANIC MOLECULAR CRYSTAL AND SPECIFIC NONCONJUGATED CONDUCTIVE POLYMERS

Jitto Titus

A Dissertation

Submitted to

the Graduate Faculty of

Auburn University

in Partial Fulfillment of the

Requirements for the

Degree of

Doctor of Philosophy

Auburn, Alabama
August 4, 2007

STUDIES OF THE OFF-RESONANT NONLINEAR OPTICAL PROPERTIES OF AN ORGANIC MOLECULAR CRYSTAL AND SPECIFIC NONCONJUGATED CONDUCTIVE POLYMERS

Jitto Titus

Permission is granted to Auburn University to make copies of this dissertation at its discretion, upon the request of individuals or institutions and at their expense. The author reserves all publication rights.

_____
Signature of Author

_____
Date of Graduation

Style manual or journal used: *Journal of Applied Physics*, Bibliography follows *Journal of Applied Physics.*

Computer software used: Microsoft Office Word 2003

VITA

Jitto Titus son of Dr. Titus Koilpillai and Mrs. Jintha Titus was born on 20th June 1979. In 2000, he graduated with a Bachelors degree in Mechanical Engineering from Dr. M. G. R. Engineering College, Chennai, India. He joined the doctoral program in the department of Mechanical Engineering at Auburn University, Alabama in 2001.

DISSERTATION ABSTRACT

STUDIES OF THE OFF-RESONANT NONLINEAR OPTICAL PROPERTIES OF AN ORGANIC MOLECULAR CRYSTAL AND SPECIFIC NONCONJUGATED CONDUCTIVE POLYMERS

Jitto Titus
Doctor of Philosophy, 4th August, 2007
(B. E., Dr. M. G. R. Engineering College, Chennai, India, 2000)

128 Typed Pages
Directed by M. Thakur

In this dissertation, the second order nonlinear optical properties of an organic molecular crystal and the third order off-resonant nonlinear optical properties of specific nonconjugated conductive polymers have been studied in detail. Presently available electro-optic devices are based on long propagation of light through bulk crystals or waveguides. Usually more than 1 cm propagation length is necessary to produce a sufficiently large phase change at an acceptably low electric field. This is due to the relatively low electro-optic coefficients that are usually observed in commercial materials such as lithium niobate (r_{33} = 30 pm/V). Hence to compensate for the low electro-optic coefficients, the interaction length is increased. The organic molecular salt, 4′-dimethylamino-*N*-methyl-4-stilbazolium tosylate (DAST) has been proven to be an

excellent candidate for an electro-optic material for many significant and novel applications. A single-pass thin-film electro-optic modulator with a large intensity modulation (20%) at 720 nm for a low ac field (1 V/μm, at 4 kHz) using a 3-μm-thick single-crystal film of DAST (red phase) has been demonstrated. Owing to the exceptionally large electro-optic coefficient and excellent optical quality of the films, large modulation depths despite an interaction length of a few microns were observed. The magnitude of the electro-optic coefficient is found to be r_{11} = 530 pm/V at 720 nm and 445 pm/V at 750 nm. The electro-optic coefficient of DAST at a technologically important wavelength (1.55 microns) was determined to be r_{11} = 200 pm/V. Electro-optic modulation was also demonstrated at high speed (up to 1.5 GHz) and the response was found to be flat over the higher frequency range. A Novel Pockels cell device based on the single-pass field induced birefringence configuration was designed, fabricated and successfully demonstrated with significant modulation and a comparative study was done. A fiber coupled electro-optic device based on the same configuration also was designed, fabricated and successfully demonstrated. Quadratic electro-optic measurements on a novel nano-optical polymer based on nonconjugated conductive polymers were done for the first time. Both the nonconjugated polymers 1,4-cis-polyisoprene and poly(β-pinene) investigated showed exceptionally large nonlinearities. The nonlinear absorption coefficient of poly(β-pinene) was determined using a modified z-scan technique and was found to be 2.6 cm/MW and a time resolved measurement involving field-induced birefringence for the same material was performed. The experiment was also conducted using PTS-polydiacetylene as the standard. The large

optical nonlinearities observed have been accredited to the nature of the charged sites formed upon doping as well as the confinement of the charge in the sub-nanometer domain. The optical, mechanical and electrical properties of another nonconjugated conductive polymer, doped styrene-butadiene rubber were studied.

ACKNOWLEDGEMENTS

Photons came to be when You said "Let there be light"
Never since then have they ceased to shimmer for Your delight
You allowed me to worship You through my curiosity
***Jesus**, my all knowing Savior, for this I thank Thee*

My arduous journey would have never been so sweet
It is only because of you that my joy is complete
Through tests and trials you stood by me
***Sheba**, my lovely bride, for this I thank thee*

You brought me into this world and taught me life
Nurtured my dreams and sheltered me from strife
You believed in me and loved me unconditionally
*My **parents**, my refuge, for this I thank thee*

*Dr. **Thakur**, you are not only resourceful but also enlightening*
*Dr. **Riggs** and Dr. **Marghitu**, your thoughtfulness is encouraging*
You all not only have imparted knowledge unto me
You have been a part of my life and for this I thank thee

My friends who have made my life in Auburn exciting
*The '**Garden Court**' gang, y'all are amazing*
Ananth, Veera, Aditya, Raj, Vippa, Sanchit and Kutty
I cherish the memories of you and for this I thank thee

TABLE OF CONTENTS

LIST OF FIGURES xii

LIST OF TABLES xv

1. INTRODUCTION……1

2. BACKGROUND……...6
   - 2.1 Interaction of a Light Wave with an Anisotropic Medium 8
   - 2.2 Nonlinear Optical Process 13
   - 2.3 Second Order Nonlinear Optical Processes 15
     - 2.3.1 Second Order Nonlinear Optical Effects in Organic Molecules 17
     - 2.3.2 Relation Between Wavelength and Linear Electro-Optic Effect 19
     - 2.3.3 Second Order Nonlinear Optical Materials 19
   - 2.4 Third Order Nonlinear Optical Processes 24
     - 2.4.1 Conjugated Polymers 25
     - 2.4.2 Nonconjugated Polymers 28
     - 2.4.3 Quadratic Electro-Optic Effect 29
     - 2.4.4 Two Photon Absorption 32
     - 2.4.5 Other Third Order Materials 34
   - 2.5 Nano-Optics 36
     - 2.5.1 Optical Properties of Metal Nanoclusters in Dielectrics 37
     - 2.5.2 Optical Nonlinearities in Semiconductor Nanoparticles 38
     - 2.5.3 Quantum Dot Analogy of Doped Nonconjugated Conductive Polymers 39

3. OBJECTIVES……..42

4. ELECTRO-OPTIC STUDIES OF THE ORGANIC MOLECULAR SALT - DAST……..……44
   - 4.1 Characteristics and Preparation of Single-crystal Films of DAST 45
   - 4.2 Electro-Optic Studies on DAST 52
   - 4.3 Off-Resonant Electro-Optic Studies on DAST at 1.55 Microns 53
     - 4.3.1 Sample Preparation and Experimental Setup 53
     - 4.3.2 Field Induced Birefrengence Measurements 55
   - 4.4 Electro-Optic Modulation at 1.5 GHz Using a Single-Crystal Film of DAST .. 59

4.5 Electro-Optic Devices Based on Single-Pass Field Induced Birefringence Method Employing DAST 63
4.5.1 Pockels Cell Using DAST Single-Crystal Film 64
4.5.2 Fiber Coupled Electro-Optic Device 67

5. THIRD ORDER NONLINEAR OPTICAL STUDIES OF SPECIFIC NONCONJUGATED CONDUCTIVE POLYMERS 71
5.1 Electrical and Optical Properties of Styrene-Butadiene-Rubber 72
5.1.1 Electrical Conductivity Analysis 73
5.1.2 Optical Absorption Analysis 73
5.1.3 Photoluminescence Measurements 75
5.1.4 FTIR Spectroscopy 76
5.2 Quadratic Electro-Optic Measurements Using 1,4 Cis-Polyisoprene 78
5.2.1 Experimental Setup 79
5.2.2 Results 80
5.2.3 Analysis 82
5.3 Nonlinear Refractive Index and Two-Photon Measurements Using Poly(β-pinene) 84
5.3.1 Z-Scan Experimental Setup 85
5.3.2 Z-Scan Results and Analysis 87
5.3.3 Mach-Zhender Experimental Setup 91
5.3.4 Results 92
5.3.5 Time Resolved Measurements 93
5.3.6 Pump-Probe Setup and Analysis 93

6. SUMMARY 97

BIBLIOGRAPHY 99

APPENDIX 110

LIST OF FIGURES

Fig. 2.1 Schematic of intersite hopping transport in doped 1,4 cis-polyisoprene [84]. 29

Fig. 2.2 Optical AbsorptionSpectra of a) CdSe andb) Gold Nanoparticles for Different Particle Sizes [96]..... 40

Fig. 4.1 a) Molecular structure of DAST
b) The molecules as they are embedded in the crystal lattice [56]. 46

Fig. 4.2 Projection of two unit cells of the DAST crystal [57]. 47

Fig. 4.3 Directions of the dielectric and crystallographic axes in a DAST crystal [58] 47

Fig. 4.4 Crystal Structure of DAST Viewed Approximately Along the c-axis. 49

Fig. 4.5 Deviation Between the Crystal Axis a and Molecular Axix z in DAST Crystal..... 49

Fig. 4.6 Optical micrograph of a single crystal film of DAST..... 51

Fig. 4.7 Optical absorption spectrum of a single crystal film of DAST [64]..... 52

Fig. 4.8 Optical micrograph of a single crystal film of DAST with gold electrodes 54

Fig. 4.9 The experimental setup used for field-induced birefringence measurements..... 55

Fig. 4.10 Optical Configuration Showing Angular Position of polarizer and analyzer with respect to Crystal Axis of DAST..... 56

Fig. 4.11 Device Configuration of the Field-Induced Birefringence Setup. 57

Fig. 4.12 Oscilloscope trace of the signal modulation at 1.55 microns…… 58

Fig. 4.13 Modulation Signal Recorded Using a Spectrum Analyzer at 1.1 GHz [67] 60

Fig. 4.14 Modulation as a Function of Drive Voltage [67] 61

Fig. 4.15 Modulation as a Function of Frequency (0.25 - 1.5 GHz) [67] 62

Fig. 4.16 Setup for a Typical Pockels Cell 65

Fig. 4.17 Oscilloscope Trace of the Modulation Observed Using the Pockels Cell 66

Fig. 4.18 Photograph of the Pockels Cell Prototype. 66

Fig. 4.19 Photograph of the Fiber Coupled E-O Modulator Prototype. 67

Fig. 4.20 Photograph of a Fully Assembled Fiber Coupled E-O Modulator. 67

Fig. 4.21 Oscilloscope Trace of the Modulation Observed Using the Fiber Coupled E-O Modulator. 69

Fig. 5.1 Molecular Structure of Styrene-Butadiene-Rubber. 73

Fig. 5.2 Optical Absorption Spectra of SBR at Different Doping Levels. 74

Fig. 5.3 Photoluminiscence Spectra of SBR. 75

Fig. 5.4 FTIR Spectra of SBR at Different Doping Levels. 76

Fig. 5.5 Optical absorption of 1,4 cis-polyisoprene [84]. 79

Fig. 5.6 Oscilloscope trace of modulation signal in quadratic electrooptic measurement of doped 1,4 cis-polyisoprene. [84]. 81

Fig. 5.7 Quantum Dots Created Upon Doping With Iodine 82

Fig. 5.8 Schematic of the spring mass system involving a hole loosely bound to the dopant ion I_3^- 83

Fig. 5.9 Molecular Sturcture of Poly(β-pinene). 84

Fig. 5.10 Optical absorption spectra of Poly(β-pinene) at Different Doping Levels 85

Fig. 5.11 Schematic of the Z-Scan Experimental Setup 86

Fig. 5.12 Z-Scan Data (Open Aperture) for Two Photon Absorption Measurement at Varying Input Powers..... 87

Fig. 5.13 Z-Scan Data (Open Aperture) for Continuous Mode Indicating No Two Photon Absorption..... 88

Fig. 5.14 Normalized Z-Scan Plots (Open Aperture) for Two Photon Absorption Measurement (Pulsed Mode)..... 88

Fig. 5.15 TPA Coefficient Plotted as a Function of Wavelength..... 89

Fig. 5.16 Change in Transmission with Varying Input Intensity..... 91

Fig. 5.17 Schematic of Mach-Zhender Experimental Setup..... 92

Fig. 5.18 Pump-Probe Time Resolved Experimental Setup..... 94

Fig. 5.19 Time Resolved Measurement of the Two Photon Absorption..... 95

LIST OF TABLES

Table I Calculated Half Wave Voltage and Figures of Merit for Minimum Drive Power [121,122] 21

Table II Third order nonlinear optical coefficients of various materials [11]..... 26

Table III Two Photon Absorption in Various Materials [32]..... 33

Table IV Third Order Nonlinear Optical Coefficients of Various Materials [7]..... 34

CHAPTER 1

INTRODUCTION

In this new era of 'optical technology', data communication, storage and image processing technology have been the earmarks. Mankind has never been so networked and the proverbial world as we know it is indeed shrinking. This is credited to the high speeds and wide bandwidths offered by the telecommunication industry. We are nearing the point where it will be necessary to replace the role of electrons with photons in communications. Electronic switches and repeaters are no longer able to offer the speed that is required. This has caused researchers to turn to the possibility of optical switches and all optical networks. To make this not only viable but also feasible, novel optically active materials are being engineered and studied. Electro-optic modulators are devices that can control by the application of a voltage, the amplitude, phase and polarization of an optical beam that interacts with the media subjected to the electric field. To make theses devices commercially available, certain crucial characteristics of the optically active material have to be met such as, the magnitude of electro-optic susceptibility (which translates into drive voltage, V_{π}, requirements), optical loss, thermal, environmental, mechanical and chemical stability and ease of integration with fiber optics and very large scale integration (VLSI) semiconductor electronic circuitry [2].

Currently in the electro-optic modulator technology, the most used crystalline material is lithium niobate which is an inorganic material. The other not so widely used materials are organic and polymeric. However, inorganic materials' main drawback is their ineffectiveness at high speed operations due to the high dielectric constants, which is not an issue in organic and polymeric materials. These materials possessing extremely large optical nonlinearities have significantly lower dielectric constants and consequently ultrafast and broadband electronic responses. Investigating the nonlinear optical effects in such organic and polymeric materials could open the door to the answer for higher speeds and wider bandwidths.

In this research, the nonlinear optical properties of an organic molecular crystal and specific nonconjugated conductive polymers have been studied. The third order optical nonlinearities in nonconjugated conductive polymers have been observed and measured. The calculated optical nonlinearity for these polymers was found to be exceptionally large. The behavior of these nonconjugated materials has been compared to that of nano-metallics and nano-semiconductors and is found to be similar which explains the large optical nonlinearities.

In Chapter 2, of this dissertation a review of second order and third order nonlinear optical processes is presented. Based on Maxwell equations the propagation of optical waves in an anisotropic media and the various nonlinear optical interactions has been described. Some of the second order and third order nonlinear optical materials have been reviewed. Among the various third order nonlinear optical materials π-conjugated polymers (having alternate single and double bonds in the backbone) have shown great

potential. Polymers offer several advantages over organic and inorganic crystals. The advantages of such π-conjugated polymers are discussed. The Kerr electro-optic effect and the change in the refractive index of a third order optical material on the application of electric field are studied. Equations relating the change in the refractive index and Kerr coefficient have been described.

In Chapter 3, the objectives of the research have been stated.

In Chapter 4, the electro-optic effect using the field induced birefringence method at an off-resonant wavelength (1.55 microns) is discussed. The second order nonlinear optical material investigated for this work was a single-crystal film of 4-dimethylamino-N-methyl-4-stilbazolium tosylate (DAST). DAST, an organic molecular salt, is known to exhibit the highest second order nonlinearity among all materials investigated to date. The electro-optic properties of a single-crystal film of DAST are discussed. The method used for performing the experiment as well as sample preparation is described. The electro-optic modulation of the DAST sample is also demonstrated at high speeds. (up to 1.5 GHz). A Novel Pockels cell device based on the single-pass field induced birefringence configuration was designed, fabricated and successfully demonstrated with high modulation and a comparative study is discussed. A fiber coupled electro-optic device based on the same configuration also was designed, fabricated and successfully demonstrated. The advantages of single pass thin film modulators over conventional waveguide modulators and their potential applications have been stated.

In Chapter 5, quadratic electro-optic effect in nonconjugated conductive polymers has been reported for the first time. Contrary to the fundamental assumption that

conjugation is a prerequisite for a polymer to become conductive nonconjugated polymers have shown to conduct electricity upon doping with strong electron acceptors. The first nonconjugated polymer reported for its conductivity was 1,4 cis-polyisoprene. Thereafter, other nonconjugated polymers have been investigated for their conductivity. The conductivity mechanism and optical absorption of these polymers has been explained. Nano-optics deals with the interaction of light with particles in the nanometer domain. To date metal and semiconductor nanostructures have been fabricated in a dielectric media and studied for their nonlinear optical properties. While operating at wavelengths close to plasmon resonance frequency, a significant enhancement of nonlinear optical properties of the metal nanostructures has been observed. This is mainly due to the dielectric confinement effect. In semiconductors the enhancement is due to the quantum confinement effect as the excitonic radius reduces compared to the bulk. Equations explaining these phenomena have been described. Quadratic electro-optic measurements on a thin film of doped 1,4 cis-polyisoprene has been performed. The observed Kerr coefficient is exceptionally large. The large magnitude of the Kerr coefficient has been attributed to the loosely bound hole at the charge transfer site and also the confinement of the charge within a nanometer size volume. A correlation between other nanostructered materials has been established to explain the charge confinement and enhancement of the optical nonlinearity. The nonlinear absorption coefficient of poly(β-pinene) was determined using a modified z-scan technique and a time resolved measurement involving a Mach-Zehnder configuration for the same material to determine the nonlinear refractive index and its sign was performed and is

explained. The optical, electrical and mechanical properties of a nano-optical polymer, doped styrene-butadiene rubber have been discussed.

Chapter 6 summarizes the dissertation. This research comprises of a study nonlinear optical properties of a specific organic molecular crystal and nonconjugated polymers. The electro-optic measurements of DAST at off-resonant wavelength and at high speeds were conducted. These experiments have led to the characterization of single crystal films of organic molecular salts and also the demonstration of two single pass thin film modulators. The third-order studies have involved the measurement of the quadratic electro-optic effect and the nonlinear refractive index and absorption in nonconjugated polymers. The scope of this research is an attempt to understand the nonlinearities in organic crystals as well as nonconjugated conductive polymers and demonstrate specific devices based on such materials.

CHAPTER 2

BACKGROUND

Light wave is an electro-magnetic radiation comprising of a magnetic field and an electric field component [3]. When a light wave interacts with a medium, it causes the charged particles of the matter to oscillate. This perpetuates localized optical changes in the medium that the light travels through. The study of this phenomenon is called as Nonlinear Optics. These changes in materials can also be brought about by the application of a large electric field. The behavior of the electro-magnetic light radiation is governed by the equations stated by Maxwell [4, 5].

$$\overline{\nabla} \times \overline{E} = -\frac{\partial \overline{B}}{\partial t} \tag{2.1}$$

$$\overline{\nabla} \times \overline{H} = \overline{J} + \frac{\partial \overline{D}}{\partial t} \tag{2.2}$$

$$\overline{\nabla} \cdot \overline{D} = \rho \tag{2.3}$$

$$\overline{\nabla} \cdot \overline{B} = 0 \tag{2.4}$$

Where, $\overline{E}$ and $\overline{H}$ are electric and magnetic field vectors respectively. $\overline{D}$ and $\overline{B}$ are electric and magnetic field displacement vectors. $\overline{J}$ is the electric current density (A/m^2). ρ is the electric charge density (C/m^3). In optics, for most cases, one deals with propagation of electromagnetic radiation in regions that are far from the sources causing both ρ and $\overline{J}$ to become zero. The effect of electromagnetic field on material media is dictated by these equations:-

$$\overline{D} = \varepsilon \overline{E} = \varepsilon_0 \overline{E} + \overline{P} \qquad 2.5$$

$$\overline{B} = \mu \overline{H} = \mu_0 \overline{H} + \overline{M} \qquad 2.6$$

Where ε and μ are tensors of rank 2 and are known as permittivity tensor and permeability tensor respectively. $\overline{P}$ and $\overline{M}$ are electric and magnetic polarizations respectively. ε_0 and μ_0 are permittivity and permeability of vacuum respectively. These tensors are reduced to scalars when the material is isotropic or in other words, the electric displacement vector $\overline{D}$ and its corresponding electric field $\overline{E}$ become parallel and consequently, the electric polarization is proportional to the electric field which can be expressed as

$$\overline{P} = \varepsilon_0 \chi \overline{E} \qquad 2.7$$

And the relationship between the electric field and electric field displacement vector can be expressed as

$$\overline{D} = \varepsilon_0 (1 + \chi) \overline{E} \tag{2.8}$$

2.1 Interaction of a Light Wave with an Anisotropic Medium

Crystals are most often anisotropic. And in an anisotropic medium, the dynamics of light interaction is more complex than in an isotropic medium [3]. When an electric field is applied to the anisotropic medium, a polarization is induced in the medium. The induced polarization is not always parallel to the field except for certain propagation directions.

A dielectric tensor relates the displacement vector $\overline{D}$ to the electric field vector $\overline{E}$ [5][6]

$$\begin{pmatrix} \overline{D}_x \\ \overline{D}_y \\ \overline{D}_z \end{pmatrix} = \varepsilon_0 \begin{pmatrix} \varepsilon_{xx} & \varepsilon_{xy} & \varepsilon_{xz} \\ \varepsilon_{yx} & \varepsilon_{yy} & \varepsilon_{yx} \\ \varepsilon_{zx} & \varepsilon_{zy} & \varepsilon_{zz} \end{pmatrix} \begin{pmatrix} \overline{E}_x \\ \overline{E}_y \\ \overline{E}_z \end{pmatrix} \tag{2.9}$$

Where, ε_{ij} are the components of the dielectric tensor. The elements other than the diagonal in the dielectric tensor become zero when the axes of the dielectric tensor are parallel to the principal axes of the material.

When an electric field is applied to a dielectric medium the charges are rearranged and form oscillating electric dipoles corresponding to the frequency of the field applied [3]. The dipole oscillations can also be induced when an intense light like a laser beam interacts with the dielectric medium. The effect of the magnetic field part of the light and the electric quadrupoles is not significant and is usually neglected. This is called electric-dipole approximation. The cumulative effect of all the oscillating dipoles results in a macroscopic polarization $\overline{P}$ which is used to describe the response of the material. The polarization or the net dipole moment per unit volume induced by the field can be expressed as

$$\overline{P} = \sum_j N_j e_j \left(\Delta r_j\right) \tag{2.10}$$

Where N_j and e_j are the density and charge of the species j in the crystal and Δr_j is the displacement of the charged species from the equilibrium position. In an anisotropic medium such as a crystal, where ε and μ are tensors of rank 2, the induced polarization will depend, both in its magnitude and direction, on the direction of the applied field.

From equation 2.8 we have

$$\varepsilon_{ij} = \varepsilon_0 (1 + \chi_{ij}) \tag{2.11}$$

Where ε_{ij} and χ_{ij} constitute dielectric and susceptibility tensors respectively. Therefore, from Eqs. (2.8) and (2.11) we have

$$\begin{pmatrix} \overline{D}_x \\ \overline{D}_y \\ \overline{D}_z \end{pmatrix} = \begin{pmatrix} \varepsilon_{11} & \varepsilon_{12} & \varepsilon_{13} \\ \varepsilon_{21} & \varepsilon_{22} & \varepsilon_{23} \\ \varepsilon_{31} & \varepsilon_{32} & \varepsilon_{33} \end{pmatrix} \begin{pmatrix} \overline{E}_x \\ \overline{E}_y \\ \overline{E}_z \end{pmatrix} \qquad 2.12$$

For a lossless non-optically active material, the dielectric permeability tensor is represented by a real symmetric matrix, which therefore has six independent elements. Considering the principal coordinate system Eq. (2.12) reduces to

$$\begin{pmatrix} \overline{D}_x \\ \overline{D}_y \\ \overline{D}_z \end{pmatrix} = \begin{pmatrix} \varepsilon_{xx} & 0 & 0 \\ 0 & \varepsilon_{yy} & 0 \\ 0 & 0 & \varepsilon_{zz} \end{pmatrix} \begin{pmatrix} \overline{E}_x \\ \overline{E}_y \\ \overline{E}_z \end{pmatrix} \qquad 2.13$$

This new coordinate system is called the principal-axis system, as in this system, the dielectric tensor is denoted as a diagonal matrix. Most optical materials being nonmagnetic in nature, the stored electric field in the anisotropic medium is given by,

$$2U_e = \left(\frac{\overline{D}_x^2}{\varepsilon_x} + \frac{\overline{D}_y^2}{\varepsilon_y} + \frac{\overline{D}_z^2}{\varepsilon_z} \right) \qquad 2.14$$

The electrical displacement vectors corresponding to the stored electrical energy describe an ellipsoid. Where, ε_x, ε_y and ε_z are the principal dielectric constants. If the principle indices of refraction are defined as n_x, n_y and n_z by substituting $n_i^2 = \varepsilon_i$ (i = x, y, z) and $D_i^2 / 2U_e = i^2$ in Eq. (2.14) we get [3]

$$\frac{x^2}{n_x^2} + \frac{y^2}{n_y^2} + \frac{z^2}{n_z^2} = 1 \qquad 2.15$$

This is a general equation of an ellipsoid and is also called as the indicatrix or index ellipsoid, whose major axes are parallel to x, y and z directions and the respective lengths are $2n_x$, $2n_y$, $2n_z$. The two refractive indices associated with the material are the magnitudes and the directions of the major and minor axis and two corresponding directions of D associated with the two independent plane waves that can propagate along an arbitrary direction in a crystal. It is, apart from a scale factor, equivalent to the surface mapped out by the D vectors corresponding to a constant energy density at a given frequency.

The index ellipsoid becomes a sphere in cubic crystals called isotropic indicatrix. Whereas crystals belonging to the tetragonal, hexagonal and trigonal crystal systems the crystal symmetry requires that $n_x = n_y$ and the indicatrix reduces to an ellipsoid of revolution. In this case there is only one optic axis, oriented along the axis of highest symmetry of the crystal, the z axis (or c axis). These crystals are said to be uniaxial crystals and the equation for such a uniaxial indicatrix is

$$\frac{x^2 + \quad y^2}{n_o^2} + \frac{z^2}{n_e^2} = 1 \qquad 2.16$$

Where n_o is the index of refraction faced by ordinary waves and n_e is the index of refraction experienced by extraordinary waves. If $n_e > n_o$ the indicatrix is said to be positive uniaxial. If $n_e < n_o$ the indicatrix is said to be negative uniaxial. The crystals belonging to the orthorhombic, monoclinic and triclinic symmetry, all crystallographic directions, are distinct and none of the principal indices are identical. In this case there exist two unique directions and for propagation along these directions the refractive index is polarization independent and so these materials are called biaxial media whose equation is given by Eq. (2.16).

For the linear electro-optic effect, an applied field changes each of the of coefficients $(1/n^2)_i$ i=1,…...6 in a way that is linearly dependent on electric field $\overline{E}$ ($\overline{E}_x$, $\overline{E}_y$, $\overline{E}_z$). The linear changes in the coefficients is described by the electro-optic tensor which is given by

$$\begin{pmatrix} \Delta(1/n^2)_1 \\ \Delta(1/n^2)_2 \\ \Delta(1/n^2)_3 \\ \Delta(1/n^2)_4 \\ \Delta(1/n^2)_5 \\ \Delta(1/n^2)_6 \end{pmatrix} = \begin{pmatrix} r_{11} & r_{12} & r_{13} \\ r_{21} & r_{22} & r_{32} \\ r_{31} & r_{32} & r_{33} \\ r_{41} & r_{42} & r_{43} \\ r_{51} & r_{52} & r_{53} \\ r_{61} & r_{62} & r_{63} \end{pmatrix} \begin{pmatrix} \overline{E}_1 \\ \overline{E}_2 \\ \overline{E}_3 \end{pmatrix} \qquad 2.17$$

where the 6×3 matrix with elements r_{ij} is called the electro-optic tensor.

2.2 Nonlinear Optical Processes

As discussed earlier, induced polarization is due to the interaction of the material of the medium and the electro-magnetic wave traveling through it or due to the application of an external electric field [6, 7, 8]. This polarization is a characteristic that is used to define nonlinear optical phenomenon because, a polarization varying with time can give rise to new electromagnetic field components. The wave equation for a nonlinear optical media is given by

$$\nabla^2\overline{E} - \frac{n^2}{c^2}\frac{\partial^2\overline{E}}{\partial t^2} = \frac{4\pi}{c^2}\frac{\partial^2\overline{P}^{NL}}{\partial t^2} \qquad 2.18$$

In the above inhomogeneous wave equation, the polarization P^{NL} associated with the nonlinear response drives the electric field $\overline{E}$.

A simple Lorentz oscillator model can be used to better understand this interaction. Lorentz considered an oscillating mass on a spring as an analogy for the model of an atom. The tethered mass would represent the electron which is held close to the nucleus by a force (spring). The natural frequency of the system and the equilibrium displacement would be ω_0 and r. When an electric field is applied to the system analogous to a force acting on the mass, the electron begins to oscillate according to the nature of the force applied. The field either repels or attracts the electron. The electric field component of the optical field encountered by the electron varies sinusoidally. At high optical frequencies, the heavier nuclei, due to the inertia is unable to respond in

phase with the rapid oscillation frequencies of the applied field. Only the electrons in the valence orbit have the most displacement. This displacement is proportional to the applied electric field. However at large magnitudes of the applied field, the system becomes nonlinear. The behavior of the electron is governed by an oscillation equation

$$\left[\frac{d^2x}{dt^2} + 2\Gamma\frac{dx}{dt} + \omega_0^2 x + \frac{b}{m}x^2 + \frac{c}{m}x^3 + ...\right] = -e\overline{E}(t) \qquad 2.19$$

Where $\omega_0 = \sqrt{\frac{k}{m}}$ is the resonance frequency and Γ is the damping term. The terms $(b/m)x^2 + (c/m)x^3 + ...$ are anharmonic terms. Due to these anharmonic terms the nonlinear optical properties in a material can be visualized. The instantaneous optical response can often be described by expressing the polarization as a power series in the field strength E (t) as

$$\overline{P}(t) = \chi^{(1)}E(t) + \chi^{(2)}E^2(t) + \chi^{(3)}E^3(t) + ... \qquad 2.20$$

$$= \overline{P}^{(1)}(t) + \overline{P}^{(2)}(t) + \overline{P}^{(3)}(t) + ...$$

Where $\chi^{(1)}$ is linear susceptibility, $\chi^{(2)}$ second order nonlinear susceptibility and so on.

2.3 Second Order Nonlinear Optical Processes

Let us consider an optical field incident upon a nonlinear optical medium which is characterized by a nonlinear susceptibility $\chi^{(2)}$ consisting of two distinct frequency components, which are represented in the form

$$\overline{E}(t) = \overline{E}_1 e^{-i\omega_1 t} + \overline{E}_2 e^{-i\omega_2 t} + c.c \tag{2.21}$$

The second order nonlinear polarization that is induced in such a crystal is described by

$$\begin{aligned}\overline{P}^{(2)}(t) = \chi^{(2)}[E_1^2 e^{-2i\omega_1 t} + E_2^2 e^{-2i\omega_2 t} + 2E_1 E_2 e^{-i(\omega_1+\omega_2)t} + 2E_1 E_2^* e^{-i(\omega_1-\omega_2)t} + c.c] \\ + 2\chi^{(2)}[E_1 E_2^* + E_2 E_2^*]\end{aligned} \tag{2.22}$$

Where, c.c. stands for complex conjugate. It is convenient to express this result using the notation

$$\overline{P}^{(2)}(t) = \sum_n \overline{P}(\omega_n) e^{-i\omega_n t} \tag{2.23}$$

Where, the summation is over the positive and negative frequencies of ω_n. The complex amplitudes of various frequency components of the nonlinear polarization and the physical processes that they describe are given by

$$\overline{P}(2\omega_{(1)}) = \chi^{(2)} E_1^2 \qquad \text{Second-Harmonic Generation (SHG)} \tag{2.24}$$

$$\overline{P}(2\omega_{(2)}) = \chi^{(2)} E_2^2 \qquad \text{Second-Harmonic Generation (SHG)} \tag{2.25}$$

$$\overline{P}(\omega_1 + \omega_2) = 2\chi^{(2)} E_1 E_2 \qquad \text{Sum Frequency Generation (SFG)} \tag{2.26}$$

$$\overline{P}(\omega_1 - \omega_2) = 2\chi^{(2)} E_1 E_2^* \quad \text{Difference Frequency Generation (DFG)} \quad 2.27$$

$$\overline{P}(0) = 2\chi^{(2)}\left(E_1 E_1^* + E_2 E_2^*\right) \quad \text{Optical Rectification (OR)} \quad 2.28$$

However, only one of these frequency components of significant intensity will be present in the radiation resulting due to the nonlinear optical interaction because the nonlinear polarization can efficiently produce an output signal only when the condition for phase-matching is satisfied. Most often, this condition cannot be satisfied for more than one frequency component of nonlinear polarization. The static component of the input field gives rise to a phenomenon known as the Pockel's or Electro-Optic (EO) effect. This can be described in terms of second order nonlinear susceptibility as

$$\overline{P}_i(\omega) = 2\sum_{jk} \chi_{ijk}^{(2)}(\omega = \omega + 0) E_j(\omega) E_k(0) \quad 2.29$$

This nonlinear interaction precipitates a phase shift that is dependent on the propagation length. This is equivalent to a change in the refractive index. Linear electro-optic effect can be observed only in materials that are noncentrosymmetric. For isotropic materials that are centrosymmetric (i.e. possess a center of inversion) the $\chi^{(2)}$ nonlinear susceptibility vanishes.

When Kleinman symmetry conditions are valid d_{ijk} coefficients are often used where,

$$d_{ijk} = \frac{1}{2}\chi_{ijk}^{(2)} \quad 2.30$$

The nonlinear coefficients d_{ijk} are related to the linear electro-optic coefficients r_{ijk} by

$$d_{ijk} = -\frac{\varepsilon_{ii}\varepsilon_{jj}}{4\varepsilon_0} r_{ijk} \qquad 2.31$$

Using linear approximation, the change in the refractive index Δn_i is given by

$$\Delta n_i = -\frac{1}{2} n_i^3 r_{ijk} E_k \qquad 2.32$$

An important parameter to characterize electro-optic crystals for modulator applications is the half-wave voltage, V_π, which is the voltage required to obtain a phase shift of π in the transmitted beam in an appropriate modulator configuration. This half–wave voltage, V_π, can be written as

$$V_\pi = \frac{\lambda}{(n^3 r)_{eff}} \frac{d}{l} \qquad 2.33$$

Where, $(n^3 r)_{eff}$ is the effective electro-optic coefficient, *d* is the gap between the electrodes and *l* is the length of the device. In order to get low modulation voltages one must have large values of $(n^3 r)_{eff}$ and large values of the device geometry (*l/d*). This can be realized in a traverse configuration where the light propagation direction is perpendicular to the applied electric field.

2.3.1 Second Order Nonlinear Optical Effects in Organic Molecules

Davydov and co-workers in 1970 [9] demonstrated that organic molecules exhibit large second-order optical nonlinearities due to the strong donor-acceptor intra-molecular

interaction. The large nonlinear-optical response observed in certain organic systems is due to the ability of the optical fields to affect the motions of the π-electrons. The electrons in these π-conjugated systems are not tightly bound to the individual nuclear sites. Hence their orbital motion can span distances, even as far as the entire molecule. Therefore, the π-electrons excitations in individual molecular units give rise to the optical nonlinearity. And, each one of them can be considered as an independent source of nonlinear optical response. The polarization $\overline{P}$ of the molecule in the presence of an electric field $\overline{E}$ can be written as [11]

$$\overline{P}_i = \textit{Ground state dipole moment} + \varepsilon_0(\alpha_{ij}E_j + \beta_{ijk}E_jE_k + \gamma E_jE_kE_l + ____) \qquad 2.34$$

Where α_{ij} is the polarizability tensor, β_{ijk} is first order hyperpolarizability tensor, γ_{ijkl} is second order hyperpolarizability tensor. *i*, *j*, *k* denote the molecular coordinates. Most organic materials being centrosymmetric, do not exhibit second order optical nonlinearities. However, when an acceptor and donor group is chemically substituted across the π-conjugated chain, strong intramolecular interaction between the donor-acceptor groups which provides maximum acentricity to the molecule can be realized giving rise to a noncentrosymmetric crystal structure. Both β value and its orientation in a crystal dictate the second order nonlinear optical susceptiblity. The effective β is the sum of two parts [12].

$$\beta_x = \beta_{add} + \beta_{CT} \qquad 2.35$$

Where β_{add} results from the interaction between the substituent and the conjugated system and β_{CT} the predominating part arising from the donor acceptor charge transfer contribution. The β_{CT} value increases remarkably with the increase of the π-conjugation length and the strength of donor and acceptor groups, although reducing the optical transparency of the material.

2.3.2 Relation Between Wavelength and Linear Electro-Optic Effect

The linear electro-optic coefficient of organic materials depends on the wavelength of the electromagnetic wave and can be derived as [13]

$$r_{IJK}^{(\omega)} = K \frac{1}{n_I^2(\omega) n_J^2(\omega)} \frac{n_I^2(\omega)+2}{3} \frac{n_J^2(\omega)+2}{3} \frac{3\omega_{eg}^2 - \omega^2}{(\omega_{eg}^2 - \omega^2)^2} \qquad 2.36$$

Where, K is a constant that depends on the material parameters such as the dielectric constant, number density of molecules, the difference between excited-state and ground state dipole moments and the transition dipole moment, and ω_{eg} is the resonance frequency of the optical medium.

2.3.3 Second Order Nonlinear Optical Materials

From the earlier discussions, it is apparent that the ideal material in regard to potential applications in nonlinear optical devices should possess the perfect combination of favorable physiochemical properties such as large nonlinearities, wide optical transparency, architectural flexibility for molecular design and morphology, ease of fabrication, wide phase matchable angle, high laser damage threshold, etc.

The invention and the development of laser technology, new nonlinear optical materials of both inorganic and organic types have caused an explosion in the area of nonlinear optics research. The scientific development of organic molecules took place simultaneously with that of inorganic molecules. For the very first time, the phenomenon of second harmonic generation in single crystal quartz was observed in 1961, by Franken and coworkers [14]. The linear electro-optic effect was discovered for the first time in quartz and tourmaline crystals by Röntgen and Kundt [15]. The electro-optic effect in uniaxial crystals of some dihydrogen phosphates were measured by Billings [16, 17, 18]. Carpenter [19] measured the electro-optic coefficients of ammonium dihydrogen phosphate (ADP) and potassium dihydrogen phosphate (KDP). This led to the development of other nonlinear optical materials such as lithium niobate ($LiNbO_3$) [20], potassium niobate ($KNbO_3$), barium titanate ($BaTiO_3$), potassium dihydrogen phosphate (KDP) etc. and a variety of semiconductors such as gallium arsenide (GaAs) [21], cadmium sulfide (CdS) [22], cadmium selenide (CdSe) [23] etc. in the recent years, $LiNbO_3$ has been the prime SHG material. Optical waveguide devices compatible with laser diodes and devices for light switching and fast modulation have been fabricated using this material [24]. However, most of these inorganic and semiconductor materials are limited in their speed of operation because of the relatively large dielectric constants. Organic and polymer based electro-optic modulators however, due to their low dielectric constants show high potential and has been the center of attention for researchers.

Rentzepis and Pao [25] are noted to be the first to observe SHG in an organic material benzenepyrene. Following them, Heilmer [26] in the same year, 1964 also

observed SHG in Hexamethylenetetramine single crystal. Few other materials to follow were hippuric acid [27] and benzyl [28]. In 1970, Davydov and co-workers reported strong SHG from organic compounds having electron donor and acceptor groups attached to a benzene ring. This provided the basis for the understanding of the organic structure that could potentially display large SHG. This caused a renwed interest in the search for new organic materials that have large second order optical nonlinearities, such as NPP, COANP, PNP, NPAN, MBANP and DAN [12]. These materials can be classified into categories, such as: (1) single crystals; (2) Langmuir-Blodgett films; (3) self assembled systems; (4) liquid crystals; (5) poled polymers. Controlled nonlinearity, ease of processibility and low cost can be realized using polymeric materials. However, due to lack of reliability and stability, they are not practical for device technology. Langmuir-Blodgett (L-B) films again due to poor long term stability, has not been very successful in device technology. Many other nonlinear optical crystals have shown potential. Some of the techniques used to grow bulk crystals are vapor growth, melt growth, solution growth). Thakur *et al.* [29] developed a novel technique called the *shear method* to prepare single-crystal thin films of organic materials. Diacetylene crystals were grown using this method and later various other organic crystals for applications in second-order optics.

The recently engineered organic nonlinear optical materials have shown to posses better nonlinear optical properties than inorganic materials. The high nonlinear susceptibility in organic materials is mainly due to the electronic origin as opposed to the inorganic counterparts. The dielectric constant is also much lower in organic materials.

Hence, nonlinear effect is as fast as the speed of light in the medium. This has shown tremendous practical potentials for high speed optical devices. Organic materials have good mechanical properties and can be grown into thin crystalline layers, fabricated into structures. They are also environmentally and thermally stable. Because of their unique chemical structures (π bonding), organic molecular materials exhibit the largest nonresonant optical nonlinearities.

Material	Wavelength (nm)	n	ϵ^s	r^s (pm/V)	V_π (kV)
$KNbO_3$ (r_{33})	632.8	2.167	24	34	1.8
$KNbO_3$ (r_{33})	1300	2.109	24	34	4.1
$LiNbO_3$ (r_{33})	632.8	2.196	28	28.8	2.1
$LiNbO_3$ (r_{33})	1300	2.134	28	28.8	4.6
GaAs (r_{41})	1020	3.50	13.2	1.2	20
MNA (r_{11})	632.8	2.0	3.5	67	1.2
MNBA (r_{11})	632.8	2.024	~4	30	2.5
Optimized stilbene (r_{33})	1300	~2	~3–7	~330	~0.5
Optimized stilbene (r_{33})	1500	~2	~3–7	~310	~0.6
Alternating styrene-malcic-anhydrid copolymer (see Table 4) (r_{33})	1300	1.66	~3.6	~20	~14.2

Table I - Calculated reduced half-wave voltages and figures-of-merit for minimum drive power in electro-optic modulators employing bulk crystals in the transverse configuration [121, 122]

The table lists the characteristics of some of the commercially used organic, inorganic and polymeric nonlinear materials.

Some of the main disadvantages or limitations in using inorganic materials are as follows:

1. High absorption coefficients which leads to large losses as the light propagates through the active material usually up to 1cm in length.
2. Possible nonuniformities and impurities being present in the active material could cause damage to the material when high power laser beams propagating through, could cause the combustion of such impurities.
3. High insertion losses leading to lower efficiencies. Hence AR coating and index matching liquids are necessary.
4. Highly susceptible to induced refractive index changes.
5. These materials are usually piezo-electric and could give rise to ringing. This largely reduces the efficiency at higher repletion rates.
6. Relatively higher dielectric constants make them sluggish at high speed opterations.

Advantages of DAST as an electro-optic material in comparison with the commercially available materials are:

1. DAST crystals have a high melting point of 256˚C.
2. They can be grown in the form of crystals of reasonable size and high optical quality. They have good mechanical stability and are environmentally stable.

3. Like other organic crystals, the nonlinear optical effects in DAST originate from the extended π-electron system, so its response time is very short.
4. DAST's low dielectric constants as compared to conventional inorganic materials and the electronic origin of nonlinear effects make it suitable for high-speed modulation and detection of THz-wave radiation.
5. DAST crystals show large birefringence with $n_1 = 2.8$ (633nm) being much larger than $n_2 = 1.8$ and $n_3 = 1.68$ which is advantageous for electro-optic applications, since an electro-optic material figure-of-merit (FOM) = n^3r.
6. Highest known electro-optic coefficients (r_{11}~770 pm/V at 633 nm)
7. It has low absorption in the technologically important wavelength range (1.3 and 1.55 microns).
8. Nearly optimum chromophore orientation, hence large nonlinear optical and electro-optic coefficients.
9. High tendency to crystallize non-centrosymmetrically.
10. Insignificant insertion and propagation losses compared to waveguide structures.

2.4 Third Order Nonlinear Optical Processes

The third order nonlinear susceptibility is the third term in the power series expansion of the induced polarization which is given by

$$\overline{P}^{(3)}(t) = \sum_{n} \overline{P}(\omega_{(n)}) e^{-i\omega_n t} \qquad 2.37$$

As described in the previous section, when we consider the optical field comprising of three distinct frequency components, various nonlinear optical processes due to third order susceptibility of the material can be derived by separating different frequency components of the induced polarization. The refractive index of the material is affected by the frequency of the optical wave, as given by $n = n_0 + n_2 I$, where n_0 is the linear refractive index (low-intensity), n_2 given by

$$n_2 = \frac{12\pi^2}{n_0^2 c} \chi^{(3)} \qquad 2.38$$

is an optical constant that characterizes the strength of the optical nonlinearity, and where $I = (n_0 c/8\pi)E^2$ is the intensity of the incident wave. One of the processes that can occur as a result of the intensity-dependent refractive index is self-focusing in where when n_2 is positive the material acts as a positive lens causing the rays to converge.

2.4.1 Conjugated Polymers

Conjugated polymers are a class of polymers which have alternating single and double bonds. Conjugated polymers have very large $\chi^{(3)}$ values as they are isotropic. The electrical conduction in such conjugated polymers occurs as a result of the formation of solitons, polarons or bipolarons formed upon doping [30]. Polydiacetylene, in a certain form exhibits a third order susceptibility of 10^{-9} esu as compared to the value of 1.9×10^{-12} esu for carbon disulphide. The favorable properties of the π-conjugated organic

polymers are: a) Fast response time in subpicoseconds, b) High resistance to laser radiations (GW/cm^2), c) Low dielectric constant and wide bandwidth, d) Chemical tailoring of physical and optical properties, e) Ease of processing into ultra thin films, fibers, and even as liquid crystals, f) Mechanical strength, flexibility and environmental stability, g) Compatibility with semiconductor integrated structures. A few such π-conjugated organic polymers are polydiacteylenes (PDAs), Poly (p-phenylene vinylene) (PPV) and polythiophenes among others can be processed into thin films which have shown resonant and off resonant third order nonlinear susceptibilities in the range of 10^{-5} to 10^{-12} esu [9]. The delocalization of the π electron from one repeat unit to the other along the backbone of the polymer is the key to the high nonlinearity. The delocalization of these electrons depends on the nature of the repeat unit electronic structure and order. When all the polymeric chains are aligned in the same direction, the polymer will exhibit a larger value of $\chi^{(3)}$ when compared to those with amorphous or disordered chains. $\chi^{(3)}$ is maximized when the polymeric chains are packed closely.

One of the most commonly investigated conjugated polymer for third order optics is polydiacetylene. Their advantages over other conjugated polymers are their one dimensional, delocalized electronic system. Single crystals can be prepared which have the molecules oriented in the same direction and the off-resonant nonlinearity is extremely large and is ultra fast.

Material	$\chi^{(3)}$ (10^{-10} esu)	Wavelength (μm)	Experimental Technique
PDA-PTS (single crystal)	90	0.6515	DFWM

PDA-PTS (single crystal)	2×10^5	1.97	SA
PDA-4-BCMU (thin film)	1.0	1.86	THG
PDA-4-BCMU (thin film)	2.0	0.620	DFWM
Polyacetylene (single crystal)	170	1.907	THG
Polyacetylene (single crystal)	90	1.064	THG
Polyacetylene (thin film)	500	0.620	DFWM
Polyacetylene (thin film)	1800	2.25	THG
PPV (thin film)	16	1.064	THG
PPV (thin film)	2.0	0.620	DFWM
Poly(thiophene) (thin film)	3.52	1.907	THG
Poly(thiophene) (thin film)	66	0.532	DFWM
Polypyrrole (thin film)	0.03	0.602	THG

Table II Third order nonlinear optical coefficients of some important π-conjugated polymers at resonant and off-resonant wavelengths performed by several groups [11].

DFWM = Degenerate Four Wave Mixing

THG = Third Harmonic Generation

SA = Saturation Absorption

2.4.2 Nonconjugated Polymers

Rustagi and *Ducuing* (1974) studied the importance of π-conjugation in determining the third-order nonlinear optical properties. Following them, π-conjugated organic polymers have received a lot of attention as nonlinear materials. The high optical nonlinearity arises due to the π-electron delocalization in the repeat of the polymer structure. However no direct correlation has been noted between high conductivity and the third-order susceptibility ($\chi^{(3)}$) although the extensive π-conjugation is often associated with conductivity of organic systems. Polyacetylene and polythiophene, that are nonconductive in the undoped state, become highly electrical conductivity when doped with an electron acceptor such as the halogens. These polymers exhibit large third-order nonlinear optical effects in the undoped state and decreases upon doping. Immense research effort has been out into conjugated polymers for their electrical conductivity until Thakur [72] in 1988, demonstrated that conjugation is not a necessary condition for a polymer to be conductive. His observations of a nonconjugated polymer becoming electrically conductive when doped with appropriate dopants, led him to many other investigations on nonconjugated polymers. Since then [79][80][81], research work on many other nonconjugated conductive polymers like, 1,4-polybutadiene, cis-1,4-polyisoprene and polyalloocimene have been reported. The third-order nonlinear optical effects in nonconjugated polymers were first reported by Thakur *et al* on cis-1,4-polyisoprene.

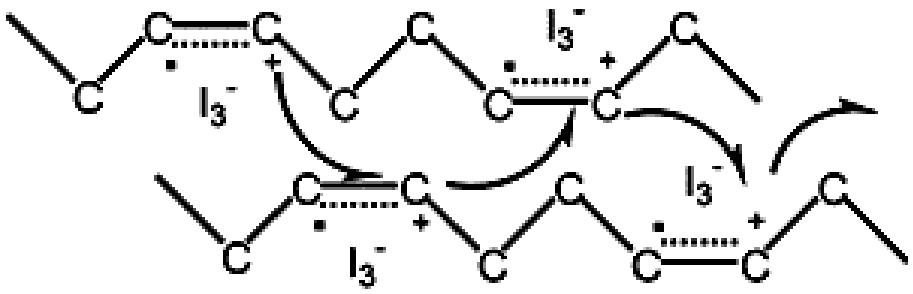

Fig 2.1 Schematic of the intersite hopping transport in a doped nonconjugated conductive polymer (polyisoprene) [84].

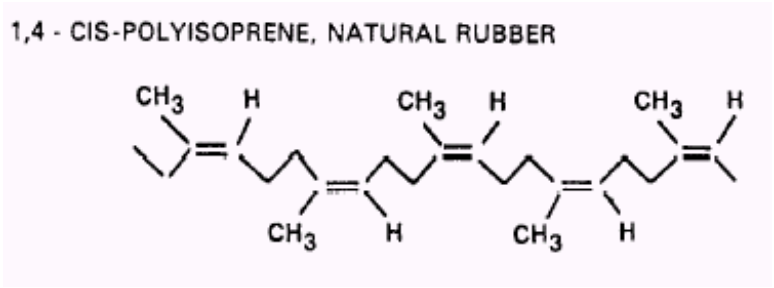

Fig 2.2 Undoped Polyisoprene

Considering the known bond length of the carbon-carbon double bond (~1.4 Angstroms), the dimension of the doped site has been estimated to be a few angstroms. This sub-nanometer confinement leads to such a large nonlinear effect.

2.4.3 Quadratic Electro-Optic Effect

Crystals that have a center of symmetry (isotropic medium) show no linear electro-optic effect. But there is a change in the constants of the index ellipsoid that is related to the second order products of applied electric field components. The induced polarization in the material is quadratically proportional to the applied electric field. This effect is called the quadratic or the Kerr electro-optic effect. This interaction of the

optical radiation with the material subjected to an electric field can be described completely in terms of the impermeability tensor η_{ij} by the relation [5]

$$\overline{E}_i = \sum_j \eta_{ij} \overline{D}_j \qquad 2.39$$

Quantum theory of solids, dictates that the optical dielectric impermeability tensor depends on the distribution of charges in the crystal. When an electric field is applied, redistribution of the bound charges occur and also possibly a slight deformation of the ion lattice causing a change in the optical impermeability tensor. This change in the impermeability tensor can be related to the applied electric field by the following relation

$$\Delta\eta_{ij} = r_{ijk} E_k + s_{ijkl} E_k E_l \qquad 2.40$$

Where, r_{ijk} is the linear electro-optic coefficient as described in section 2.1 and s_{ijkl} is the quadratic electro-optic coefficient. The s_{ijkl} coefficient varies as the square of the applied electric filed therefore it's called the quadratic electro-optic effect which was first discovered by J. Kerr in 1875 in optically isotropic media such as glasses and liquids. Unlike linear electro-optic effect which is observed in anisotropic media, the quadratic electro-optic effect is seen in all media and there are no symmetry restrictions. In noncentrosymmetric media the linear electro-optic effect is more predominant than the quadratic effect. But in centrosymmetric media it's the prominent nonlinearity. When an electric field is applied, the dimensions and orientation of the index ellipsoid change depending on the direction of the applied electric field and also on the symmetry properties of the 6 × 6 matrix elements of the s_{ijkl} coefficient. In an optically isotropic

media such as polymers, the application of electric field makes the media birefrengent which mainly depends on the alignment of the molecules affected by the electric field. The media then behaves as a uniaxial medium where the direction of the applied electric field defines the optical axis. Usually, the z-axis is chosen to be the direction of the applied field. The quadratic electro-optic coefficients for an isotropic crystal are given by

$$\begin{pmatrix} s_{11} & s_{12} & s_{12} & 0 & 0 & 0 \\ s_{12} & s_{11} & s_{12} & 0 & 0 & 0 \\ s_{12} & s_{12} & s_{11} & 0 & 0 & 0 \\ 0 & 0 & 0 & 1/2(s_{11}-s_{12}) & 0 & 0 \\ 0 & 0 & 0 & 0 & 1/2(s_{11}-s_{12}) & 0 \\ 0 & 0 & 0 & 0 & 0 & 1/2(s_{11}-s_{12}) \end{pmatrix} \quad 2.41$$

The index of ellipsoid for such an isotropic medium on the application of E reduces to

$$x^2\left(\frac{1}{n^2}+s_{12}E^2\right)+y^2\left(\frac{1}{n^2}+s_{12}E^2\right)+z^2\left(\frac{1}{n^2}+s_{11}E^2\right)=1 \quad 2.42$$

Where s_{11} and s_{12} are the quadratic electro-optic coefficients and E is the magnitude of the applied electric field. Comparing Eq. 2.42 with Eq. 2.17 we get

$$n_0 = n - \frac{1}{2}n^3 s_{12}E^2 \quad 2.43$$

$$n_e = n - \frac{1}{2}n^3 s_{11}E^2 \quad 2.44$$

The birefringence $n_e - n_o$ is given by

$$n_e - n_0 = \Delta n = \frac{1}{2}n^3(s_{12}-s_{11})E^2 \quad 2.45$$

By using the relationship $s_{44} = \frac{1}{2}(s_{11}-s_{12})$ Eq. 2.45 can be written as

$$\Delta n = -n^3 s_{44} E^2 \qquad 2.46$$

Eq. 2.46 is often written in terms of the Kerr coefficient (K) in m/V^2 as

$$\Delta n = K\lambda E^2 \qquad 2.47$$

where

$$s_{44} = -\frac{K\lambda}{n^3} \qquad 2.48$$

There is a better understanding of the basic requirements for materials with high third order nonlinearities after almost a decade of research and development. π-conjugated organic polymers have emerged as interesting third order nonlinear optical materials which exhibit very large $\chi^{(3)}$ values. Although these polymers offer large optical nonlinearities and ultrafast response time, there are high optical losses. Several applications for of these materials have been proposed and various promising devices have been fabricated.

2.4.4 Two Photon Absorption

When an electron absorbs a single photon and reaches an excited state, the observed phenomenon is linear absorption. But when the electron absorbs two photons almost at the same time to reach an excited state that corresponds to the sum of the energy of the absorbed photons, this phenomenon is called nonlinear absorption or two photon absorption. The atom does not necessarily reach an intermediary state. The excited virtual state so reached does not correspond to any electronic or vibrational energy eigenstate.

The nonlinear optics community has widely accepted the z-scan [31,32,39-43,107] technique as a standard method in determining the nonlinear refractive index and absorption. This is due to the simplicity of the technique and the efficiency. Just by performing some simple mathematical operations on the data sets obtained, the nonlinear refractive index and absorption coefficient can be quite accurately determined.

A closed aperture setup is used when the nonlinear refractive index is to be studied. In this setup, the aperture is placed far from the sample to be studied. In order to determine the nonlinear absorption coefficient, the aperture is placed in the near field or completely removed. The sample is then translated along the z axis such a manner that it travels equidistantly on either sides of the beam waist area. The transmitted light is then studied as a function of the position of the sample. To calculate the range to be traversed, the beam parameters and the sample thickness L are used where, the diffraction length, Z_0, of the beam that is focused using a lens is defined as $\pi w_0^2/\lambda$ for a Gaussian beam where w_0 is the focal spot size (half-width at the $1/e^2$ maximum in the irradiance). When the sample used is thin where, $L \leq Z_0$, the scan range is $\approx \pm 5Z_0$ or more. To get rid of the noise and to factor out laser instability, a reference detector can be used to normalize the observed data. [31][32]. In this setup, also called the open aperture setup, the effect of nonlinear refractive index is latent. Nonlinear absorption is more prominent in the frequency range where the sample absorbs the most.

When the data obtained from the open and closed setups are subjected to simple mathematical division, a curve is obtained that would be very similar to that obtained with a closed aperture Z-scan on a sample with the same Δn but with Δα=0.

Two-photon Absorption: λ = 1.06μm				$2\hbar\omega$ = 2.34 eV			
Material	form[a]	n(λ)	Eg(eV)	$E_p^{(b)}$(eV)	E_b/E_g	$\beta_2^{exp}(\frac{cm}{GW})$	$\beta_2^{theor.}(\frac{cm}{GW})$
ZnTe[c]	Z	2.79[c]	2.26[i]	19.1	0.004[o]	4.5	0.89
CdSe[c]	W	2.56[c]	1.74[j]	21	0.007[i]	18	18.6
CdTe[d]	Z	2.84[c]	1.44[c]	20.7	0.003[o]	22	25.1
CdTe[d]	Zp	2.84[c]	1.44[c]	20.7	0.003[o]	15	25.1
$CdS_{.5}Se_{.5}$[c]	W	2.45[l]	1.93[k]	21	0.010[l]	10	12.1
$CdS_{.25}Se_{.75}$[c]	W	2.51[l]	1.78[k]	21	0.008[l]	15	17.7
GaAs[e]	Z	3.43[i]	1.42[i]	25.7	0.003[o]	23	19.7
Two-photon Absorption:		λ = 0.53μm		$2\hbar\omega$ = 4.68 eV			
Material	form	n(λ)	Eg(eV)	Ep(eV)	E_b/E_g	$\beta_2^{exp}(\frac{cm}{Gw})$	$\beta_2^{theor.}(\frac{cm}{GW})$
ZnS[f]	Zp(c)	2.40[i]	3.66[i]	20.4	0.010[i]	2.0	2.10
ZnS[f]	Zp	2.40[i]	3.66[i]	20.4	0.010[i]	3.5	2.10
ZnSe[g]	Zp	2.70[i]	2.67[i]	24.2	0.008[o]	5.5	4.27
CdS[c]	W	2.60[i]	2.42[c]	21	0.012[i]	5.5	4.87
ZnO[h]	W	2.05[i]	3.20[n]	21	0.020[i]	5.0	4.77

Table III Two Photon absorption of various materials [32]

2.4.5 Other Third Order Materials

In the telecommunications industry, usually, optical fibers are used to transmit signals and are amplified and switched by electronic components. However, we have reached a bottleneck in speed as the electronic switches can go only upto the nanosecond time domain. This has demanded an urgent need for all optical switches where the maximum limit would only be the speed of light. This requires materials with high

optical nonlinearities, so that less power is needed for the switching action. The range of potential material structures is wide because, third order nonlinear effects do not require noncentrosymmetric materials, or intramolecular charge transfers. Classifications of third order nonlinear optical organic and polymeric materials are : 1. Liquids; 2. Molecular solids; 3. Charge-transfer complexes; 4. Conjugated polymers; 5. Nonlinear optical dye-functionalized polymers; 6. Organometallic compounds; 7. Composites; 8. Liquid crystals and 9. Biomaterials. Recent research has shown that organic crystals have some of the largest nonlinear optical susceptibilities ever measured. The drawbacks however are the difficulties in fabrication, poor optical quality resulting in scattering losses and the need for large interaction lengths. But polymers have been promising candidates due to the ease of processiblity, higher optical quality, their ability to be fabricated on planar passive waveguides and their cost effectiveness.

Material	**n_0**	**$\chi^{(3)}$ (esu)**	**$n_2(cm^2/W)$**
Crystals (wavelength - 1.06 microns)			
Al_2O_3	1.8	2.2×10^{-14}	2.9×10^{-16}
CdS	2.34	7.0×10^{-12}	5.1×10^{-14}
GaAs	3.47	$1.0 \times 10\text{-}^{10}$	3.3×10^{-13}
ZnSe	2.7	4.4×10^{-12}	3.0×10^{-14}
Nanoparticles (wavelength – 532nm)			
CdSe in glass	1.5	1.0×10^{-12}	1.8×10^{-14}
Gold in glass	1.5	1.5×10^{-8}	2.6×10^{-8}

Polymers (wavelength – 1.06 microns)			
Polydiacteylene(PTS)		10^{-9}	10^{-11}
Liquids			
Benzene	1.5	6.8×10^{-14}	1.2×10^{-15}
CCl_4	1.45	8×10^{-14}	1.5×10^{-15}
Nitrobenzene	1.56	4.1×10^{-12}	6.7×10^{-14}
Other Materials			
Air	1.003	1.2×10^{-17}	5.0×10^{-19}
Ag		2.0×10^{-11}	
Au		5.4×10^{-11}	

Table IV Third Order Nonlinear Optical Coefficients of Various Materials [7]

2.5 Nano-Optics

When light interacts with matter of nanometer sizes, it results in some interesting optical nonlinearities. The science of this phenomenon is called nano-optics. It has been observed that the nano-optical sites enhance third order nonlinearities that are localized in the close proximity of the nano-optical sites [33]. Better understanding and manipulation of this phenomenon can be vital in areas of high resolution optical microscopy, highly improved data storage, telecommunication, optical computation, holography, optical correlators, phase conjugators and medicine.

2.5.1 Optical Properties of Metal Nanoclusters in Dielectrics

With the objective of manipulating and tuning of these nano-optical properties, studies have been conducted where nano-clusters of gold, silver and copper are embedded in different matrices [97][100][101][102][103]. The nonlinear properties observed are of the third order as these composite materials are centrosymmetric. These metal nanoclusters in glass matrices are prepared using ion implantation and conventional melt and heat treatment methods. Particle sizes down to 10 nm can be achieved with the mean free conduction path being much smaller compared to bulk metals. This results in changing the quantum states of the electrons and the dynamics of their interaction with the applied optical fields. When the wavelength of the interacting light is larger than the nanocluster, it induces polarization of the free charges and it modifies the dielectric constant of the medium. This phenomenon is called as dielectric or classical confinement. For metal nanocluster whose diameter is less than $\lambda/20$ the theories of Mie and of Maxwell-Garnett can be used to calculate the absorption coefficient of the composite in the electric dipole approximation which is as follows,

$$\begin{aligned}\alpha &= \frac{\omega}{n_0 c}\,\mathrm{Im}\left[\chi^{(1)}(\omega)\right] = p\frac{18\pi n_d^3}{\lambda}\frac{\varepsilon_2}{\left(\varepsilon_1 + 2n_d^2\right)^2 + \varepsilon_2^2} \\ &= p\frac{\omega}{n_0 c}\left|f_1(\omega)\right|^2 \varepsilon_2\end{aligned} \qquad 2.50$$

Where, $\varepsilon(\lambda) = \varepsilon_1 + i\varepsilon_2$ is the frequency-dependent dielectric constant of the metal, p is the volume fraction of the metal particles, n_d is the refractive index of the dielectric host, and $\chi^{(1)}$ is the first order optical susceptibility. The quantity $f_1(\omega)$ is the mean-field

enhancement factor. The absorption coefficient has a maximum value at the surface plasmon resonance frequency ω_{sp} where $\varepsilon_1 + 2n_d^2 = 0$. The metal particle size directly dictates the surface plasmon resonance frequency.

2.5.2 Optical Nonlinearities in Semiconductor Nanoparticles

The enhancement of second and third order nonlinearities in semiconductor nanoparticles are mainly due to the quantum confinement whereas, in metals, it is due to the dielectric confinement [34][100]. The large third order optical nonlinearities for silicon nanostructures reported in the range of 10^{-8} - 10^{-9} esu shows tremendous potential in optoelectronic devices. The optical transitions occurring in metals are usually intraband and in semiconductors, it is interband. In silicon nanoclusters that were prepared by ion implantation, the observed nonlinear optical effects were directly proportional to the size of the nanoclusters. The internal electric field $\overline{E}_i$ on a nanocluster is because of the surrounding clusters' fields and the resonating characteristics of the cluster itself. The internal electric field can be written as $E_i = Cp/\varepsilon$ where C is the coupling between the clusters. The total expression for polarization can be written as

$$\overline{P} = N\alpha^{(1)}\frac{\overline{E}}{1-\alpha^{(1)}C} + 3N\alpha^{(1)}\alpha^{(3)}\left|\overline{E}\right|^2\frac{\overline{E}}{\left(1-\alpha^{(1)}C\right)^4} \qquad 2.55$$

Where $\alpha^{(1)}$ and $\alpha^{(3)}$ are linear and third order polarizabilties respectively. N is average number of dipoles in the material per unit volume. When the dipoles are excited in the proximity of electronic resonance, enhancement of linear polarizability coefficient

is observed. In a condition where clusters are in close proximity, coupling among the clusters give rise to a very large nonlinear coefficient [102][103]. Since the contributing factor in the semiconductor quantum dots in the quantum confinement effect, the exciton effective Bohr radius a_B^* decreases and the third order nonlinear susceptibility depends on a_B^* as the inverse fourth power of a_B^* $\left(\chi^{(3)} \sim 1/\left(a_B^*\right)^4\right)$. This implies that if a_B^* reduced, large enhancement in $\chi^{(3)}$ can be expected.

2.5.3 Quantum Dot Analogy of Doped Nonconjugated Conductive Polymers

When one or more free electrons are confined within a space typically ranging from a few nanometers to microns, the system is called as a quantum dot. The number of confined electrons, which can be accurately manipulated, dictates the size and shape of the q-dot. The behavior of quantum dots is analogous to that of atoms. Just as there are energy levels in atoms, q-dots also posses energy levels which exist due to the confinement of the electrons

The Nonconjugated polymer cis-1,4-polyisoprene exhibits the same properties of that of q-dots when it is doped with iodine. Since the bond lengths of the polymer are known, it can be deduced that the charge transfer sites have dimensions less than 1 nm. The optical absorption spectra of polyisoprene obtained at different doping concentrations when compared with nanometer-sized CdSe [96], a semiconductor, show that about 1.2 nm size particles of CdSe exhibit same optical properties as that of doped polyisoprene (wavelength ~ 300-550nm). In the case of Au nanoparticles [120], it has been reported that the third order nonlinear susceptibilities are largely dependent on the

particle size and the distance of separation from the neighboring dielectrics. This is consistent with the dimension of the charge transfer site in the polymer which is less than 1nm obtained from the bond length calculation.

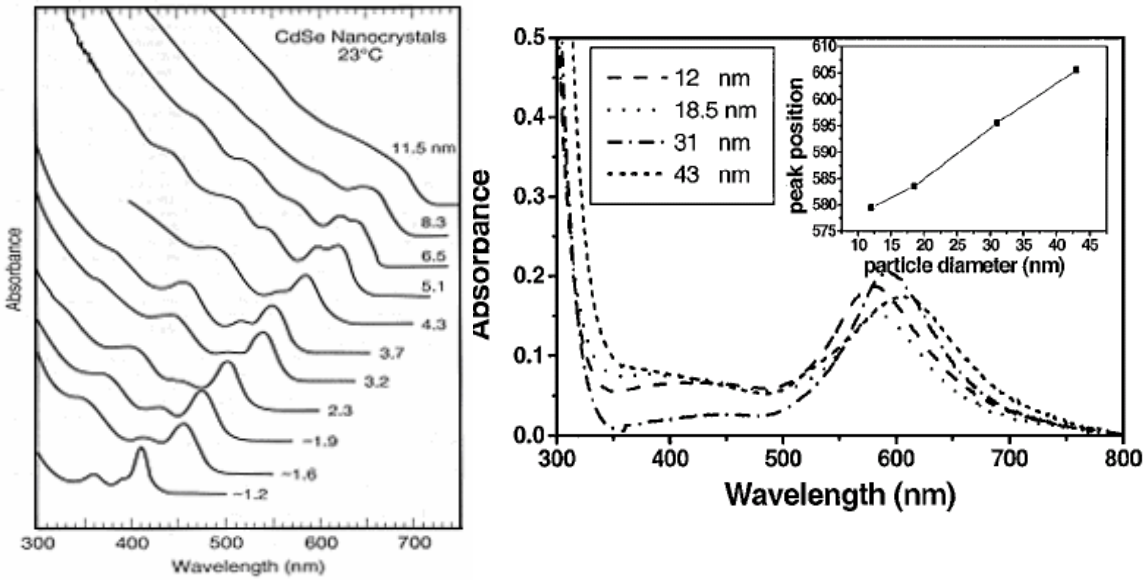

Fig. 2.2 Optical absorption spectra of a) CdSe nanoparticles for different sizes [96] and b) Gold nanoparticles[120].

When a comparative study [80][84] is done between the conduction in indium metal and polyisoprene, it is apparent that the maximum conductivity attained by polyisoprene (0.1 S/cm) corresponds to the conductivity of nanometer size indium particles (~10 nm). The electrical conductivity is also found to be directly proportional to the particle size. The third order nonlinearity can be significantly enhanced in the order of the fourth power by operating at or close to the plasmon resonance frequencies.

In low doping conditions where the average distance between the dopants substantial, the charged sites are well confined. At heavier doping conditions, the distance between the dopants reduce hence the confinement effect is also largely reduced.

CHAPTER 3

OBJECTIVES

The goal and scope of this research work is to study the off-resonant nonlinear optical properties of a single crystal film of an organic material, 4'-dimethylamino-N-methyl-4-stilbazolium tosylate (DAST) and specific nonconjugated conductive polymers; 1, 4 cis-polyisoprene (Natural Rubber), poly(β-pinene) and styrene-butadiene-rubber (SBR). These nonconjugated polymers possessing isolated double bonds become electronically conductive upon doping with electron acceptors due to the formation of charge transfer sites. These sites being in the nanoscale domain enhances the nonlinearities of these doped polymers.

Single crystal film of DAST has the largest known electro-optic coefficient. This is mainly attributed to the optimum molecular orientations in the crystal. The electronic origin of the effect allows the material to operate at high speeds and at longer wavelengths like 1.55 micrometers. The specific research objectives employing DAST are:-

1. To prepare good quality single crystal films of large areas using the modified shear method and to prepare the samples for the study by depositing electrodes.

2. To demonstrate a single pass thin film modulator using the field induced birefringence method by applying an electric field along the dipole axis of a single crystal film of DAST, at a longer wavelength.
3. To measure the electro-optic coefficient of DAST film at 1.55 microns.
4. To calculate the real part of the electro-optic coefficients at these wavelengths.
5. To demonstrate good electro-optic modulation at high speed (GHz).
6. To design, fabricate and demonstrate working devices based on the single pass field induced birefringence method employing DAST.

The specific research objectives concerning the nonconjugated conductive polymers are:-

1. To study the optical absorption, photoluminescence and FTIR characteristics of specific nonconjugated conductive polymers.
2. To study the quadratic electro-optic effect in a specific nonconjugated conductive polymer.
3. To determine the nonlinear refractive index and the two-photon absorption coefficients of a specific nonconjugated conductive polymer.
4. To correlate the nonlinear optical characteristics with the electronic structures and analyze the reason for the exceptionally large nonlinearities of these polymers.

CHAPTER 4

ELECTRO-OPTIC STUDIES OF THE ORGANIC MOLECULAR SALT - DAST

We are stepping into an era where the technological world powered and controlled by photons is becoming more of a reality. Electro-optic materials and devices play a significant role in photonics technology. Just as the transistor can be said to be the building blocks of electronics, an optical modulator would be the optical equivalent. An optical modulator can be defined as a device used to modify any characteristic of an optical signal (light wave) which could be the phase or the amplitude by the application of an electric field. It can also be used to steer or reroute the light beam. There are two types of light modulation namely, direct or external. When the driving voltage of the light source is varied, direct modulation is achieved. In the case of external modulation, the intensity of light can be modulated by changing (i) the optical absorption (electro-absorption modulator) of the material interacting with the light beam or (ii) the refractive index (electro-optic modulator) where the phase is modulated. Reasonably high power signals could be generated by direct modulation. However, the drawbacks are that such modulators are affected by 'chirp' which is essentially a moment of laser instability due to the change in center wavelength. This could occur due to the changes in the refractive index of the active crystal induced either by the flash lamp or the voltage changes. Also

the lifetime of the laser is significantly due to the frequent changes in voltage. Initially telecommunication did not demand wider bandwith and higher frequencies making direct modulation feasible. However due to the increased transmission rates of the telecommunication industry, direct modulation is no longer feasible. External modulation is more apt due to the fact that the laser is operating continuously and the output light is modulated. The most commonly and successfully used modulators employ inorganic materials like $LiNbO_3$ [53]. The downside to these inorganic materials is the inability to go to speeds over 10 GHz where they become sluggish due to their high dielectric constants. This has led to the advent of organic crystals and polymers whose very large second order nonlinear susceptibility $\chi^{(2)}$ have a purely electronic origin.

4.1 Characteristics and Preparation of Single Crystal Films of DAST

Meredith studied several organic chromophores of the form $(CH_3)_2NC_6H_4CH{=}CHC_5H_4N(CH_3)^+X^-$ and found that they posses large molecular hyperpolarizabilities β. Nakanishi et al. and Marder et al. following suit researched further and reported that by varying the counterions in the stilbazolium salts, crystalline materials with very large macroscopic optical nonlinearities could be engineered. Many stilbazolium salts have been examined until now and the organic molecular salt, 4-dimethylamino-*N*-methyl-4-stilbazolium tosylate (DAST) has shown the highest potential for second harmonic generation.

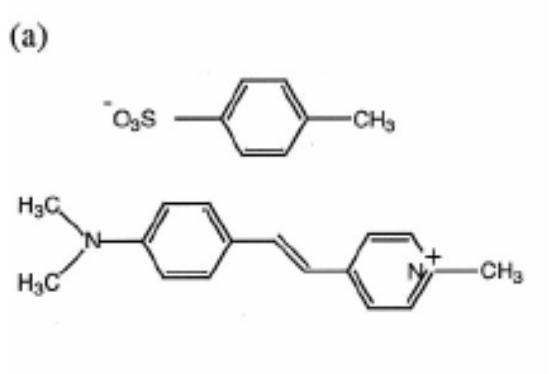

Fig. 4.1 a) Molecular structure of DAST [56]

In DAST, the cationic layers of stilbazolium chromophores are interlaced with p-toluenesulfonate anion layers forming a noncentrosymmetric structure [55]. Fig. 4.1 (a) shows the molecular structure of DAST. Fig. 4.1 (b) shows the p-toluenesulfonate anions stacked in a plane almost perpendicular to the molecular plane of the cationic chromophore. In DAST the stilbazolium chromophores are aligned at an angle of less than 20° with respect to the dipole axis *a*.

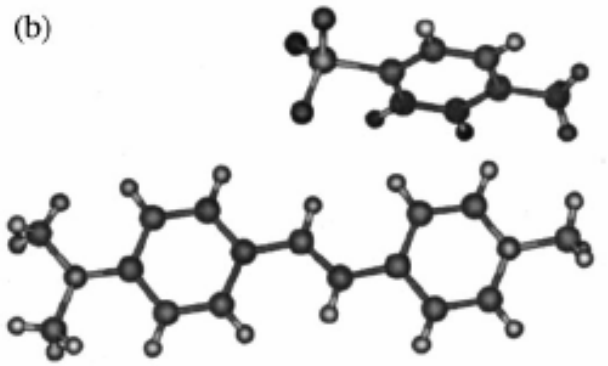

Fig. 4.1 b) The molecules are shown as they are organized in the crystal lattice [56]

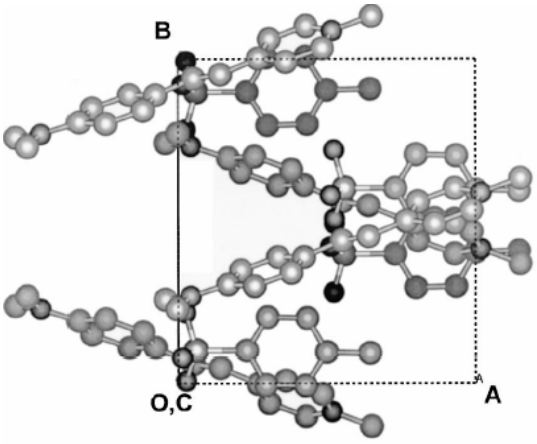

Fig. 4.2 Projection of two unit cells of the DAST crystal along the crystallographic axis c. The chromophores are stacked along the c axis and make an angle of 20° with respect to the polar axis a [57].

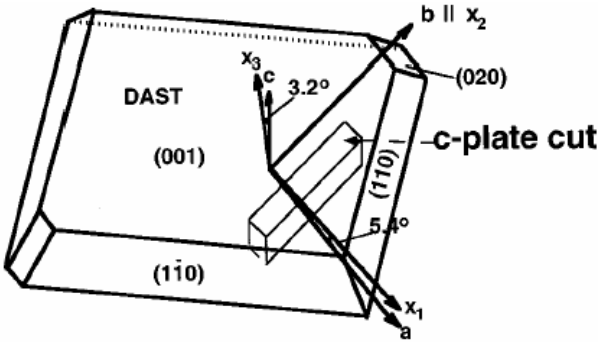

Fig. 4.3 Directions of the dielectric axes and crystallographic axes on a c plane cut DAST crystal [58].

In Fig. 4.2, the orientation of the stilbazolium chromophores with respect to the polar a axis can be observed. DAST which is a positive biaxial crystal, comes under the monoclinic space group Cc (point group m, Z = 4). The optical indicatrix x_2 is parallel to b and x_1 and x_3 (as well as a and c) are in the plane perpendicular to x_2. The angle contained within a and x_1 is 5.4°, and that between c and x_3 is 3.2°. as shown in Fig. 4.3

the dielectric axis makes an angle with the crystallographic axis on a ‘c’ cut plane crystal of DAST [56-58]. DAST crystals are mechanically and environmentally stable with a melting point of 256˚C. They are ease to process and crystals can be grown by various methods with very good optical quality. The dielectric constant of DAST is low and typical of other organic crystals, DAST has high nonlinear optical properties that originate from the extended π-electron system, hence has a very short response time. This makes DAST more suitable for high-speed switching and detection of THz-wave radiation than its inorganic counterpart $LiNbO_3$ [27]. DAST crystals are great candidates for electro-optics because the $n_1 = 2.8$ (633nm) is much larger than $n_2 = 1.8$ and $n_3 = 1.68$ [59]. DAST crystals have been employed in electro-optic modulators (EO), gratings, frequency doublers, optic parametric oscillators in the near infrared, electro-optic sampling systems, and THz pulse generation [55-61].

The active materials used in the commercially available electro-optic modulators require significantly large interaction length to produce sufficient modulation. This is due to the low electro-optic coefficients. And also, there are insertion losses and propagation losses. But in devices employing thin film crystals of DAST, the beam propagates perpendicular to the surface of the film, greatly reducing the losses. The required interaction length is also much less and can produce sufficient modulation with relatively lower electric fields.

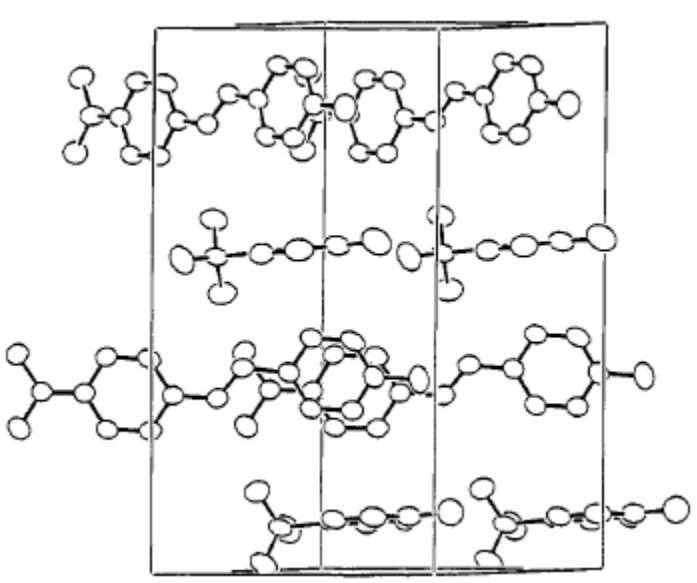

Fig. 4.4 Crystal Structure of DAST viewed approximately along the c axis.

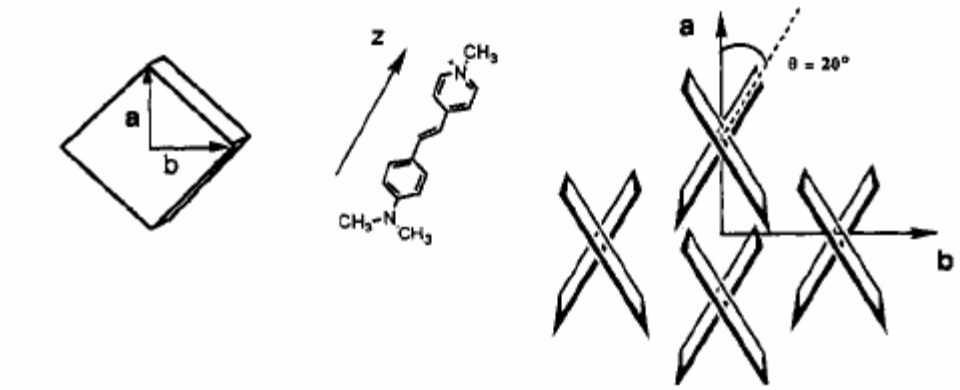

Fig. 4.5 Deviation between the crystal axis a and molecular axis z in DAST crystal

In bulk DAST crystals that are grown, surface imperfections are unavoidable. This can cause scattering losses and also some degradation of the phase information. It can also give rise to destructive interference that can make it ineffective. Therefore not

surprisingly, the electro-optic coefficients for bulk crystals of DAST are low [55,59]. The highest reported electro-optic coefficient for DAST bulk crystal was r_{11}~100pm/V at 750nm with an applied frequency of 1 KHz [66]. Electro-optic coefficient of single crystal thin film of DAST measured at high speed (1.5 GHz) was r_{11}=445pm/V at 750nm [67]. It is apparent that the electro-optic coefficient of single crystal thin film of DAST is significantly higher than bulk crystals. Single crystals thin films of DAST are also more environmentally stable.

There have been many attempts at growing optically good DAST thin film single crystals [56, 57, 69]. Thakur et. al. for the first time successfully grew very high quality thin film single crystals of DAST by using a technique called "Modified shear method" [72]. First a super-saturated solution of DAST in methanol is made. This solution is then introduced between two quartz substrates that are hydrophilic by nature. While applying a constant pressure, the substrates are moved with respect to each other. With the aid of the polar forces between the substrate and the DAST molecules, they align themselves in a direction parallel to the substrate surface. As the solution is evaporated in a controlled environment, the mobility of the molecules reduces resulting in the crystallization of the molecules [60]. These thin films so formed have excellent optical quality as they mimic the surface of the substrate and their dipole axis is parallel to the surface of the film. Areas up to 30-40mm^2 and thickness varying from 1 to 18 microns were obtained. X-ray diffraction of the films showed the single crystallinity with a [001] orientation [66].

Fig. 4.6 Optical micrograph (in transmission) of a single crystal thin film of DAST.

Organic materials, as expected, show large absorption at the surface plasmon resonance wavelength range. The optical absorption spectrum [64] for single crystal thin film of DAST is shown in Figure 4.7. The optical absorption spectroscopy at resonant and non-resonant wavelengths for different angles showed strong dichorism at the resonant wavelength. The film absorbed the most when light is polarized along the dipole axis and is the least when polarized perpendicular to the dipole axis. The absorption peak was at ~550nm.

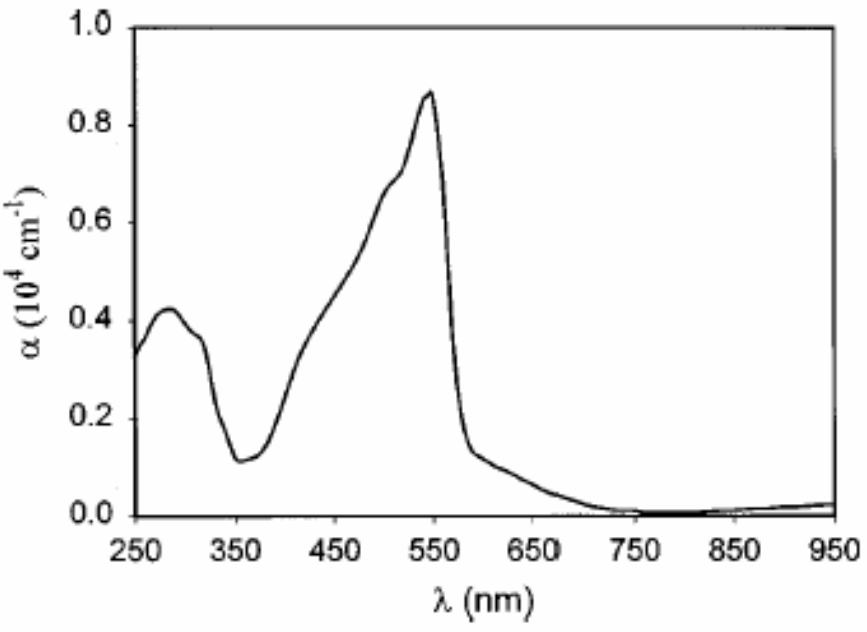

Fig. 4.7 Optical absorption spectrum of single crystal thin film of DAST [64].

4.2 Electro-Optic Studies on DAST

Different magnitudes of the electro-optic coefficients of DAST have been reported. This is due to the inability in factoring in the surface quality of the crystal while determining the electro-optic coefficients. Foreseeing the tremendous potential applications for such single crystal thin films, the electro-optic properties were studied. A single-pass thin-film electro-optic modulator with a large intensity modulation (20%) at 720nm for a low AC field (1 V/μm, at 4 kHz) using a 3 μm thick single crystal film of DAST (red phase) has been demonstrated. Subsequently, 80% modulation depth was observed in a 4 μm thick film for a field of 4 V/μm at 750nm. Such large modulation depths despite an interaction length of a few microns were observed because of the exceptionally large electro-optic coefficients of DAST and excellent optical quality of the

films. Modulation due to electroabsorption and the near-resonant electro-optic measurements in a single-crystal film of DAST have also been recently reported. At a wavelength near resonance the change in the real part of the refractive index can be related to the real part of the electro-optic coefficient and the change in the imaginary part of the refractive index, change in the absorption coefficient, can be related to the imaginary part of the electro-optic coefficient.

4.3 Off-Resonant Electro-Optic Studies on DAST at 1.55 Microns

4.3.1 Sample Preparation and Experimental Setup

Single crystal films of DAST with excellent optical quality were prepared using the modified shear method. Once the solution completely evaporates, the two substrates are separated and are cut so as to suit the device needs. Gold and aluminum electrodes are then deposited by Ladd Vacuum evaporation sputter, in such a way that the applied electric field is parallel to the dipole axis of DAST single crystal. The electrodes are separated by a narrow gap so that a large electric field can be obtained for a relatively small voltage. An optical micrograph of DAST sample with the gold electrodes deposited is shown in Figure 4.8. The gap between the electrodes varied from 50-100μm. Conducting epoxy was used to attach copper tape to the gold coating. The electric field is then applied across the sample though the copper tapes.

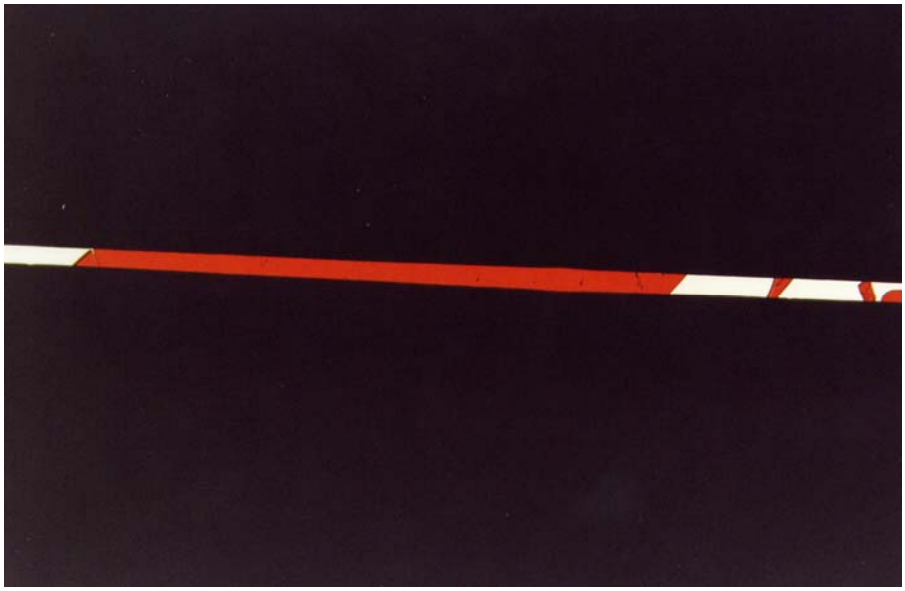

Fig. 4.8 Optical micrograph of a single crystal thin film of DAST with gold electrodes deposited on the surface.

The electro-optic modulation through DAST single crystal thin film was obtained using field induced birefringence measurements in the cross polarized geometry as shown in Figure 4.9. A fiber coupled semiconductor laser diode (1.55 microns) purchased from B&W Tek, was used as the source of optical beam for electro-optic measurements. The optical beam passes through a polarizer kept at 45° to the dipole axis of DAST and then was focused on the sample through the slit. The light passing through the sample then is compensated for phase due to the inherent birefringence of DAST using a Babinet-Soleil compensator and also to fix a bias point. Then the light passes through an analyzer, which was kept cross-polarized with respect to the polarizer. Finally, the light from the analyzer is focused on a photodiode. A 4 KHz AC field was applied along the dipole axis of the crystal and the output from the photodiode is analyzed using a Lock-in-Amplifier, and the

applied frequency is used as the reference. A mechanical chopper is used to chop the optical beam at fundamental frequency (4 KHz) and is sampled in order to obtain the DC component of the optical beam.

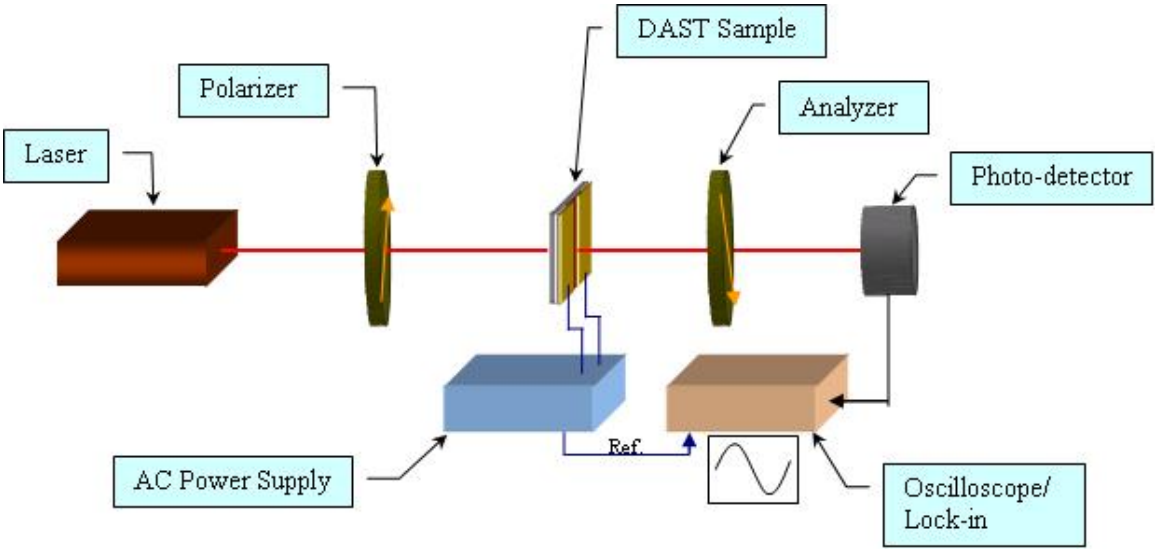

Fig. 4.9 Experimental setup used for field induced birefringence measurement of Electro-optic modulation in Single crystal thin film of DAST

4.3.2 Field Induced Birefringence Measurements

The schematic of the sample used is shown in Figure 4.10. The total optical intensity that is available at the photo diode is measured and the magnitude of the modulation is also observed and is then used to calculate the Electro-optic coefficient of DAST at λ = 1550nm.

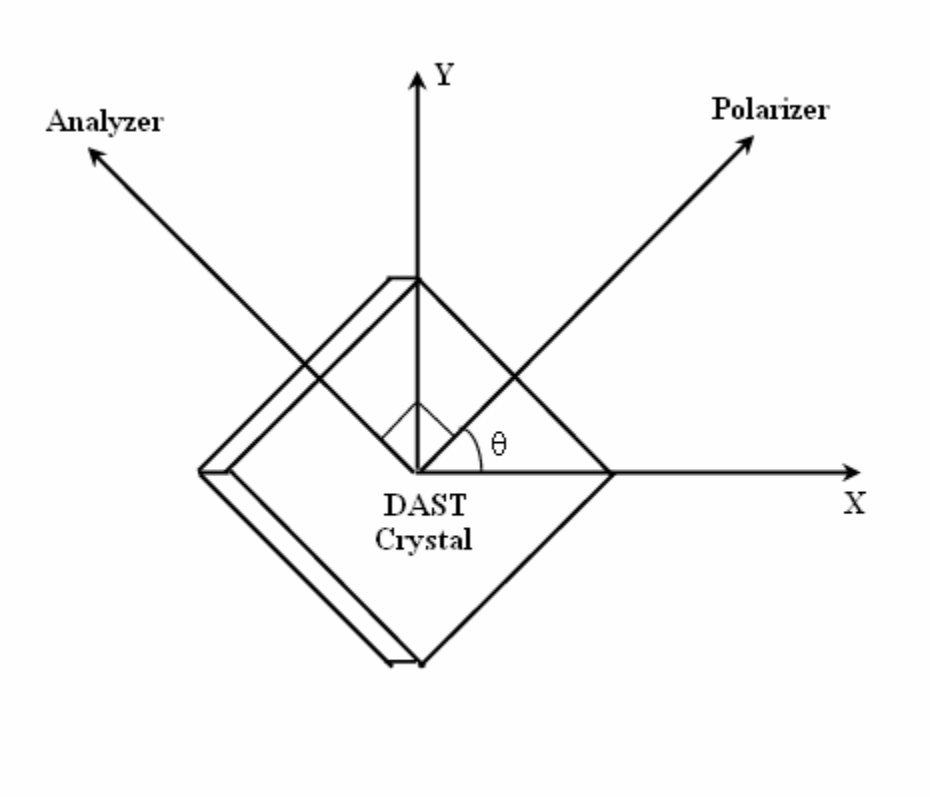

Fig. 4.10 Optical configuration showing angular position of the polarizer and analyzer with respect to the crystal axis.

It can be shown that percentage modulation

$$\frac{\Delta T}{T} = \sin\delta \tag{4.2}$$

Where, δ is the phase change due to the electro-optic effect.

Hence change in refractive index is given by

$$\Delta n = -\frac{1}{2}\left(n_x^3 r_{11} - n_y^3 r_{21}\right)\overline{E} \tag{4.3}$$

The phase retardation caused due to the change in refractive index is given by

$$\delta = \frac{2\pi}{\lambda} \cdot \Delta n \cdot t \tag{4.4}$$

Substituting Eq. (4.4) in Eq. (4.3) we get

$$\delta = -\frac{\pi}{\lambda}\left(n_x^3 r_{11} - n_y^3 r_{21}\right) \cdot \overline{E} \cdot t$$
$$\overline{E} = \frac{V_m}{l} \tag{4.5}$$

Where, λ is the wavelength of the laser beam, V_m is the peak to peak amplitude of the applied ac field, l is the separation between the electrodes deposited on the sample, t is the thickness of the sample, n_x and n_y are the refractive indices of DAST along x and y direction respectively.

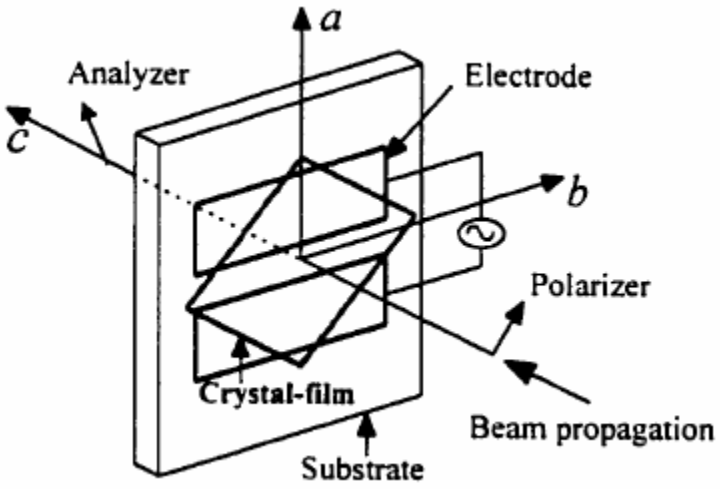

Fig. 4.11 Device configuration of the field induced birefringence setup in the cross-polarized geometry to measure electro-optic modulation in single crystals thin film of DAST.

In DAST single crystal films, the electro-optic coefficient, $r_{21} \cong r_{11}/3$. From the modulation depth observed, the real part of the electro-optic coefficient r_{11} can be calculated. The Electro-optic coefficient of DAST single crystal thin film at 1.55 microns was calculated to be about 200pm/V. Figure 4.11 shows the device configuration of the single-pass electro-optic modulator. In this scheme, the light propagates perpendicular to the film surface and the electric field applied along the dipole axis. Figure 4.12 shows the oscilloscope trace of the modulation of light using the single-pass electro-optic modulator for an applied ac field of 1V/μm at 4KHz**.**

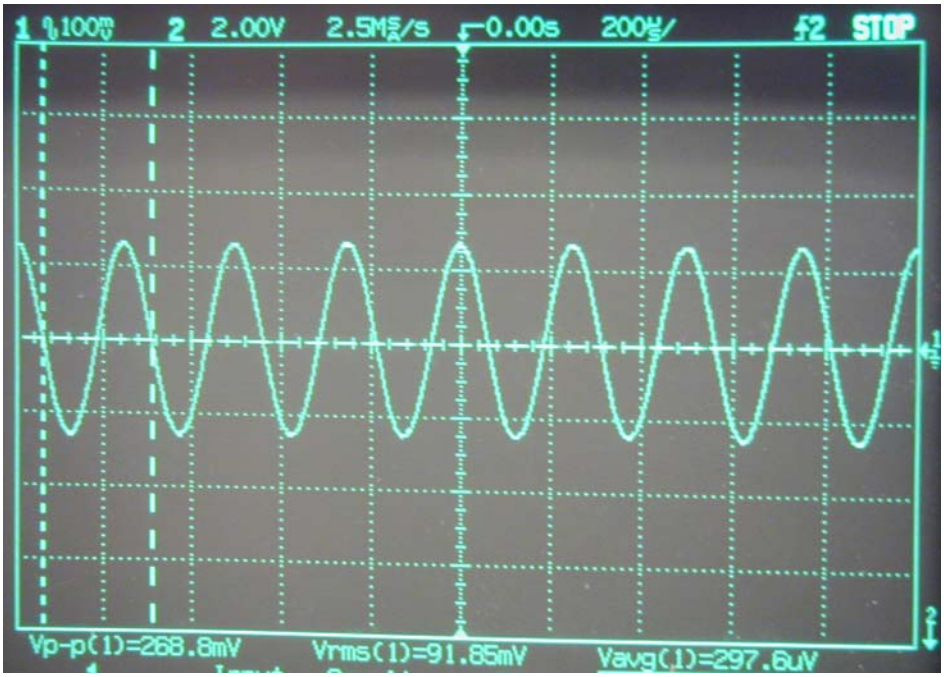

Fig. 4.12 Oscilloscope trace of modulated light in a single pass thin film electro-optic modulator based on DAST at λ=1.55 microns.

4.4 Electro-Optic Modulation at 1.5 Ghz Using a Single Crystal Film of DAST

As stated earlier, DAST single crystal thin films have a low dielectric constant. Hence they can effectively be used for high speed modulation and also for high speed electric field sensing.

To perform the high speed measurement, the DAST sample was prepared using the modified shear method discussed earlier. The electrode gap on the crystal was 15 microns. The sample was completely enclosed in a half inch thick aluminum casing to prevent any radiation that could result due to the open ended electrodes which could be easily picked up by the equipment used for analyzing the modulation of the light beam. The laser source used in this setup was a Ti:sapphire laser at wavelengths ranging from 730-860 nm. The experimental setup used was the same as that used for the linear direct electro-optic modulation. An RF field is applied across the sample through the gold electrodes using a HP signal generator ranging up to 2.5 GHz. One of the electrodes is connected to the aluminum casing and the other is connected to a 50 Ohms impedance matched cable to prevent the RF signal from bouncing back. The modulated signal is observed using a spectrum analyzer using a high speed photodiode.

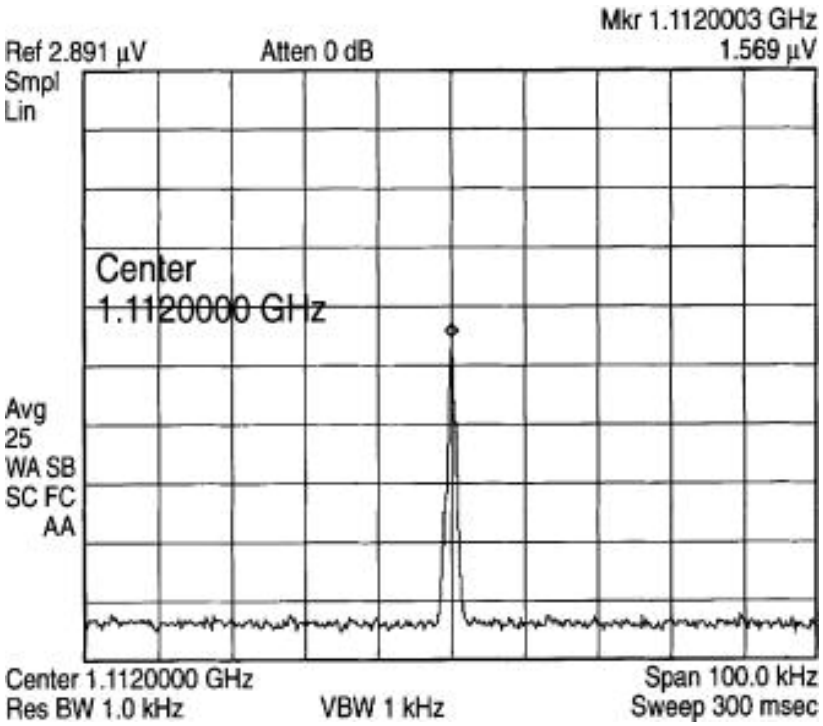

Fig. 4.13 Modulation signal recorded using a spectrum analyzer at 1.1 GHz [67].

Figure 4.13 shows a spectrum analyzer trace of a 1.11 GHZ modulated signal. Measurements were continued up to 1.5 GHz. A modulation depth of ~1% was observed [67] for a field of ~0.06 V/µm and a film thickness of 3 µm. This is extremely large modulation depth considering exceptionally low field that is applied. The modulation depth can be further enhanced by increasing the film thickness and decreasing the electrode gap.

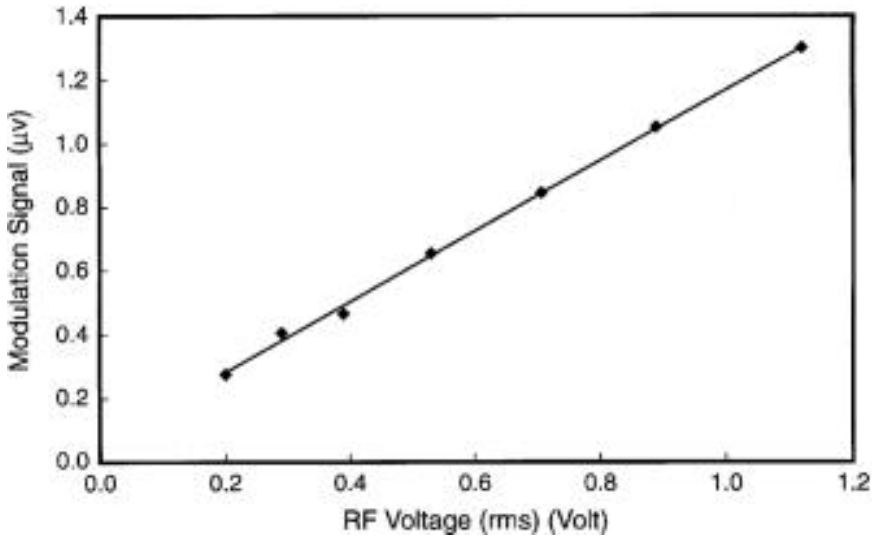

Fig. 4.14 Modulation as a function of driving voltage showing linearity of response [67].

When the magnitude of the RF voltage was increased, the modulation depth observed also increased. Figure 4.14 shows that the modulation signal is directly proportional to the applied field characteristic of direct linear electro-optic modulation. Since the throughput of such a device is substantially larger than that of waveguide devices, the effective modulation depth relative to the input power is comparable to that of waveguide devices. For example, in devices that are based on waveguides, there losses due to insertion of the laser beam. There are also losses throughout the length of the waveguide due to the absorption of the active material. The total losses are usually in the order of about 6 dB. So the effective throughput is about 25%. Hence achieving a 100% modulation depth in a waveguide device is equivalent to about 25% modulation relative to the input power. In the single pass device configuration considered using single-crystal film of DAST, a 25% modulation depth should be straightforward to produce at a low voltage and at a high frequency by increasing the film thickness and reducing the

electrode gap. As stated earlier, the observed signal-to-noise ratio (Fig. 4.13) is about as high as that of a waveguide device even though the interaction length is only a few microns and the applied voltage is 1 V. This is probably because of highly simplified propagation geometry in this configuration compared to that in a waveguide. The devices based on these films have much greater design flexibility and versatility. Such flexibility can be comparable to liquid crystal devices with the additional advantage of orders of magnitude higher speed than liquid crystals. As stated earlier, these can operate in transmission and reflection, can be integrated with optical fibers or in free-space interconnects, and also in this configuration a large number of devices on one film may operate in parallel thus substantially enhancing the speed.

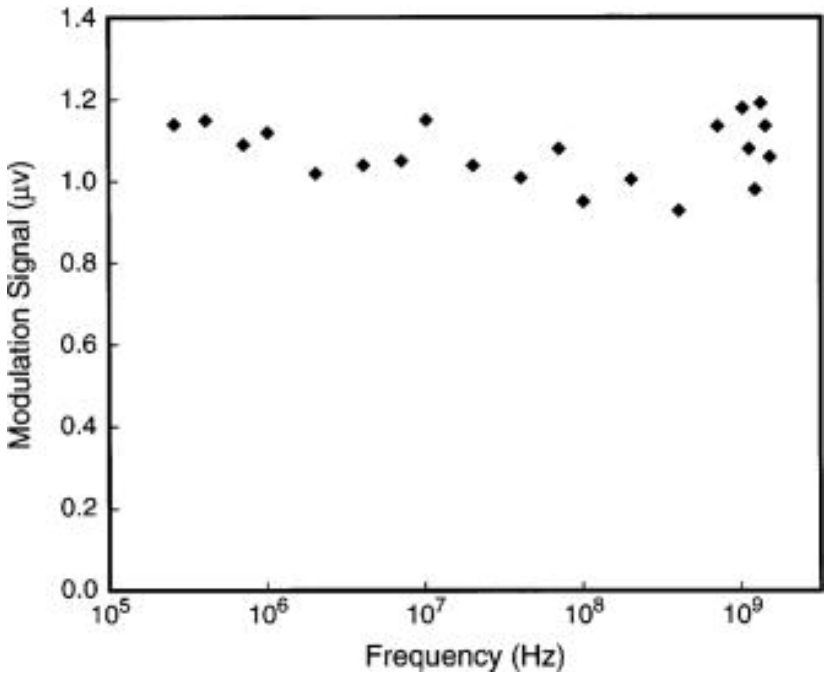

Fig. 4.15 Modulation as a function of frequency (0.25 – 1.5 GHz) [67].

Modulation depth was observed over a frequency range up to 1.5 GHz. The modulation depth remained almost constant over the entire frequency range (Fig. 4.15) [67]. This indicates that even at higher frequencies, one can expect to observe the same modulation depth. This is attributed to the electronic origin of the electro-optic effect and the low dielectric constant. This indicates that DAST single crystals have huge potentials in the telecommunication industry where, more bandwidth and higher speeds are the imminent needs. These results show a high signal-to-noise ratio, comparable to that of waveguide based electro-optic modulators.

4.5 Electro-Optic Devices Based on Single-Pass Field Induced Birefrengence Method Employing DAST

The early types of electro-optic modulators used bulk crystals as the active media. However, after the development of optical fibers, the optical losses were reduced drastically. This also has led to a surge in the evolution of fiber optical telecommunication as higher bandwidths with practically no cross talk were made possible. But along with this development came the need to process signals at high speed. The answer to this was waveguide based electro-optic modulators. Although they have been constantly improved upon, they are still stymied by two major factors which are the non-practicality of producing high density devices and also the high optical losses due to insertion and the absorption of the active material. These limitations are however overcome by using the single pass field induced birefringence method employing a single

crystal film of DAST. In this case, the input beam passes through a polarizer oriented at an angle (usually 45 degrees) with respect to the principal axes x and y. the electric field changes the refractive index of the crystal in the x or y direction which in turn changes the polarization of the light beam. After the beam passes through the output polarizer, which in essence acts as an analyzer, the intensity of the light beam will vary according to the frequency of the applied electric field.

In this section of the dissertation, two types of electro-optic modulators based on DAST thin film single crystals are discussed.

4.5.1 Pockels Cell Using DAST Single-Crystal Film

A Pockels cell is device which is capable of modulating the phase of the intensity of the light passing through an electro-optical material which is subjected to an electric field. This is due to the Pockels effect.

The Pockels cell based on DAST is based on the single pass field induced birefringence method. The schematic of the device is as shown in the figure 4.16. The active electro-optic material used in this particular Pockels cell is a 4 micron thick single crystal film of DAST on which aluminum electrodes are deposited with a gap of about 70 microns. The sample is then coated with a micron thick layer of polystyrene which acts as a dielectric coating offering hermetic protection to the DAST sample and also prevents the arcing of current due to air break down hence enabling high voltages to be applied across the sample.

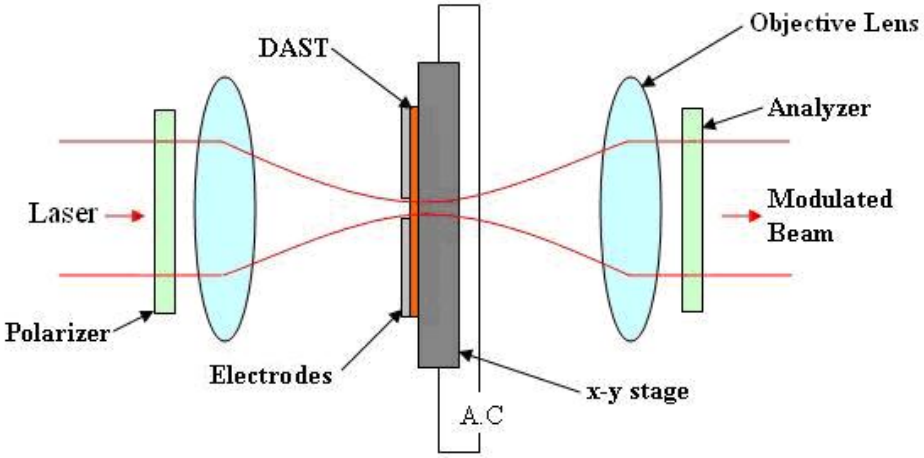

Fig. 4.16 Setup Configuration for a typical pockels cell.

The components of the prototype Pockels cell device are enclosed in a casing. The lower and the upper panels of the casing are made of aluminum and the side panels are made of plexiglas. The components integrated in the device are a polarizer, analyzer and two 10x lenses purchased from Newport. At the center is an x-y stage on which the DAST single crystal film sample with the electrodes is mounted on. The voltage is applied onto the electrodes by means of wires with gator clip terminations. All these optical components are fastened onto the lower aluminum panel by means of screws. A He-Ne laser was used as the light source and the frequency of the field applied was 4 KHz. The modulated signal is collected using a photodetector which is studied using either an oscilloscope or a lock-in amplifier. A reference signal from the voltage driver is fed to the oscilloscope/lock-in to filter out the noise. The modulation observed is directly proportional to the magnitude of the voltage applied. Figure 4.17 is an oscilloscope trace showing a modulation of about 56 percent for an applied field of about 125 volts.

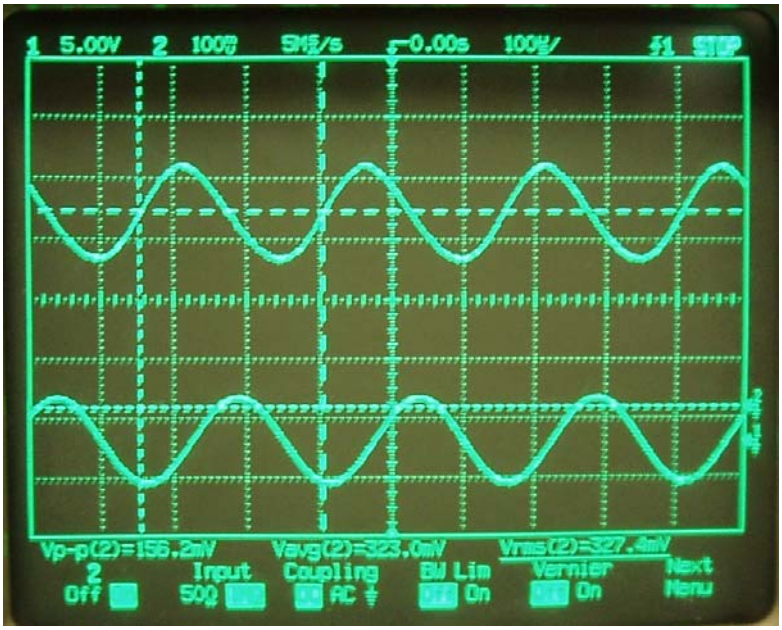

Fig. 4.17 Oscilloscope trace of the modulation observed using the Pockels cell.

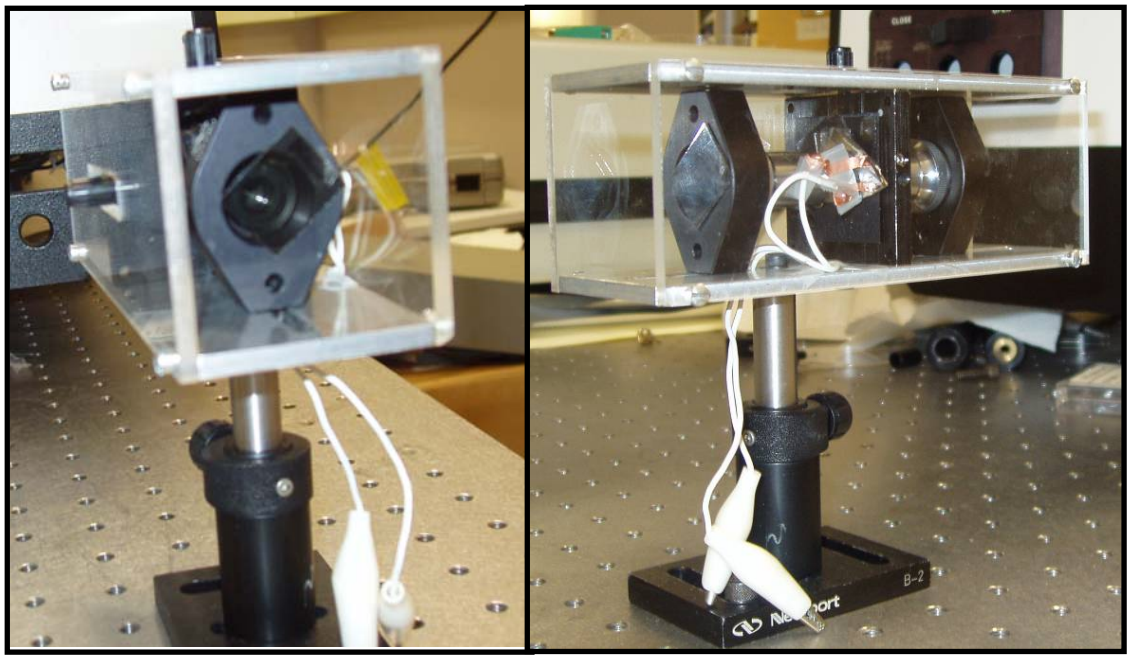

Fig. 4.18 Photograph of the Pockels cell prototype based on DAST

The design of this Pockels cell was improved upon and a compact device was fabricated and demonstrated successfully. The AutoCAD drawings are included in the Appendix.

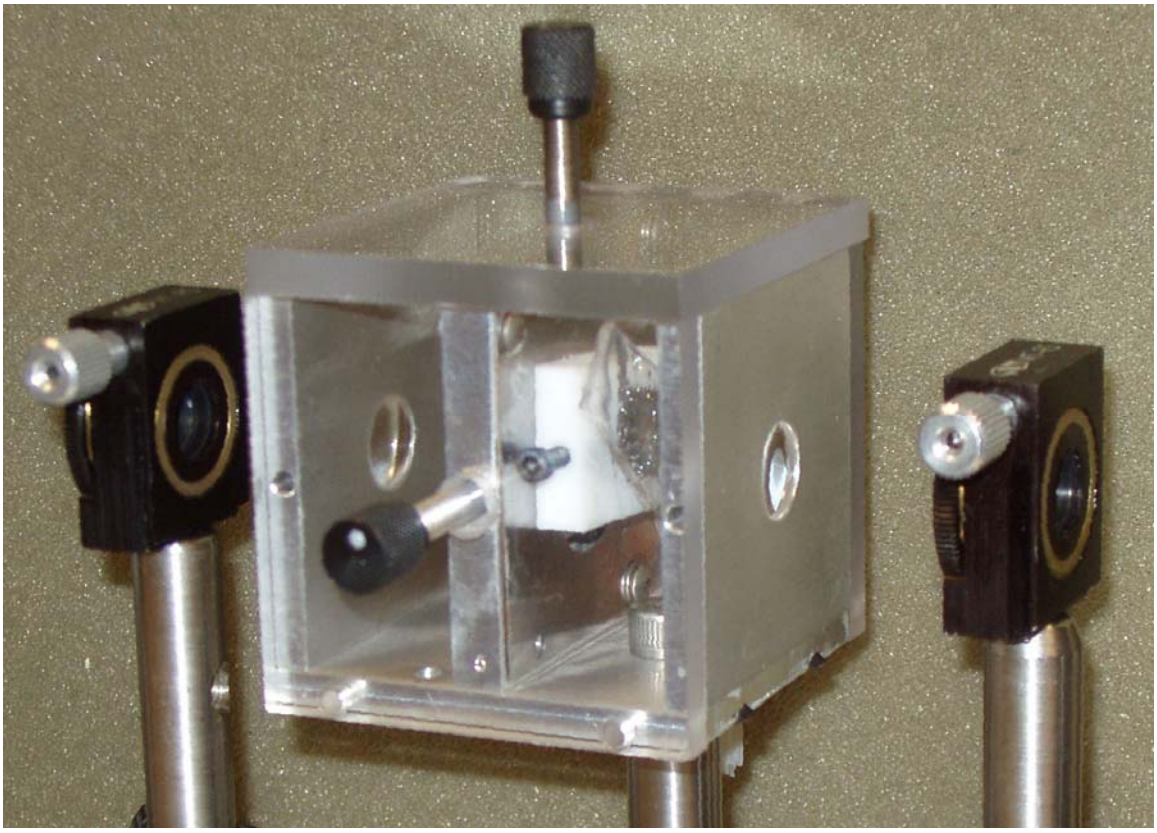

Fig. 4.19 Photograph of the revised Pockels cell based on the final design.

This prototype Pockels cell can be used as a teaching tool which could benefit graduate and undergraduate students in learning about linear direct electro-optic modulation.

4.5.2 Fiber Coupled Electro-Optic Device

The field of nonlinear optics involving the study of the optical properties of materials interacting with light, has attracted intense research interest not for the purpose of exploring new frontiers but also due to the exciting and potential applications in technology. Light modulators find application as optical gates, signal and image

processing, q-switching and modulators. Optical modulation is achieved by inducing a phase shift in the light beam by applying an electric or an optical beam to the medium that it propagates through. In this section a fiber coupled electro-optic modulator based on the single pass birefringence method is discussed.

In this electro-optic modulator, light beam of a He-Ne laser is coupled into a multimode fiber of core diameter of 10 microns with a coupling ratio of about 70%. At the end connector of the fiber, a 2 micron diameter ball lens is mounted using a silicone sleeve in such a way that the light exiting from the fiber end connector is focused at a distance of 5mm in front of the ball lens. The end connector is then connected to a specially manufactured micro stage which allows two degrees of freedom along the x and y axis with a resolution of a few microns. This stage is then immediately followed by a polarizer sheet which is mounted on the x-y stage. A single crystal film of DAST with aluminum electrodes with polystyrene dielectric coating is then sandwiched between two such stages and the whole device is held together by two screws in such a way that the polarizer is at an angle of 45 degrees to the dipole axis of the DAST sample and the analyzer is at an angle of 90 degrees to the polarizer.

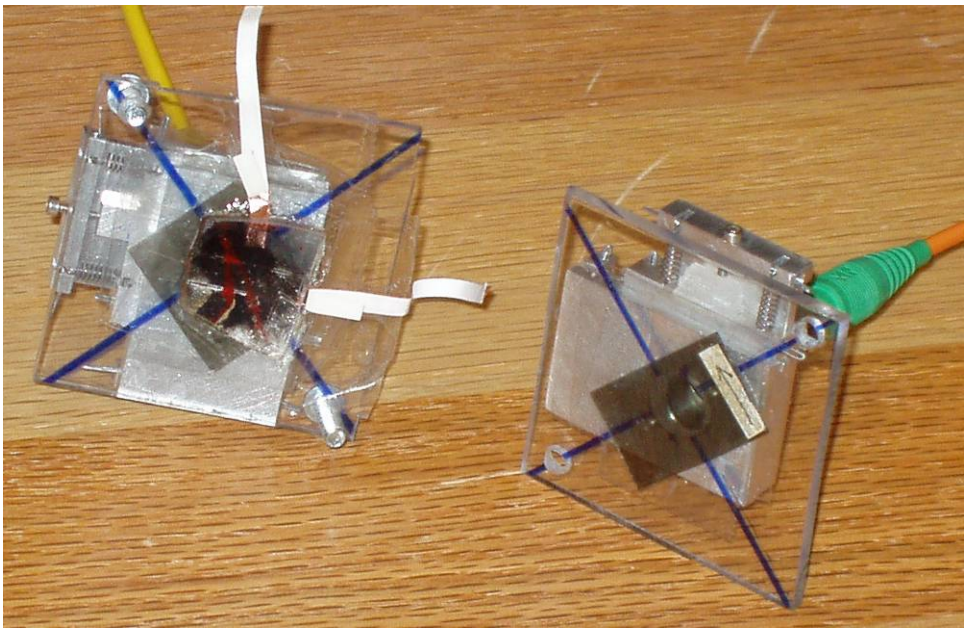

Fig. 4.20 Photograph of a prototype fiber optic electro-optic modulator based on DAST.

Hence the input light that is coupled into the multimode fiber is then made to focus between the electrodes and on the DAST sample. The light then is collected by another ball lens which couples it into a polarization maintaining single mode fiber after passing through the analyzer.

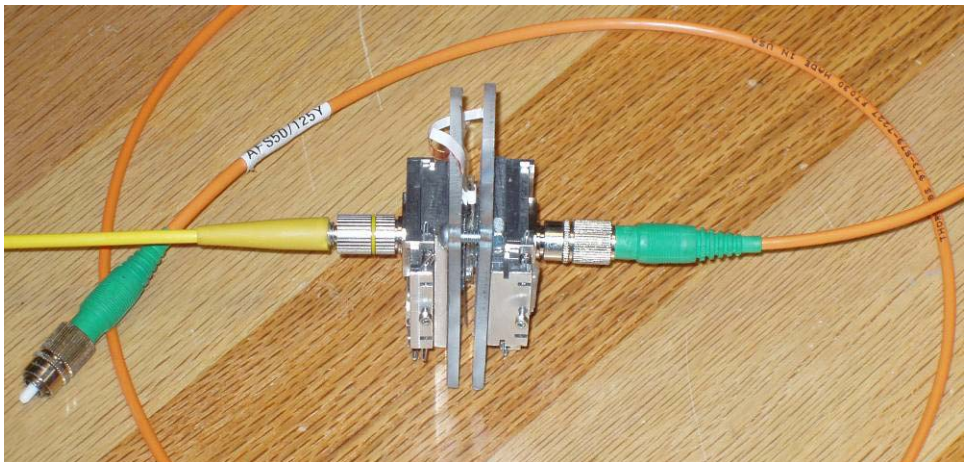

Fig. 4.21 Photograph of a fully assembled fiber optic electro-optic modulator.

The modulated beam is then detected using a photodiode and analyzed using an oscilloscope. For a field of 1 volt/micron at 4 KHz, a modulation depth of 2% was observed.

Fig. 4.22 Oscilloscope trace of the modulation observed using the fiber optic electro-optic modulator.

Although the prototype is the first of its kind, the reason for the reduction in the modulation depth observed in the fiber-optic e-o modulator is mainly due to the challenges in coupling light efficiently from one fiber to the other. As optical technology develops, better integration of lenses with the optical fiber will rectify or greatly improve the modulation that can be observed.

CHAPTER 5

THIRD ORDER NONLINEAR OPTICAL STUDIES OF SPECIFIC NONCONJUGATED CONDUCTIVE POLYMERS

"**A key property of a conducting polymer is the presence of conjugated double bonds along the backbone of the polymer. In conjugation, the bonds between the carbon atoms are alternately single and double –** Shirakawa *et al*. [76]". The research work leading to this statement (found in the Nobel Foundation webpage) led to the bestowing of the 2000 Nobel Prize in Chemistry [77]. π-conjugated conductive polymers since then have attracted a lot of research work as, till then, polymers were considered synonymous to insulators or nonconductors of electricity. However, this statement is fallacious considering the works of Thakur, first reported in his article in 1988 [79]. Through this and subsequent articles [80-84] he reported that certain non-conjugated polymers with one double bond and three single bonds in the repeat also become conductive upon doping with iodine. This phenomenon has been observed in the cases of cis-polyisoprene, trans-polyisoprene, polyalloocimene etc [83,84], where the conductivity of the material increases from less than 10^{-10} S/m in the undoped state to about 10 s/m in the doped state, which is about a change of 100 billion times.

In this section, the third order nonlinear optical properties of specific nonconjugated polymers namely, 1,4 cis-polyisoprene and poly(β-pinene) and the optical characterization of styrene butadiene rubber (SBR) are discussed.

5.1 Electrical and Optical Properties of Styrene-Butadiene-Rubber

Sample of SBR latex was obtained from the Goodrich Chemical company. As opposed to conjugated polymers, SBR being a Non-conjugated co-polymer is easily soluble in common organic solvents like toluene and hexane. Thin films of SBR were prepared by evaporating a solution of SBR rubber dissolved in toluene on quartz substrates. The rubber films thus obtained have a thickness of about 100 microns. These films are held above crystallized iodine. Due to thermal evaporation of the iodine, the SBR films get doped. On doping the films change color from colorless to black depending on the amount of dopant (i.e) iodine that has interacted with the SBR film. The films at regular intervals during the process of doping are left exposed under fume hoods so that the iodine that has sublimed on the surface of the films which do not contribute to the doping of the films is evaporated. The absorption spectra were obtained for these films, at different doping concentrations, exposed to a range of wavelengths of light by using a Hitachi U-2000 Spectrophotometer. FTIR Spectroscopic analyses were also done by using a Nicolet FTIR Spectrometer. For the FTIR Spectroscopic analysis, the thin films were prepared by the same evaporation method on Sodium Chloride windows which are transparent to the Infra-red rays. The analysis was done at different doping levels also. Electrical conductivity experiments were also conducted on these thin films using a Keithley programmable electrometer at various doping levels. Platinum probes

were used since they are not affected by iodine. These probes were placed about 5 millimeters apart and the resistance of the film was measured between the two probes.

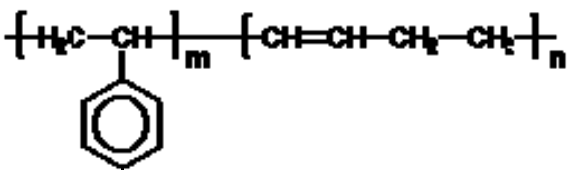

Fig. 5.1 Molecular structure of styrene butadiene rubber.

5.1.1 Electrical Conductivity Analysis:

The styrene butadiene rubber film is non-conducting in its original form. Electrical conductivity experiments were conducted at various degree of doping. It was observed that the conductivity of the film reaches a value of about 0.01 S/cm and then the value remains a constant as the film is saturated with the iodine. In a previous article, this phenomenon of electrical conductivity in a similar non-conjugated polymer namely polyisoprene has been observed and explained [79]. The iodine dopant interacts with the double bond of the polymer backbone causing the double bond to lose an electron hence rendering the site positive forming a polaronic state. The transfer of charges occurs due to the movement of the positive carriers or holes across the many polaronic sites that are created upon doping. The darkening of the film upon doping is attributed to the breaking up of the double bonds.

5.1.2 Optical Absorption Analysis:

The optical absorption spectra are shown in Fig. 5.2 for different doping levels. As expected the films are non-absorbing in the visible region since they are colorless in

their pristine state. The color of the rubber film changes from colorless to black depending on the amount of iodine in the material and correspondingly the absorption as expected increases. After a low level of doping the absorption spectrum shows two peaks – one at 4.13 eV and another at 3.18 eV. The peak at 3.18 eV broadens and red shifts as the amount of iodine in the material increases. This has been attributed to the reduction of the average distance between the dopant or the electron acceptor which in this case is iodine, and the radical cation. The peak at 4.13 eV has been explained in previous articles using a theoretical model involving Coulomb correlation in the cation radical, similar to an ethylene ion [81]. This analysis gives a Coulomb energy which is equivalent to the known optical gap of the ethylene molecule.

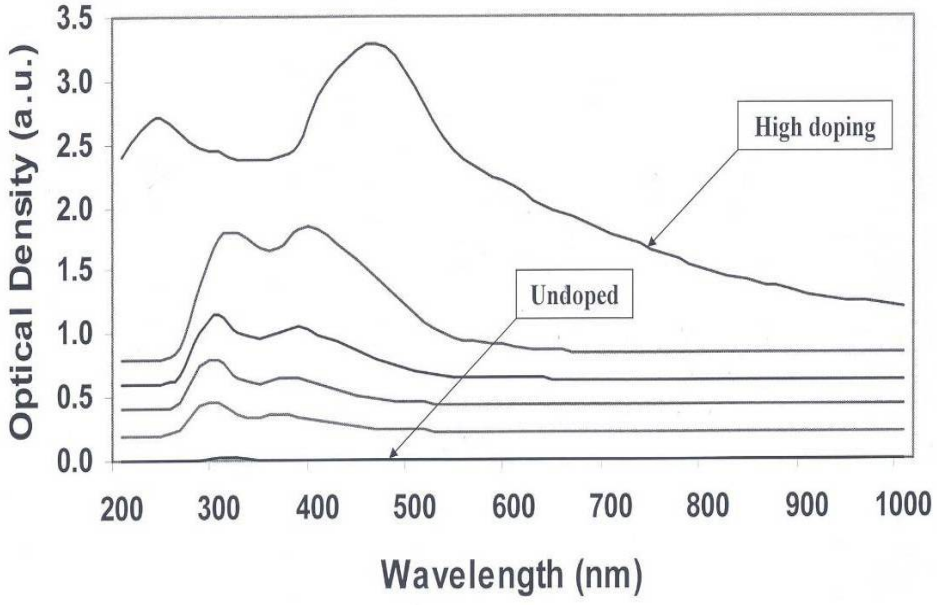

Fig. 5.2 Optical absorption spectra of SBR at different doping levels of iodine.

5.1.3 Photoluminescence Measurements

Thin films of styrene butadiene rubber were prepared on glass substrates from a toluene solution. The photoluminescence spectra of the films were recorded using a Perkin Elmer LS-55 spectrometer before and after doping. The undoped film has a weak absorption at 280 nm. Excitation at 280 nm results in an emission spectrum with a peak at 355 nm as shown in Fig. 5.3. Upon doping with iodine, the emission is substantially reduced due to quenching by iodine.

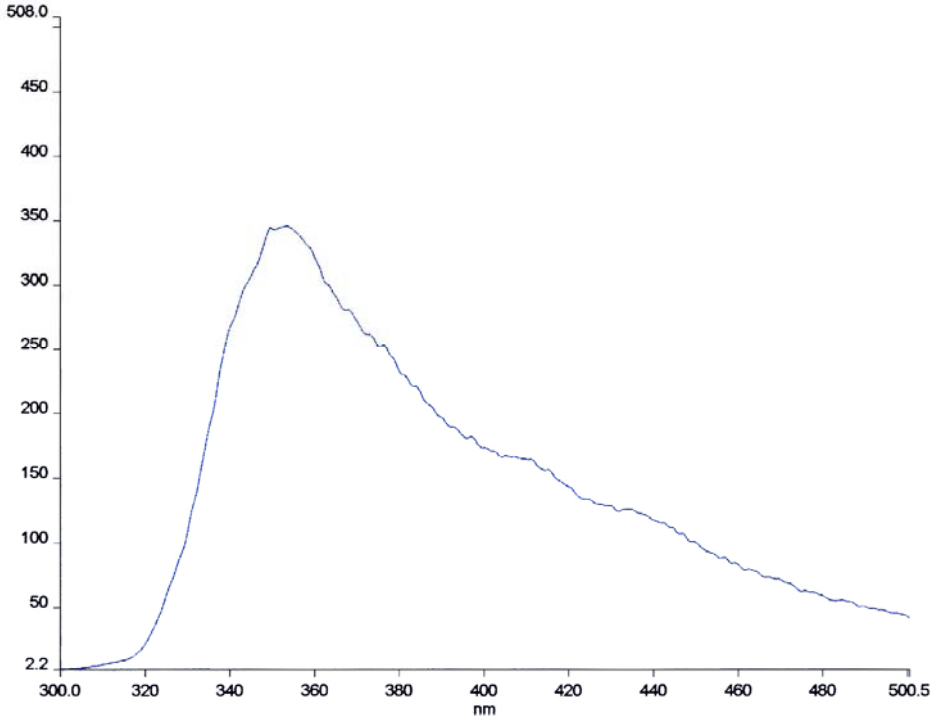

Fig. 5.3 Photoluminescence spectrum of SBR

5.1.4 FTIR Spectroscopy

Styrene butadiene rubber thin film cast on a sodium chloride substrate was used for FTIR spectroscopic studies. A Perkin Elmer spectrometer was used for these measurements. The spectra were recorded for different dopant concentrations. In the undoped film, peaks corresponding to the methyl vibrations (1447 and 1376 cm^{-1}) and the =CH-CH bending mode (964 cm^{-1}) were pronounced. As the film was doped, the peak corresponding to the =CH-CH bending mode rapidly reduced because of the charge transfer from the double bond to the dopant and consequent formation of radical cations. This result is similar to that observed for polyisoprene in which case also a reduction of the peak corresponding to the =CH-CH bending mode was observed with the increase of doping. The peak corresponding to the symmetric vibration (1376 cm^{-1}) of methyl group attached to the double bond is also relatively reduced upon doping.

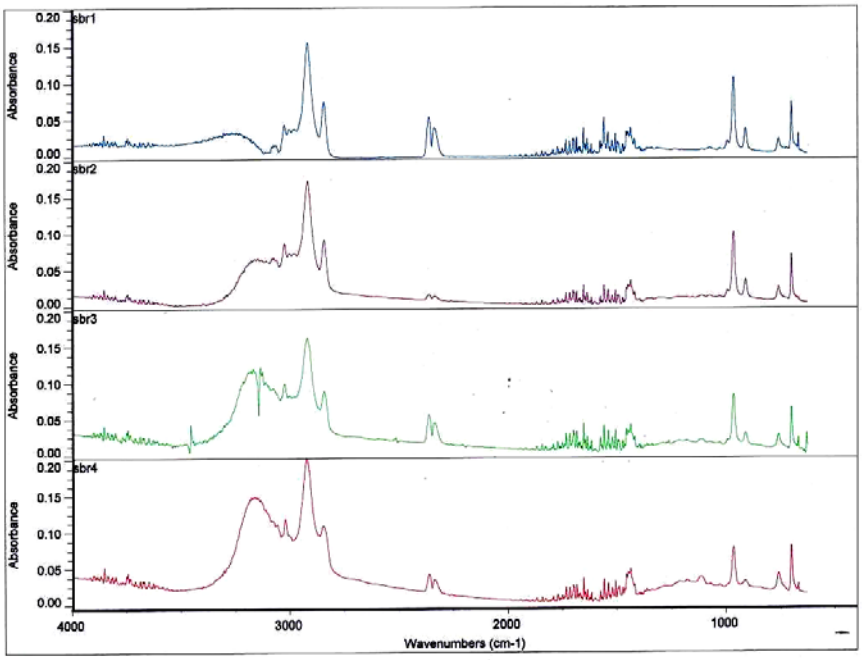

Fig. 5.4 FTIR spectra of SBR at different doping levels.

As the absorption spectra show, the undoped film is essentially nonabsorbing in the visible with a small absorption in the ultraviolet. Upon doping, a peak similar to that observed in lightly doped polyisoprene but at a lower energy is observed. This is assigned to the optical transition of the radical cation formed upon doping and charge-transfer. The shift of this peak to a lower energy is explained as due to a reduction of the average distance between the double bonds in the repeat compared to that in polyisoprene. The peak at the lower energy corresponds to the charge-transfer state formed between the cation and the dopant. The reduction in the average distance between the double bonds in the repeat causes a slight red shift of this peak as well compared to that observed in lightly doped polyisoprene. This band becomes broader and stronger with doping because of the reduction in the average distance between the double bond and dopant molecules. The transition in the radical cation is explained using the valence band approach, which involves Coulomb correlation. The value of the hopping integral between the carbon atoms obtained from the experimental optical gap leads to the correct estimation of the optical gap in ethylene molecule in the valence band approach including the appropriate Coulomb term.

The FTIR results show that double bonds decrease with doping and charge-transfer. A broad background-absorption appears in the infrared region due to the band-tail of the electronic absorption. This is a common characteristic of conductive polymers upon doping. As previously shown using solid-state ^{13}C-NMR spectroscopy in the case of 1,4-cis-polyisoprene, doping does not lead to conjugation. No new double-bonded carbon

resonance appears upon doping. The peaks corresponding to the double-bond carbon atoms decrease in intensity with doping as the radical cations are produced. Theoretical studies of the FTIR spectrum of radical cations of polyisoprene have been reported. Formation of I_3^- upon doping and charge transfer from the isolated double bonds in polyisoprene has been reported. Doping of conjugated polymers also leads to formation of I_3^-. The maximum conductivity of doped polyisoprene after saturation is about 0.1 S/cm. In doped styrene butadiene rubber the conductivity reaches about 0.01 S/cm. As reported in the literature, the maximum conductivity in doped polyacetylene for iodine doping is about 100 S/cm. With these results, the final electrical conductivities can be correlated with the different number fractions of double bonds in the polymers.

Besides the number-fraction of double bonds there are other critical factors to enhancement of conductivity in polymers upon treatment with a dopant. These include rigidity of the polymer chain, that is, whether the polymer is glassy, crystalline, or flexible. In rigid polymers including polymer crystals, dopants cannot diffuse easily to interact with the unsaturated bonds.

5.2 Quadratic Electro-Optic Measurements Using 1,4 Cis-Polyisoprene

A latex sample of 1,4 cis-Polyisoprene or natural rubber was procured from Firestone Inc. When the water in the latex is evaporated, a film of natural rubber is left behind. This dehydrated rubber is then dissolved in hexane to prepare a solution. Gold electrodes with a gap of approximately 100 μm were deposited on a glass slide. Thin films of natural rubber are cast on glass slides with the gold electrodes by evaporating the

solvent. The films so obtained are about 0.9 – 2 microns thick. Upon doping with iodine, the film became dark in color. The absorption spectra of the polymer film for different doping levels are given in Fig. 5.5.

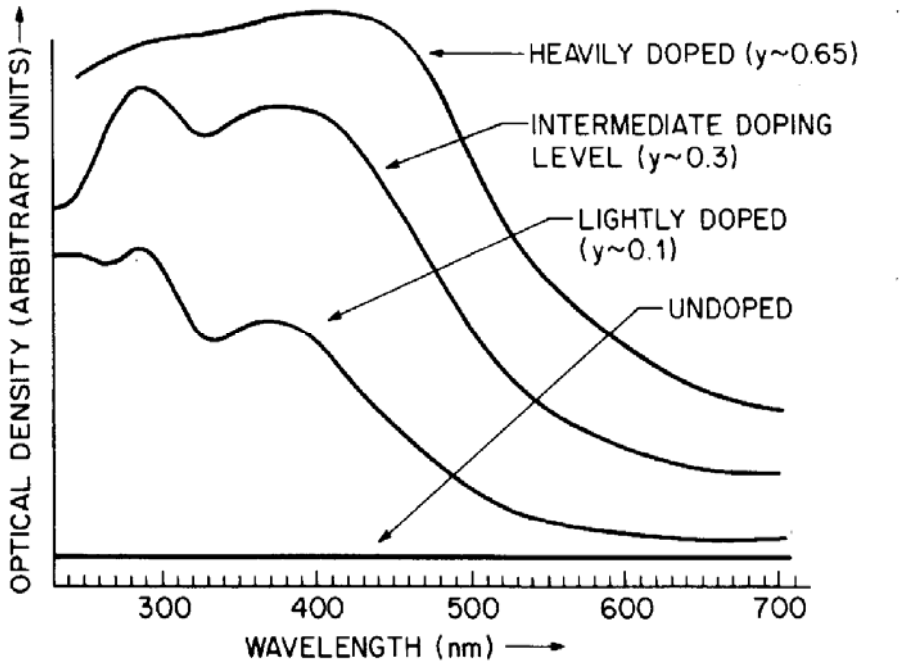

Fig. 5.5 Optical absorption spectra of 1,4 cis-polyisoprene at different doping levels.

5.2.1 Experimental Setup

A 633 nm He–Ne laser with 1 mW power is employed as the light source. The experiment was performed using field induced birefringence method. Here, the laser beam was polarized at an angle of 45 degrees (using the polarizer) with respect to the electric field and passed through the doped film. The transmitted beam was passed through an analyzer, which was cross polarized with respect to the polarizer and the final beam was collected on a photo detector. Due to the instability of the received signal, a

Lock-in amplifier (2f synchronization) was used to record the modulation signal. The modulation signal was recorded for various applied ac electric fields.

5.2.2 Results

The signal as obtained for a field of 1 V/μm is shown in Fig. 5.. The lower waveform represents the applied AC field at 4 kHz. The modulation shown in the waveform above is due to the quadratic electro-optic effect in the doped polyisoprene film. The modulation signal was also recorded using a lock-in amplifier (with 2f synchronization). The signal increased quadratically with the applied voltage. A modulation of 0.8% was observed for a field of 2.0 V/μm and the film thickness was 0.5 μm. The magnitude of the quadratic electro-optic effect is exceptionally large. The change in refractive index, Δn, is 1.6×10^{-3} at a field of 2.0 V/μm. The Kerr constant as determined is about 6.3×10^{-10} m/V^2 [84]. The Kerr constant of nitrobenzene at 589 nm is 2.4×10^{-12} m/V^2.

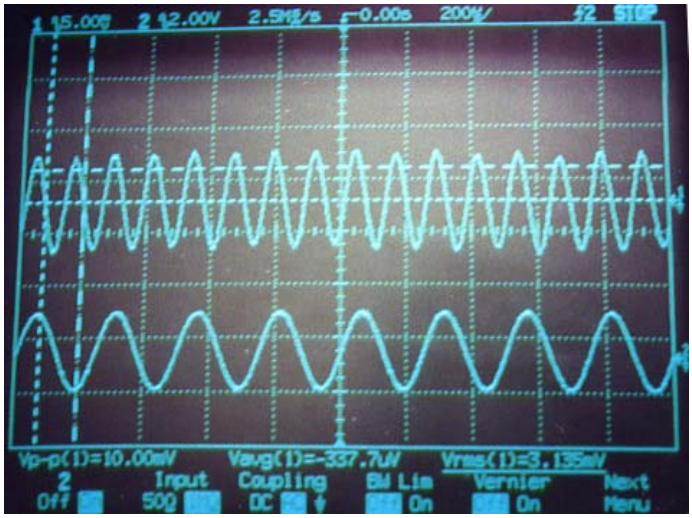

Fig. 5.6 Oscilloscope trace of modulation signal in quadratic electrooptic measurement of doped 1,4 cis-polyisoprene. The waveform at the bottom represents the applied voltage at 4 KHz. The waveform above corresponds to the quadratic electro-optic modulation signal.

The Kerr constant is determined using the equation: $K = (\Delta n)/ (\lambda E^2)$ (Eq. 2.52), where Δn is the change in refractive index caused by the applied field, λ is the wavelength and E is the strength of the applied electric field. Δn is related to the observed modulation (δ) by the formula $\delta = 2\pi \Delta n L/\lambda$, where L is the thickness of the film. The derivation for the Kerr coefficient is explained in Chapter 2. In comparison, the quadratic electro-optic effect measured in natural rubber is significantly larger than that of polyacetylene at a wavelength with a similar detuning with respect to the absorption maximum [85, 86]. The response speed threshold in doped polyisoprene however, has not been measured yet. There is strong absorption in doped polyisoprene over the wavelength range of 250 – 600nm (peak at 400nm) at a medium doping level (iodine molar concentration ~ 0.3). At high doping (iodine molar concentration ~ 0.65), the film becomes dark as the double bonds are broken, and absorbs throughout the visible. The

experiment performed here involved a film with a doping level of about 0.2 molar concentration of iodine. The electrical conductivity was about $6x10^{-4}$ S/cm and the wavelength used (633 nm) was just outside the resonance frequency (400 nm).

5.2.3 Analysis

The measured large quadratic electro-optic effect has been attributed to two reasons. First, the hole (positive charge) is loosely bound to the acceptor molecule (I_3^-) in the doped film. The formation of I_3^- upon doping has been shown earlier [87].

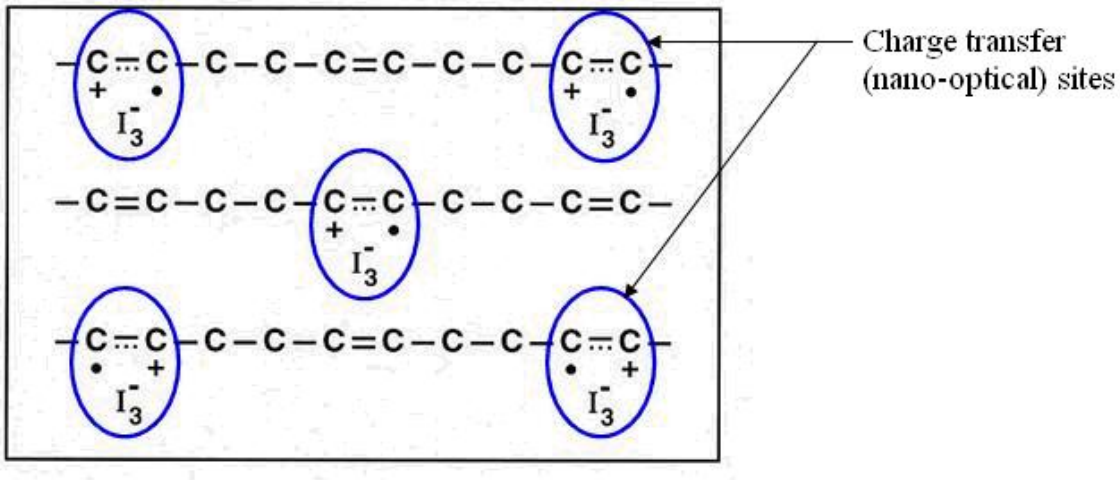

Fig. 5.7 Quantum dots created upon doping with iodine.

The loosely bound positive charge can be modeled as a spring-mass system with a quartic term in the potential energy which is shown in Fig. 5.8.

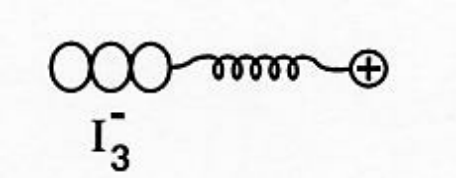

Fig. 5.8 Schematic of the spring mass system involving a hole loosely bound to the dopant ion I_3^-.

The equation for anharmonic potential energy V(x) as a power series is written as

$$V(x) = 1/2\,kx^2 + 1/3\,bx^3 + 1/4\,cx^4 + 1/5\,dx^5 + \ldots\ldots \qquad 5.2$$

where b, c, d… are the anharmonic terms. $\partial V/\partial x$ gives the restoring force acting on each particle which is substituted in the electron oscillation equation (Eq. 2.19). The quadratic and cubic terms (k, b) in the anharmonic oscillator potential energy lead to the first order and second order optical susceptibilities respectively. The quartic term involving c, leads to the third order optical susceptibility or the quadratic electro-optic effect. The contribution of the quartic term for a loose spring can be significant leading to exceptionally large third order optical effects in this system. The material being isotropic, the cubic term is not present and therefore it does not display second order optical or linear electro-optic effect. The third order optical or the quadratic electro-optic effect is large because of the higher magnitude of the quartic term. The second reason for such large nonlinear effect is due to the confinement of the charge within a small volume (nanometer scale). A discussion of nano-optics has been carried out in the following section in order to explain the enhancement of optical nonlinearities in nanometer domain.

5.3 Nonlinear Refractive Index And Two Photon Measurements Using Poly(β-Pinene)

In the last three decades we have seen an increased interest in the area of optical communication system. In particular, the area of All-Optical systems is especially important, because as it is evident in the industry of technology, it all comes down to the response time of a system. And all-optical systems are the key. All-optical systems employ ultra-fast nonlinear effects which are faster and simpler in principle than electronically controlled systems.

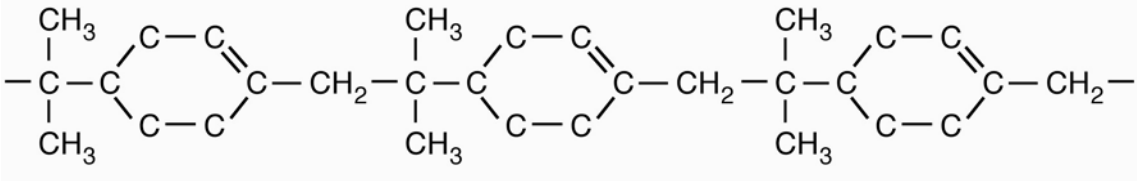

Fig. 5.9 Molecular structure of poly(β-pinene).

The molecular structure of poly(β-pinene) is shown in Fig. 5.9. When the films of this material cast on glass slides are exposed to iodine, the 'pi' bond of the double bonds in the polymer chain break up to form charge transfer sites. The iodine molecule accecpts and electron form the double bond forming an iodium complex which is loosely attached to the double bond site which is now a hole. This gives rise to a dipole. Considering the known bond length of the carbon-carbon double bond to be ~1.4 Angstroms, the charge is effectively contained within this double bond site. This essentially is a quantum dot. Hence, poly(β-pinene) doped with iodine is a nano-optical polymer. As seen in many

semiconductor and metallic quantum dots, large third order nonlinear optical effects can be expected from these materials.

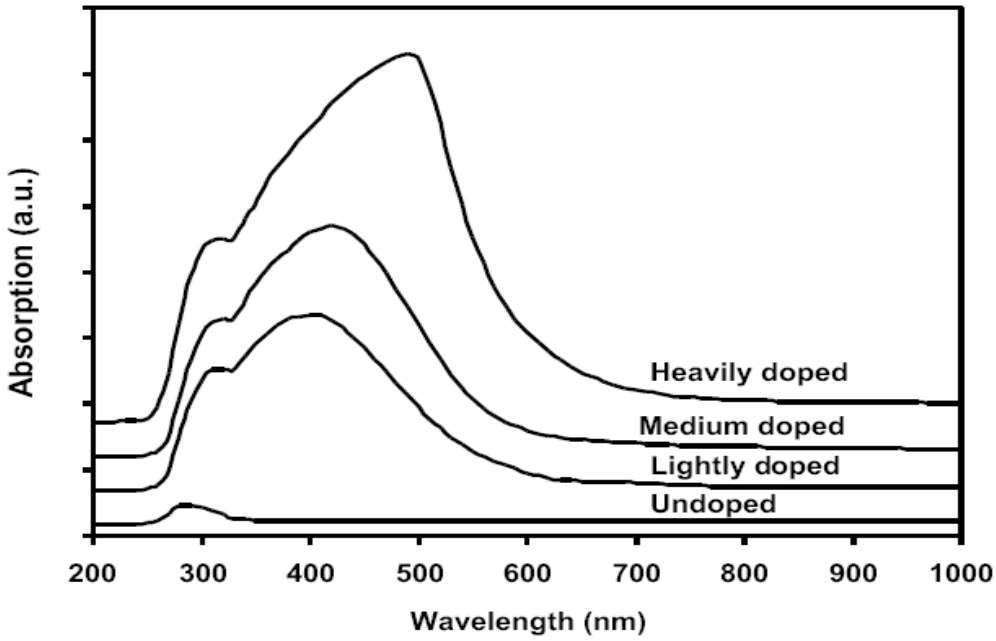

Fig. 5.10 Optical absorption spectra of poly(β-pinene) at different doping levels [110].

5.3.1 Z-Scan Experimental Setup

A modified version of the standard "closed aperture" Z-scan apparatus (i.e. aperture placed in the *far field*) is used for determining nonlinear refraction [105, 106]. The transmittance of the sample through the aperture is monitored in the far field as a function of the position, Z, of the nonlinear sample in the proximity of the focal position of the lens. The required scan range in an experiment depends on the beam parameters and the sample thickness.

The TPA coefficient of a novel nonconjugated polymer namely, Poly(β-pinene) was determined [110] using a slightly modified far-field z-scan technique. In this setup, a Ti:Saphire laser was used as the source pulsing at 82 Mhz frequency with a pulsewidth of about 150 femtoseconds. An attenuator was used right after the laser to regulate the input intensity. The sample followed by the detector is held by a fixture which is capable of very fine movements along the z axis. The initial position of the sample and the detector is before the point of focus of the beam right after the lens. The sample and the detector are then moved along the z-axis while simultaneously recording the power after the sample using the detector.

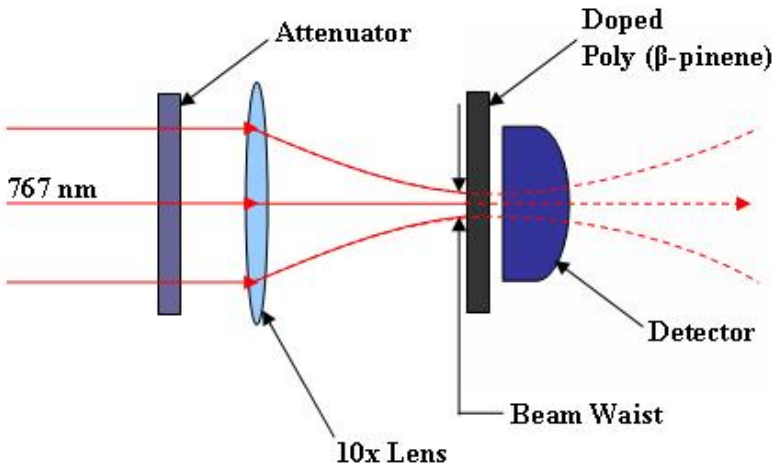

Fig. 5.11 Schematic of the z-scan experimental setup.

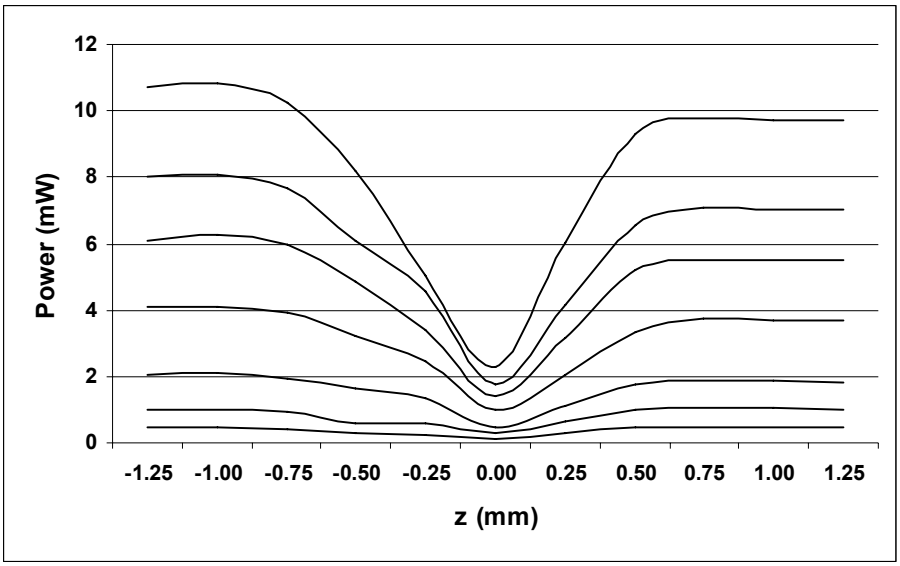

Fig. 5.12 z-scan data (open aperture) for two photon absorption measurement at varying input powers.

5.3.2 Z-Scan results and analysis

The experiment was conducted for varying degrees of incident power and as shown in Fig. 5.12, the TPA effect increases nonlinearly as the incident power increases which is typical of third order nonlinear optical effects. Fig. 5.13 shows that when the experiment is conducted in the continuous wave mode, TPA effect vanishes and the transmitted power, within experimental error margin, remains constant. This is observed because, in the CW mode, the effective incident intensity is much less compared to the modelocked mode, where the intensity of each pulse is much higher. This clearly indicates that the effect observed is due to two photon absorption.

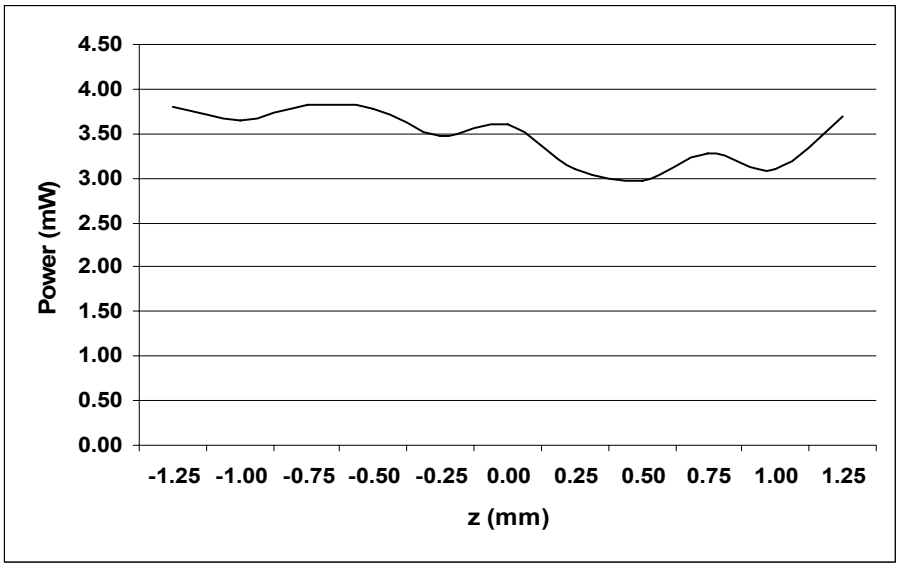

Fig. 5.13 z-scan data (open aperture) for continuous wave mode indicating no TPA.

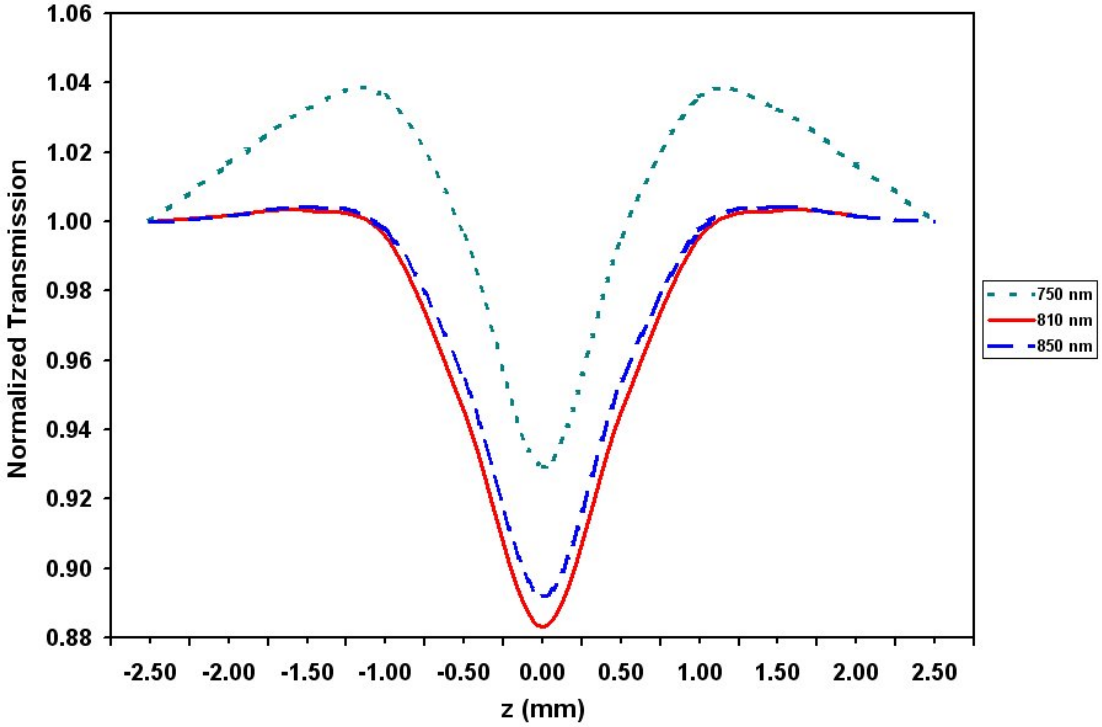

Fig. 5.14 Normalized z-scan plots (open aperture) for two photon absorption measurement (pulsed-mode).

Fig. 5.14 shows a set of z-scan plots obtained using the open aperture setup at wavelengths 750, 810 and 850 nm. It is also apparent from the plot that there is partial saturable absorption at lower wavelengths and then it vanishes for higher wavelengths. This is because; the lower wavelengths are closer to the resonance frequency of the sample giving rise to the saturation of absorption. TPA is given by $\Delta\alpha=\alpha_2 I$, where $\Delta\alpha$ is the change in linear absorption coefficient, α_2 is the TPA coefficient and I is the peak intensity. From the z-scan plots at wavelengths ranging from 730 – 860 nm, the TPA coefficient was determined. The maximum TPA coefficient as shown in Fig. 5.15, was observed at 810 nm (1.53 eV) with a magnitude of 2.6 cm/MW.

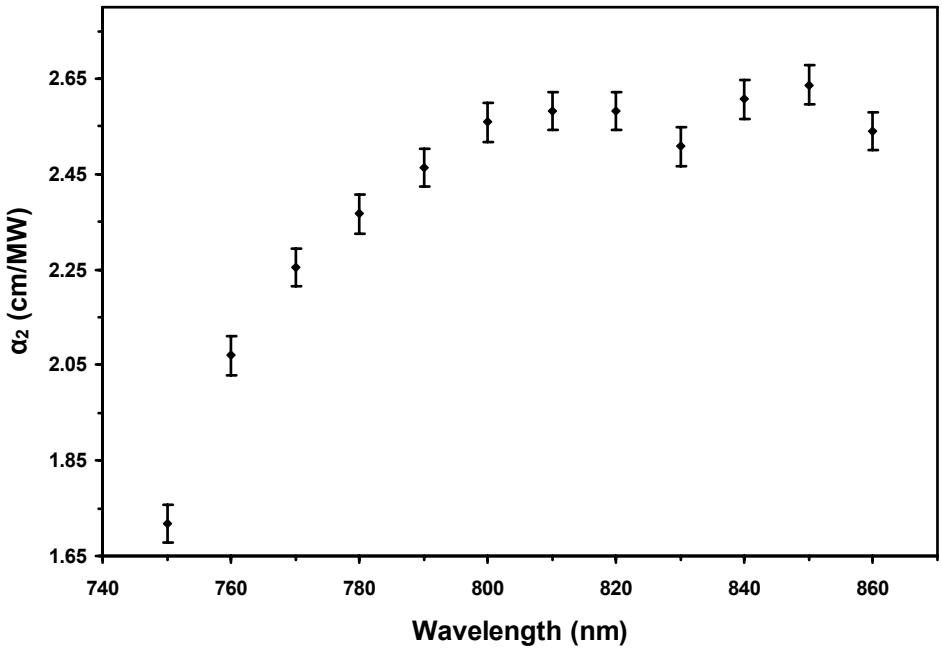

Fig. 5.15 TPA coefficient plotted as a function of wavelength.

The maximum is near half of the optical gap (3.1 eV) corresponding to the charge transfer in doped poly(β-pinene). It is also evident that there is an additional peak at 850 nm (1.46 eV) which could have its origin from the electron-phonon interaction involving

a phonon band of the charge-transfer complex. The origin of the exceptionally large TPA is attributed to the formation of a charge transfer site which are The TPA coefficient determined is comparable to that of semiconductor and metallic nano-clusters [111-116]. The saturation of absorption observed decreases at longer wavelengths as expected as the linear absorption decreases at longer wavelengths. Saturable absorption was also observed in metallic quantum dots at lower intensities [114]. The magnitude of the TPA coefficient depends on the dopant concentration since the linear absorption changes according to the doping level. As the results indicate, the linear absorption due to the charge transfer between the double bond and the dopant has the dominant contribution to the two photon effect. As discussed earlier, the large TPA coefficient is attributed to the special structure of this electronic system confined within a sub-nanometer dimension which can be inferred by knowing the chemical bond length. The magnitude and the response time of the optical nonlinearities are mainly dependent on the size of the quantum dot [111-120]. Since femtosecond pulses were used, the effect seen is mainly due to the TPA as the ultra fast pulses probe only the electronic or fast effect. In addition, the peak appears at 810 nm, which is about half of the optical gap, corresponding to the charge transfer in doped poly(β-pinene).

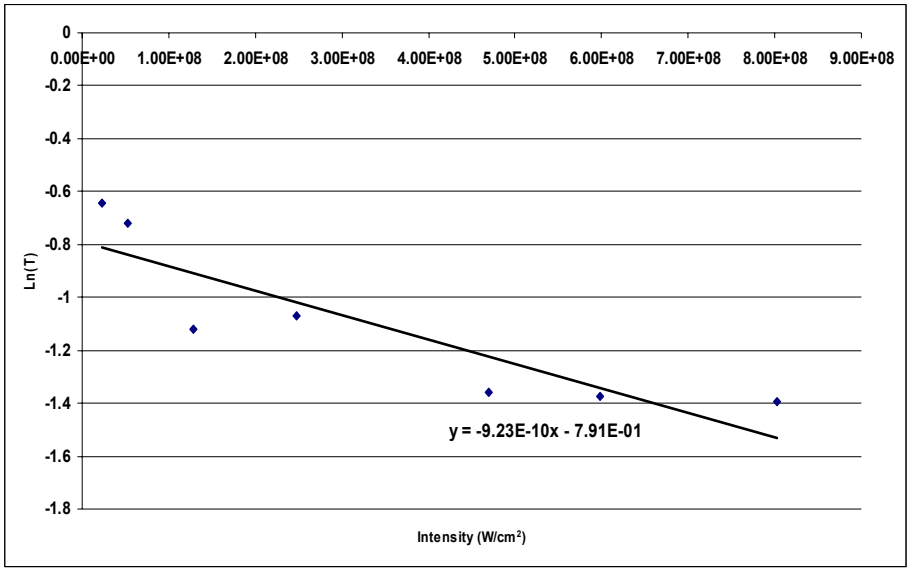

Fig. 5.16 Change in transmission with input intensity. The transmission decreases as intensity increases.

The plot of the Input intensity and the natural log of the transmission of the sample plotted show that the transmission of the sample decreases as the input intensity increases. Knowing the slope of the curve and the thickness of the doped poly(β-pinene) sample (~4 microns), the nonlinear absorption coefficient is determined to be ~ 2.6 $x10^{-6}$ cm/W or 2.6 cm/MW.

5.3.3 Mach-Zhender Experimental Setup

To measure the nonlinear refractive index of poly(β-pinene) a Mach-Zhender interferometer was constructed. Ti:Saphire laser pulsing at 82 MHz frequency with a pulsewidth of about 150 femtoseconds was used for this measurement.

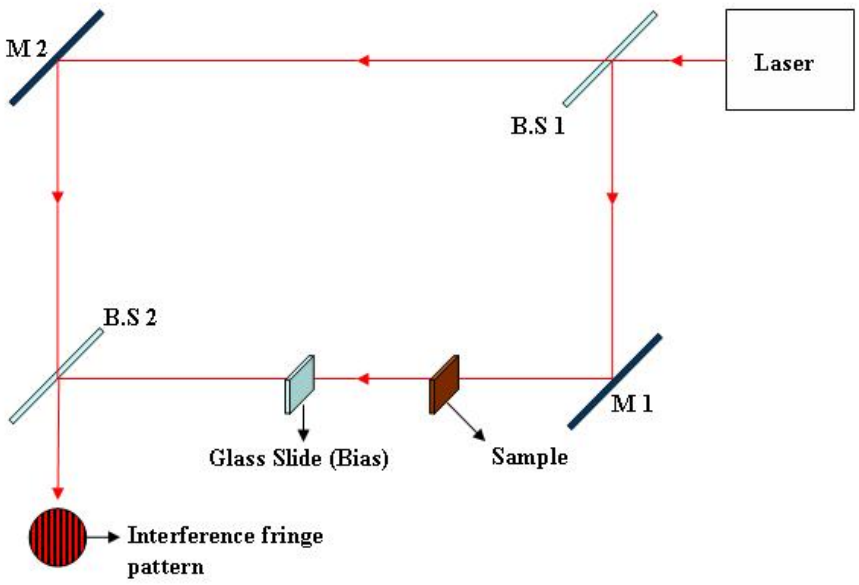

Fig 5.17 Schematic of a Mach-Zhender experimental setup.

In one arm of the interferometer, an iodine doped poly(β-pinene) sample was placed while the beam in the other arm passed through air. The fringes were observed using a charge coupled device camera and the direction of the fringe shift as a function intensity was recorded photographically. The intensity of the beam was regulated using an attenuator that was placed before the mach-zhender setup.

5.3.4 Results

Fringe patterns were observed when the doped poly(β-pinene) sample was placed on one of the arms of the setup. As the intensity of the light was increased, a shift in the fringe pattern was observed. For calibration of the sign, the doped poly(β-pinene) sample was replaced by a 100-micron-thick glass micro-slide and the fringe shift was recorded as

the glass micro-slide was rotated. The rotation of the glass micro-slide introduced positive changes in phase and the corresponding direction of the fringe shift was noted as the calibration of the sign of phase change. For the doped poly(β-pinene) sample the phase changes as the intensity increased, was found to be positive as the fringe shift was observed to be in the same direction for a decrease of intensity. Hence the nonlinear refractive index n_2 is determined to be positive. The total phase change measured was л/4 for a decrease in intensity of 150 MW/cm^2 for a sample thickness of about 10 microns. However, it became difficult to determine the magnitude of the nonlinear refractive index accurately due to the jitter and instability of the laser pulses.

5.3.5 Time resolved Measurements

Although the z-scan and the mach-zhender experiments were helpful in determining the TPA coefficients, they do not entirely eliminate the contribution due to the thermal effect. Hence the need for a time-resolved measurement became necessary.

5.3.6 Pump-probe setup

In this setup, the laser beam was split into a pump beam and a probe beam of equal path lengths such that, the probe intensity is approximately 4% of that of the pump. The doped poly(β-pinene) sample was placed at the intersection of the pump and probe beams and the beams were made to focus on the sample using objective lenses. The two beams are temporally and spatially overlapped by employing a motion controlled retro-reflective setup on the probe. The probe is made to pass through a polarizer before interacting with the sample and then passes through an analyzer. To determine the TPA

coefficient, the polarizer and the analyzer are parallel to each other orthogonal for the determination of the nonlinear refractive index. The pump beam is then chopped using a mechanical chopper which also serves as the reference for a lock-in amplifier. The probe is then collected into a photodiode connected to the lock-in amplifier.

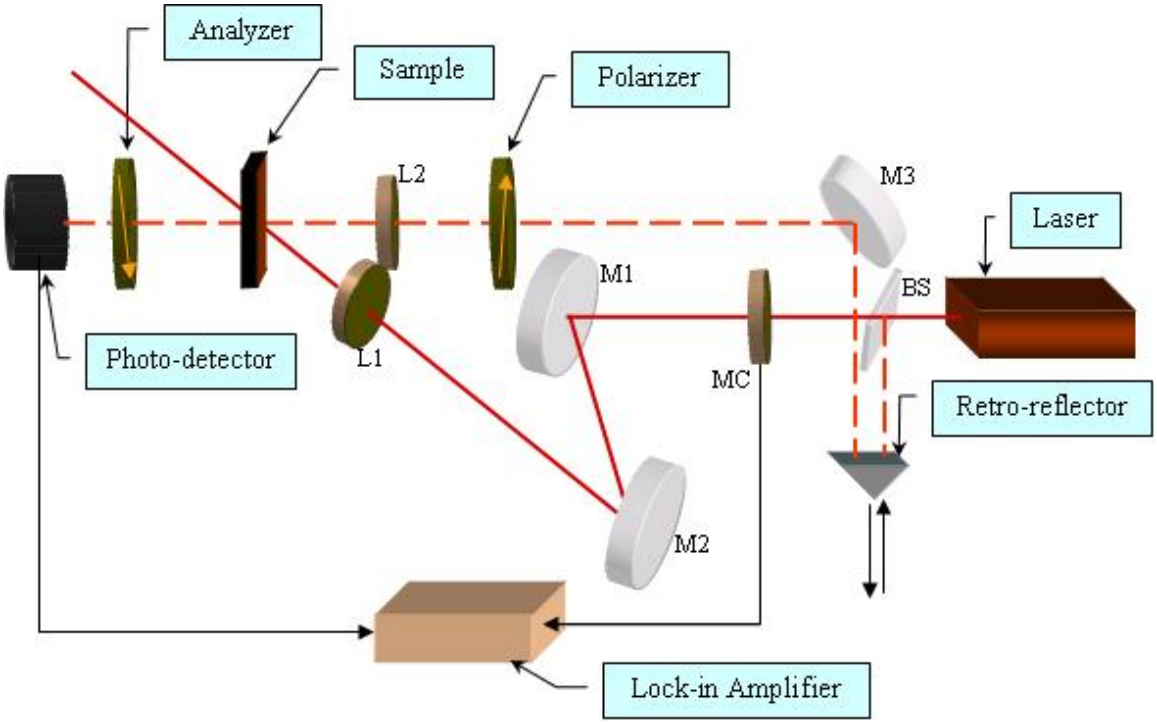

Fig. 5.18 Pump-probe time resolved experimental setup.

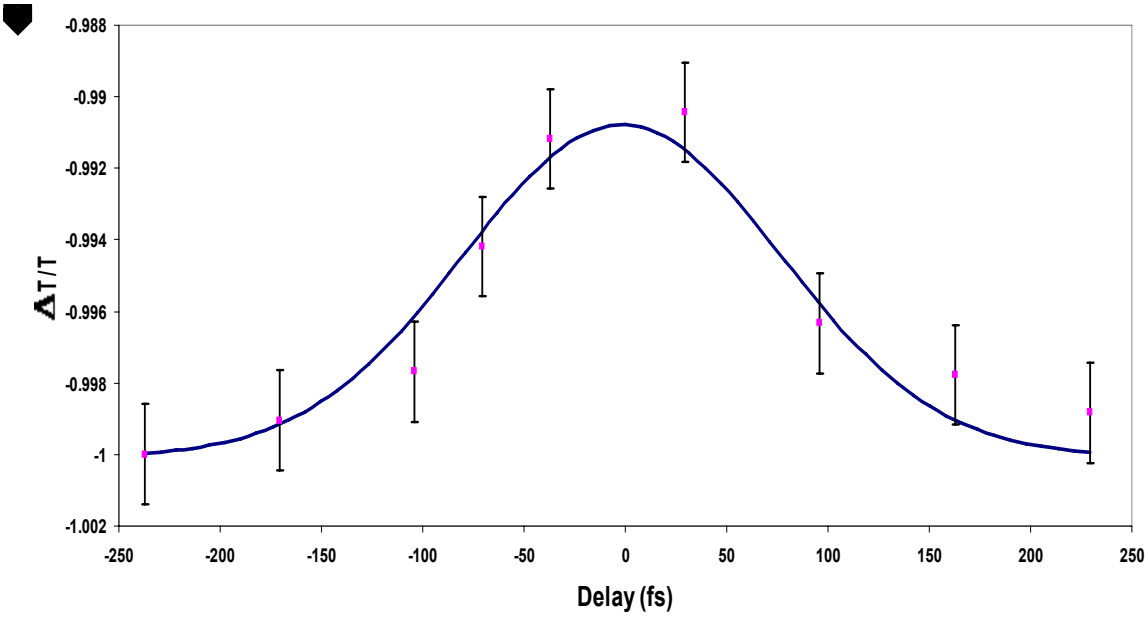

Fig. 5.19 Time resolved measurement of the two photon absorption.

When the pump and the probe are overlapped, the pump beam causes a change in the local absorption of the sample which lasts for the duration of the pulse (150 fs). During this time the probe experiences this change in absorption and hence the transmission changes and is recorded by the lock-in amplifier. The path length of the probe was changed using the retro reflector so that a time delay plot could be obtained. As seen in Fig. 5.19, the absorption decreases when the pulses of the pump and probe overlap and increases when the pulse of the probe is either ahead or behind the pump. The duration of the decrease in absorption exactly matches the pulse with of the laser beam which is 150 fs. The TPA coefficient of the doped sample of polybetapine was thus determined and was found to be in accord with the results obtained using the z-scan technique. The nonlinear refractive index of the sample was also found employing the pump-probe technique by using a cross polarized setup. The response time involved in

the observed two-photon process is ultra-fast (shorter than the pulsewidth used). This indicates that any excited state absorption was not significant at the wavelengths used.

CHAPTER 6

SUMMARY

In this dissertation, the nonlinear optical properties of an organic polymer, DAST and nonconjugated conductive polymers namely, 1,4 cis-polyisoprene, poly(β-pinene) and styrene butadiene rubber (SBR) were studied and discussed.

DAST thin-film single crystals were prepared with excellent optical quality by employing the modified shear method using a super-saturated solution of DAST in methanol as the starting material. A field induced birefringence method was used to observe phase modulation in these crystals at 1.55 microns which is a technologically important wavelength. The electro-optic coefficient at this wavelength was determined to be 200 pm/V. High speed electro-optic measurements up to 1.5 GHz were successfully demonstrated with excellent signal to noise ratio comparable to that of waveguides. The modulation depth was found to be almost constant over the frequency range up to 1.5 GHz. This indicates that the response will remain flat at higher frequencies. This is due to the electronic origin of the optical nonlinearities. Two devices namely, Pockels cell and fiber coupled electro-optic modulator, based on DAST thin-film crystals were designed, fabricated and successfully demonstrated. Using the Pockels cell, modulation depth up to 57% was observed at a low field. This kind of Pockels cells can be used as a teachers' aid in demonstrating the electro-optic effect for undergraduate and graduate students as well

as in other applications. Using the fiber coupled e-o modulator with a single mode input fiber, a modulation depth of 2% was observed.

Nonconjugated polymers 1,4 cis-polyisoprene and poly(β-pinene) when doped with iodine which is an electron acceptor, become electrically conductive. Moreover, the charge transfer sites behave as quantum dots because the radical cation that is formed due to a charge-transfer is confined within the double bond site. Knowing the carbon-carbon bond length, it is shown that the charge transfer site is in the sub-nanometer domain. These nano-optical conductive polymers have been compared to that of semiconductor and metallic quantum dots. This quantum confinement gives rise to large third order optical nonlinearities. Quadratic electro-optic measurements were done on doped 1,4 cis-polyisoprene and the Kerr constant and the change in refractive index were determined. Exceptionally large Kerr constant has been observed. Two photon absorption measurements were done on doped poly(β-pinene) using a modified open aperture z-scan technique with 150 fs pulses from a Ti:Sapphire laser and the nonlinear absorption coefficient was found to be 2.6 cm/MW. This value is exceptionally large when compared to other nonlinear optical materials. Time resolved measurements were also done using a pump-probe setup to confirm the response time of the nonlinear absorption coefficient and the nonlinear refractive index was also studied. The two-photon absorption process was found to be instantaneous at the 150 fs time scale. Optical characterization of styrene-butadiene-rubber (SBR) was done by performing optical absorption spectroscopy, photoluminescence spectroscopy and FTIR spectroscopy.

BIBLIOGRAPHY

1) Sadiku, "Elements of Electromagnetics", *Saunders College Publishing*, (1989).

2) Larry R. Dalton, William H. Steier, Bruce H. Robinson, Chang Zhang, Albert Ren, Sean Garner, Antao Chen, Timothy Londergan, Lindsey Irwin, Brenden Carlson, Leonard Fifield, Gregory Phelan, Clint Kincaid, Joseph Amend and Alex Jen, J. Matl. *From molecules to opto-chips: organic electro-optic materials* (May 1999)

3) Christopher C. Davis, "Lasers and Electro-Optics Fundamental and Engineering", *Cambridge University Press* (1996).

4) D. K. Cheng, *Field and Wave Electromagnetics* (Addison-Wesley, 1992).

5) A. Yariv and P. Yeh, *Optical Waves in crystals* (John Wiley & Sons, New York, 1984)

6) Y. R. Shen, "The Principle of Nonlinear Optics", *John Wiley & Sons* (1984).

7) R. W. Boyd, *Nonlinear Optics, Second Edition* (Academic Press, San Diego, 2003)

8) N. Bloembergen, *Nonlinear Optics* (Benjamin, New York, 1964).

9) B. L. Davydov, L. D. Derkacheva, V. V. Dunina, M. E. Zhaotinskii, V. K. Zolin, L. G. Kreneva, and M. A. Samokhina, Opt. Spectrosc. 3**0**, 274 (1971).

10) J. Zyss, and J. L. Oudar, Phys. Rev. A **26**, 2028, (1982).

11) H. S. Nalwa and S. Miyata, Eds., "Nonlinear Optics of Organic Molecules and Polymers", *CRC Press, Boca Raton* (1997).

12) D. S. Chemla and J. Zyss, Eds., *Nonlinear Optical Properties of Organic Molecules and Crystals* (Academic Press, New York, 1987).

13) Ch. Bosshard, K. Sutter, R. Schlesser, and P. Gunter, J. Opt. Soc. Am. B **10**, 867 (1993).

14) P. A. Franken, A. E. Hill, C. W. Peters, and W. Weinreich, Phy. Rev. Lett., **7**, 118, (1961)

15) Narasimhamurty, *Photoelastic and Electro-otpic properties of Crystals* (Plenum Press, New York, 1981).

16) B. H. Billings, J. Opt. Soc. Am. **37,** 738-746 (1947).

17) B. H. Billings, J. Opt. Soc. Am. **39**, 797-801 (1949).

18) B. H. Billings, J. Opt. Soc. Am. **39**, 802-808 (1949).

19) R.O'B Carpenter, J. Opt. Soc. Am. **40**, 225-229 (1950).

20) P. V. Lenzo, E. G. Spencer and K. Nassau, J. Opt. Soc. Am. **56**, 633 (1966).

21) L. Ho., and C. F. Buhrer, Appl. Opt. **2**, 647-648, (1963).

22) D. J. Gainon, J. Opt. Soc. Am. **54**, 270-271 (1964).

23) I. P. Kaminow and E. Turner, *Linear Optical Materials, Handbook of lasers* (R. J. Pressley, ed.) 447-459 Chemical Rubber Co. Cleveland Ohio (1971).

24) K. Noguchi, O. Mitomi, K. Kawano, and M. Yanagibashi, IEEE Photon. Techn. Lett., **5**, 52 (1993)

25) P. M. Rentzepis, and Y. H. Pao, Appl. Phy. Lett. **5**, 229, (1964).

26) G. H. Heilmer, N. Ockman, R. Braunstein, and D. A. Karmer, Appl. Phy. Lett. **5**, 229, (1964).

27) R. Orlov, Sov. Phy. Crystallogr., **11**, 410, (1966).

28) J. R. Gott, J. Phys. B. **4**, 116, (1971).

29) M. Thakur and S. Meyler, Macromolecules **18**, 2341 (1985).

30) B. D. Malhotra *Handbook of Polymers in Electronics* (RAPRA Technology Ltd., U.K., 2002).

31) Eric W. Van Stryland and Mansoor Sheik-Bahae *Z-Scan Measurements of Optical Nonlinearities*

32) Eric W. Van Stryland, M. A. Woodall, H. Vanherzeele, and M. J. Soileau, *Energy band-gap dependence of two-photon absorption* Optics letters Vol. 10, No. 10 October 1985

33) Bert Hecht, *Nano-optics with single quantum systems* Phil. Trans. R. Soc. Lond. A (2004) 362, 881–899

34) Alain Haché, Serge-Émile LeBlanc, Michael LoCascio, and Alessandro Martucci, *Optical switching spectroscopy of PbS quantum dots with dual wavelength pump-probe* Elsevier Sci.

35) G. M. Carter, M. Thakur, Y. J. Chen, and J. V. Hryniewicz, Appl. Phys. Lett., **47**, 457, (1985).

36) G. M. Carter, J. V. Hryniewicz, M. Thakur, Y. J. Chen, and Mayler, Appl. Phys. Lett., **49**, 998, (1986).

37) F. Kajzar, L. Rothberg, S. Etemand, P. A. Chollet, D. Grec, A. Boudet, and T. Jedju, Opt. Commun. **66**, 55, (1988).

38) P. N. Prasad and D. J. Williams, *Introduction to Nonlinear Optical Effects in Molecules and Polymers* (John Wiley & Sons, New York, 1991).

39) "Third order optical nonlinearities" Mansoor Sheik-Bahae, Michael P. Hasselbeck Preprint of OSA Handbook of Optics, Vol. IV, Chapter. 17, (2000)

40) "Two-photon absorption and nonlinear refraction of amorphous chalcogenide films" R A Ganeev, A I Ryasnyansky, M K Kodirov and T Usmanov, J. Opt. A: Pure Appl. Opt. 4 (2002) 446–451

41) "Two Photon Absorption in ZnS" E. Panizza Applied Physics Letters Volume 10, Number 10 May 1967

42) "Two photon absorption of di-alkyl-amino-nitro-stilbene side chain polymer" M. Cha, W. E. Torruellas, and G. I. Stegeman, W. H. G. Horsthuis and G. R. Mo¨hlmann J. Meth Appl. Phys. Lett. 65 (21), 21 November 1994

43) "Sensitive measurement of optical nonlinearities using a single beam" Mansoor Sheik-Bahae, Ali A. Said, Tai-Huei Wei, David J. Hagan, E. W. Van Stryland Journal of quantum electronics, Vol. 26, No. 4, April 1990

44) "Two-Photon Absorption Could Advance 3-D Data Storage" Photonics Technology World May 1999 Edition

45) "Two-Photon Absorption Enables Microfabrication" Photonics Technology World May 2002 Edition

46) Sadiku, "Elements Of Electromagnetics", *Saunders College Publishing*, (1989).

47) G. R. Meredith, "Nonlinear Optical Properties of Organic and Polymeric Materials"; D. J. Williams, Ed. ;*ACS Symposium Series, American Chemical Society*, vol. **233**, pp. 27-56, (1983).

48) J. R. Gott, J. Phys. B. **4**, 116, (1971).

49) M. Thakur and S. Meyler, Macromolecules **18**, 2341 (1985).

50) B. D. Malhotra *Handbook of Polymers in Electronics* (RAPRA Technology Ltd., U.K., 2002).

51) G. M. Carter, M. Thakur, Y. J. Chen, and J. V. Hryniewicz, Appl. Phys. Lett., **47**, 457, (1985).

52) G. M. Carter, J. V. Hryniewicz, M. Thakur, Y. J. Chen, and Mayler, Appl. Phys. Lett., **49**, 998, (1986).

53) F. Kajzar, L. Rothberg, S. Etemand, P. A. Chollet, D. Grec, A. Boudet, and T. Jedju, Opt. Commun. **66**, 55, (1988).

54) K. K. Loi, L. Shen, H. H. Wieder, and W. S. Chang, IEEE Photonics Technol. Lett. **9**, 1229 (1997).

55) G. K. Gopalakrishnan, C. H. Bulmer, W. K. Burns, R. W. McElhanon, and A. S. Greenblatt, Electron. Lett. **28**, 826 (1992).

56) S. R. Marder, J. W. Perry, and C. P. Yakymyshyn, Chem. Mater. **6**, 1137 (1994).

57) Ch. Bosshard, R. Spreiter and P. Günter, J. Opt. Soc. Am. B. **18** 11 (2001).

58) S. Follonier, M. Fierz, I. Biaggio, U. Meier, Ch. Bosshard, and P. Günter J. Opt. Soc. Am. B **19**, 9 (2002).

59) F. Pan, K. McCallion, and M. Chiappetta, Appl. Phys. Lett. **74**, 492 (1999).

60) F. Pan, G. Knöpfle, Ch. Bosshard, S. Follonier, R. Spreiter, M. S. Wong and P. Günter, Appl. Phys. Lett. **69**, 13 (1996).

61) M. Thakur, J. Xu, A. Bhowmik, and L. Zhou, Appl. Phys. Lett. **74**, 635 (1999).

62) B. Cai, T. Hattori, H. H. Deng, K. Komatsu, C. Zawadzki, N. Keil, and T. Kaino, Jpn. J. Appl. Phys. **40**, L964 (2001).

63) U. Meier, M. Bösch, Ch. Bosshard, F. Pan, and P. Günter, J. Appl. Phys. **83**, 3486 (1998).

64) S. R. Forrest, P. E. Burrows, A. Stroustrup, D. Strickland, and V. S. Ban, Appl. Phys. Lett. **68**, 1326 (1996).

65) X. Zheng, S. Wu, R. Sobolewski, R. Adam, M. Mikulics, P. Kordoš, and M. Siegel **82**, 15 (2003).

66) A. Schneider, I. Biaggio, and P. Günter Optics Communications **224,** 337-341 (2003).

67) A. K. Bhowmik ," *Nonlinear Optical and light Emission Studies of Special Organic Molecules and Crystals*" (2000).

68) M. Thakur, A. Mishra, J. Titus, and A. C. Ahyi, Appl. Phys. Lett **81**, 3738 (2002).

69) F. Pan, M. S. Wong, Ch. Bosshard, and P. Günter, Adv. Mater. **8**, 592 (1996).

70) S. Sohma, H. Takahashi, T. Taniuchi, and H. Ito, Chem. Phys. **245** 359 (1999).

71) F. Tsunesada, T. Iwai, T.Watanabe, H. Adachi, M. Yoshimurs, Y. Mori, and T. Sasaki Journal of Crystal growth 237-239 (2002).

72) S. R. Forrest, P. E. Burrows, A. Stroustrup, D. Strickland and V.S. Ban Appl. Phys. Lett. **68** 10 (1996).

73) M. Thakur and S. Meyler, Macromolecules **18**, 2341 (1985).

74) G. Knöpfle, C. Bosshard, R. Schlesser and P. Günter, IEEE J. Quantum Elec. **30** 5 (1994).

75) D. A. B. Miller, D. S. Chemla, T. C. Damen, A. C. Gossard, W. Wiegmann, T. H. Wood, and C. A. Burrus, Phys. Rev. B **32**, 2 (1985).

76) D. A. B. Miller, D. S. Chemla, and S. Schmitt-Rink, Phys. Rev. B **33**, 10 (1986).

77) H. Shirakawa, E. J. Louis, A.G. MacDiarmid, C. K. Chiang, and A. J. Heeger, J. Chem. Soc., Chem. Comm., 578 (1977).

78) http://nobelprize.org/chemistry/laureates/2000/press.html.

79) N. Basescu, Z.-X. Liu, D. Moses, A. J. Heeger, H. Naarmann, and N. Theophilou Nature **327**, 403 (1987).

80) M. Thakur, Macromolecules, **21**, 661(1988).

81) M. Thakur, J. Macromol. Sci. – Pure Appl. Chem., A, **38(12)**, 1337 **(**2001).

82) M. Thakur, and B.S. Elman, J. Chem. Phys., **90**, 2042, (1989).

83) G. Yu, and M. Thakur, J. Polymer Sci., Part B: Polymer Physics, **32**, 2099 (1994).

84) M. Thakur, S. Khatavkar, and E. J. Parish, Journal of Macromolecular Science, Part A, **A40**, 1397 (2003).

85) M. Thakur, R. Swamy, and J. Titus Macromolecules (Communication), **37(8)**, 2677 (2004).

86) B. I. Greene, and M. Thakur, J. Orenstein, Appl. Phys. Lett., **54**, 2065 (1989).

87) W. Jia, K. Misawa, H. Matsuda, S. Okada, H. Nakanishi, and T. Kobayashi, Chem. Phys. Lett., **255***,* 385 (1996).

88) Y.P. Myer, Z.J. Chen, and H.L. Frisch, Polymer*,* **38**, 729 (1997).

89) N. I. Zheludev Contemporary Physics **43**, 365, (2002).

90) F. Hache, D. Ricard, and C. Flytzanis J. Opt. Soc. Am. B, **3**, 1647, (1986).

91) H. S. Nalwa Handbook of Nanostructured Materials and Nanotechnology Volume 4 (Academic Press, San Diego, 2000).

92) R. F. Haglund Jr., Li Yang, R. H. Magruder, III, C. W. White, R. A. Zuhr, Lina Yang, R. Dorinville and R. R. Alfano, Nucl. Instr. and Meth. in Phys. Res. B **91**, 478, (1994).

93) Y. Takeda, V. T. Gritsyna, N. Umeda, C. G. Lee, and N. Kishimoto, Nucl. Instr. and Meth. in Phys. Res. B **148**, 1029, (1999).

94) K. Uchida, S. Kaneko, S. Omi, C. Hata, H. Tanji, Y. Asahara, A. J. Ikushima, T. Tokizaki and A. Nakamura, J. Opt. Soc. Am. B, **11,** 1236, (1994).

95) Y. Hamanaka, A. Nakamura, N. Hayashi, and S. Omi, J. Opt. Soc. Am. B. **20**, 1227, (2003).

96) G. Wang, and K. Guo Physica B **315,** 234, (2002).

97) C. B. Murray, D. J. Norris, and M. G. Bawendi, J. Am. Chem. Soc. **115**, 8076 (1993)

98) H. S. Nalwa *Handbook of Nanostructured Materials and Nanotechnology Volume 5* (Academic Press, San Diego, 2000).

99) Q.-Y**.** Shang, S. Pramanick, and B. Hudson, Macromolecules*,* **23**, 1886 (1990).

100) K. P. J. Williams, and D. L. Gerrard, Polym. Commun., **31**, 290, (1990).

101) R. F. Haglund Jr., Li Yang, R. H. Magruder, III, C. W. White, R. A. Zuhr, Lina Yang, R. Dorinville and R. R. Alfano, Nucl. Instr. and Meth. in Phys. Res. B **91**, 478, (1994).

102) Y. Takeda, V. T. Gritsyna, N. Umeda, C. G. Lee, and N. Kishimoto, Nucl. Instr. and Meth. in Phys. Res. B **148**, 1029, (1999).

103) K. Uchida, S. Kaneko, S. Omi, C. Hata, H. Tanji, Y. Asahara, A. J. Ikushima, T. Tokizaki and A. Nakamura, J. Opt. Soc. Am. B, **11,** 1236, (1994).

103) R. P. Lang, J. Am. Chem. Soc., **84**, 4438 (1962). Z. Jiang, and A. Sen, Macromolecules, **25**, 880 (1992). 39) T. A. Skotheim, R. L. Elsenbaumer, and J. R. Reynolds, Eds., *Handbook of Conducting Polymers*, Marcel Dekker, Inc., New York (1998).

104) M. Thakur, R. Swamy, and J. Titus Macromolecules (Communication), **37(8)**, 2677 (2004).

105) "Energy band-gap dependence of two-photon absorption" Eric W. Van Stryland, M. A. Woodall, H. Vanherzeele, and M. J. Soileau, Optics letters Vol. 10, No. 10 October 1985

106) "High-sensitivity, single-beam n2 measurements" M. Sheik-bahae, A. A. Said, and E. W. Van Stryland, September 1, 1989 Vol. 14, No. 17 Optics letters

107) "Measurement of the nonlinear refractive index of polydiacetylene using Michelson interferometry and z-scan" R. Quintero-Torres and M. Thakur, Journal of Applied Physics Letters Vol. 85, No. 1

108) Michael P Hasselbeck, "NONLINEAR OPTICS BASICS" Article Number: OPTC00753

109) "Nonlinear refractive index of optical crystals" Robert Adair, L. L. Chase and Stephen A. Payne Physical Review B, Volume 39 Number 5

110) "Two-photon absorption in quantum dots based on a nonconjugated conductive polymer" Jitto Titus and M. Thakur Appl. Phy. Lett. 90 121111 (2007)

111) Q. Li, C. Liu, Z. Liu, and Qihuang Gong, Opt. Express **13**, 1833 2005.

112) R. H. Magruder III, L. Yang, R. F. Haglund, Jr., C. W. White, L. Yang, R. Dorsinville, and R. R. Alfano, Appl. Phys. Lett. **62**, 1730 1993.

113) R. del Coso, J. Requejo-Isidro, J. Solis, J. Gonzalo, and C. N. Afonso, J. Appl. Phys. **95**, 2755 2004.

114) S. Qu, Y. Song, C. Du, Y. Wang, Y. Gao, S. Liu, Y. Li, and D. Zhu, Opt. Commun. **196**, 317 2001.

115) R. A. Ganeev, M. Baba, M. Morita, D. Rau, H. Fujii, A. I. Ryasnyansky, N. Ishizawa, M. Suzuki, and H. Kuroda, J. Opt. A, Pure Appl. Opt. **6**, 447 2004.

116) G. Ma, W. Sun, S.-H. Tang, H. Zhang, and Z. Shen, Opt. Lett. **27**, 1043 2002.

117) D. Cotter, M. G. Burt, and R. J. Manning, Phys. Rev. Lett. **68**, 1200 1992.

118) L. A. Padilha, J. Fu, D. J. Hagan, E. W. Van Stryland, C. L. Cesar, L. C. Barbose, and C. H. B. Cruz, Opt. Express **13**, 6460 2005.

119) S. A. Blanton, M. A. Hines, M. E. Schmitt, and P. Guyot-Sionnest, J. Lumin. **70**, 253 1996.

120) Shixiong Qian, Guohong Ma, Wanxin Sun, Sing-Hai Tang, Hanzhuang Zhang and Zexiang Shen. Vol. 27, No. 12, Optical Letters, 2002.

121) "Cascading of Second Order Nonlinearities in Polar Materials" Christian Bosshard, Advanced Materials

122) Ch. Bosshard, K. Sutter, R. Schlesser, and P. Gunter, Vol. 10, No. 5, J. Opt. Soc. Am. B 1993

APPENDIX

The Pockels cell was fabricated by Davis Machine Works, Opelika, AL. The following are the design drawings of the Pockels cell done using AutoCAD 2006.

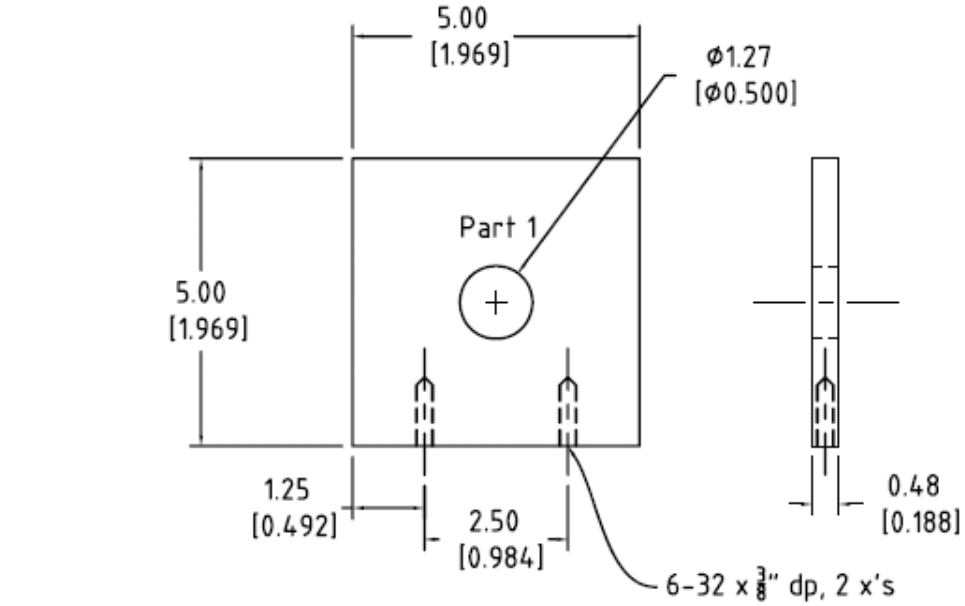
5.00
[1.969]
ø1.27
[ø0.500]
Part 1
5.00
[1.969]
1.25
[0.492]
2.50
[0.984]
0.48
[0.188]
6-32 x 3/8" dp, 2 x's

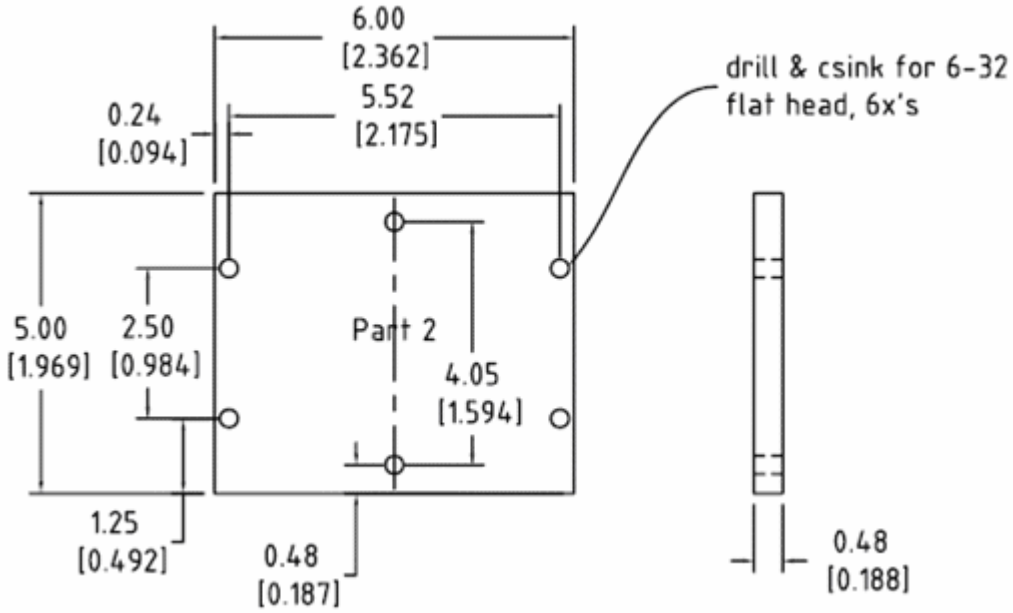
6.00
[2.362]
5.52
[2.175]
0.24
[0.094]
drill & csink for 6-32
flat head, 6x's
5.00
[1.969]
2.50
[0.984]
Part 2
4.05
[1.594]
1.25
[0.492]
0.48
[0.187]
0.48
[0.188]

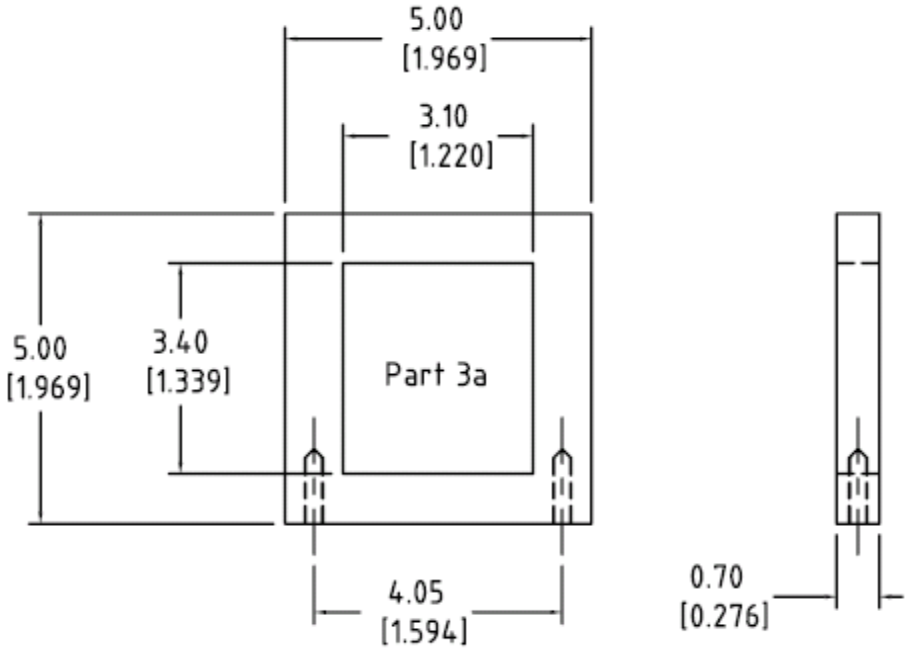
5.00
[1.969]
3.10
[1.220]
5.00
[1.969]
3.40
[1.339]
Part 3a
4.05
[1.594]
0.70
[0.276]

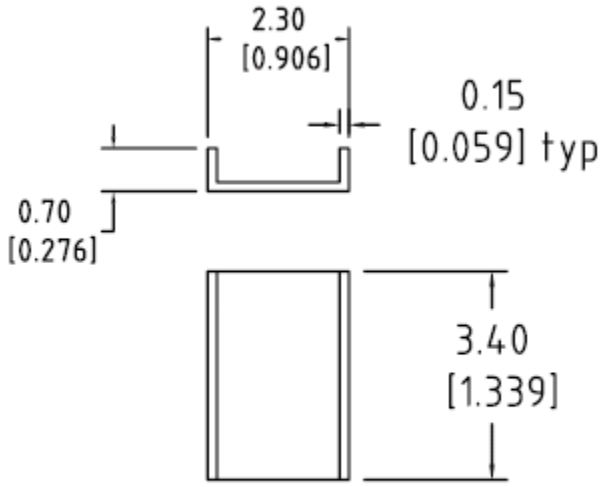
2.30
[0.906]
0.15
[0.059] typ
0.70
[0.276]
3.40
[1.339]

Part 3b

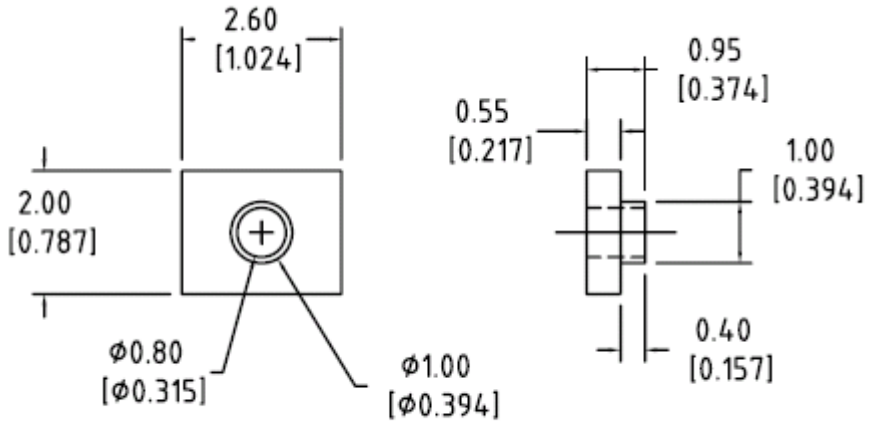

Part 3c

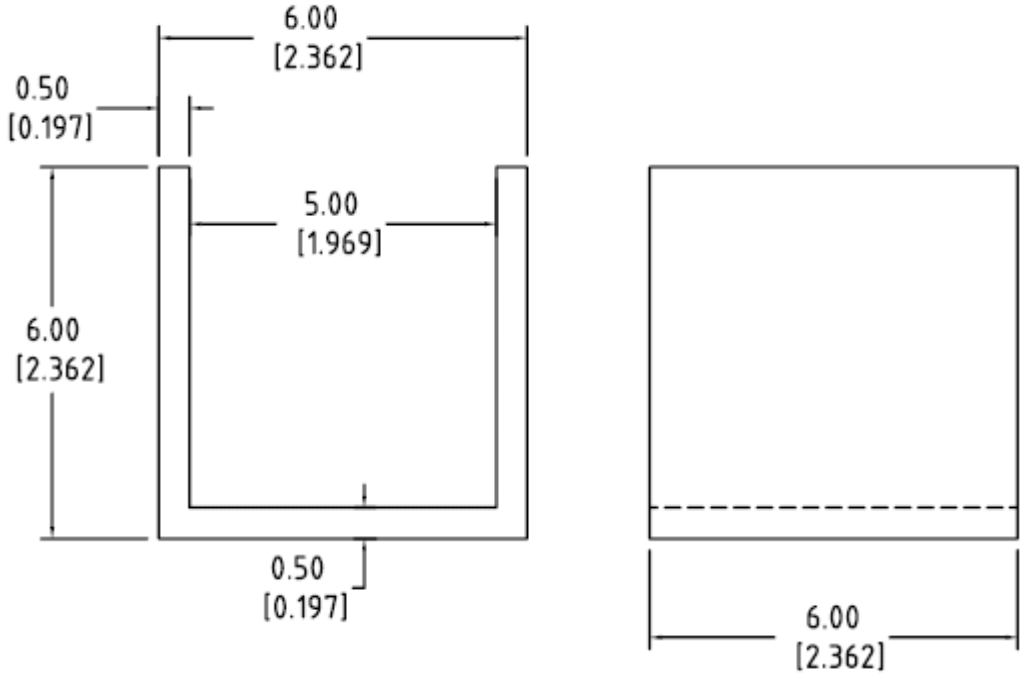

Part 4